

**Inhibiting the Actions of Essential Biomolecule Phosphopantetheine**

by

Kyle Anthony Heslip

A dissertation submitted in partial fulfillment  
of the requirements for the degree of  
Doctor of Philosophy  
(Medicinal Chemistry)  
in the University of Michigan  
2015

Doctoral Committee:

Lecturer Garry D. Dotson, Co-Chair  
Professor Ronald W. Woodard, Co-Chair  
Professor David H. Sherman  
Assistant Professor Matthew Soellner

**Dedication**

To Nicole,

Without you, none of this would have gotten finished.

## **Acknowledgements**

First and foremost I would like to express my gratitude and appreciation for my mentor Dr. Garry D. Dotson. Garry enabled me to grow as both a scientist and person. He instilled in me the importance of teaching and challenged me to keep high scientific and personal standards. I will forever be grateful for your patience and support. I would also like to express my gratitude to Dr. David H. Sherman, Dr. Matthew Soellner, and Dr. Ronald W. Woodard, for sacrificing their time to serve on my committee. Without their extreme support and invaluable insight I would not have been able to complete my doctoral work. I would like to express additional gratitude to Dr. Ronald W. Woodard for providing me a physical space and valued mentorship in the later portion of my graduate career.

I would like to thank my undergraduate mentors at Michigan State University, Dr. Mary K. Hausbeck and Dr. Leah L. Granke. I would like to express gratitude to my lab mates Dr. James Patrone, Dr. Jiangwei Yao, Dr. Ronald Jenkins, Andrew Pratt, Melissa Holt, and David Cech. You all made the long hours in lab much more entertaining and feel much shorter.

I would like to specifically thank Dr. Doug Hansen, Dr. Kris Branvold, and Dr. Ronald Jenkins, for their invaluable insights on all facets of scientific inquiry and investigation. You have provided unparalleled friendship and scholarship. I would also like to thank the friends I have made at the University of Michigan for their support both scientific and emotional: Dr. Caleb Bates, Dr. Katrina Lexa, Dr. Scott Barraza, and Dr.

Bryan Yestrepky. I would like to give a very special thanks to every member, past, present, and future of Antonio Cromartie's Kids, the best flag-football team to every play on the intramural turf.

I would like to thank my family for their support. Thank you to my parents, Brian and Elizabeth Heslip, for their guidance and support. Thank you to my siblings (Ryan, Ronnie, Katie, and Brie), for each of your own unique personalities that helped shape who I am today. And thank you to the Schaendorf family (John, Connie, Ben, and Nicole), for accepting me as one of your own.

Finally I would like to express unrelenting gratitude and love to my wife, Nicole Heslip. Thank you for your saint-like patience through the long nights and tired mornings. Without your love, understanding, and tolerance of my friends, I would not have been able to complete my doctoral work. Without your care, home management, and delicious cooking, I would have hardly survived. I owe you big.

## Table of Contents

Dedication	ii
Acknowledgements	iii
List of Figures	vi
List of Tables	viii
Abstract	ix
Chapters	
1. Introduction.	1
2. Activity of Conserved Residues of <i>Streptococcus pneumoniae</i> Type 3 Phosphopantothenoylcysteine Synthetase	26
3. Molecular Binding Mechanism of RJPXD33 to Early Raetz Pathway Acyltransferases	72
4. Conclusion & Future Directions	110

## List of Figures

Figure		Page
1.1	Structures of essential biomolecules pantothenate, phosphopantetheine, coenzyme A, and acyl-ACP	20
1.2	Biosynthetic pathway of Coenzyme A	21
1.3	Sequence similarity of CoA biosynthetic enzymes among several species	22
1.4	Selected CoA biosynthetic pathway inhibitors	23
1.5	The membranes of gram-negative bacteria	24
1.6	Biosynthetic pathway of lipid A	25
2.1	Two step reaction of PPCS	53
2.2	Growth curve of knockout strain <i>E. coli</i> MG1655 $\Delta$ PanC, $\Delta$ coaBC:: <i>Kan</i> <sup>R</sup> supplemented with various amounts of environmental pantetheine	54
2.3	Growth curve of knockout strain <i>E. coli</i> MG1655 $\Delta$ PanC, $\Delta$ coaBC:: <i>Kan</i> <sup>R</sup>	55
2.4	MIC test of JY1 (SPB03328) against <i>coaBC</i> complemented <i>E. coli</i> MG1655 $\Delta$ PanC, $\Delta$ coaBC:: <i>Kan</i> <sup>R</sup>	56
2.5	Disc diffusion of JY1 against <i>E. coli</i> MG1655 $\Delta$ PanC, $\Delta$ coaBC:: <i>Kan</i> <sup>R</sup> and <i>E. coli</i> $\Delta$ tolC	57
2.6	Full multiple sequence alignment of bacterial PPCS. Boxed and highlighted sequences represent the monofunctional Type 3 PPCS enzymes	58
2.7	Selected conserved sequences found in the multiple sequence alignment between bacterial mono and bifunctional PPCS	59
2.8	Crystal structure of <i>E. coli</i> PPCS dimer (2.37 Å resolution) bound to cytidylate intermediate mimic	60
2.9	Streaks of plasmid-based PPCS-PPCDC point mutations complementing <i>E. coli</i> MG1655 $\Delta$ dfp ( <i>coaBC</i> )	61

2.10	Results of single turnover assay in selected <i>S. pneumoniae</i> PPCS point mutations	62
2.11	<i>S. pneumoniae</i> substrates $K_m$ curves	63
2.12	<i>S. pneumoniae</i> PPCS K123 mutants phosphopantetheine apparent $K_m$ curves	64
2.13	<i>S. pneumoniae</i> PPCS K123 mutants cysteine apparent $K_m$ curves	65
2.14	<i>S. pneumoniae</i> PPCS K123 mutants cytidine triphosphate apparent $K_m$ curves	66
2.15	<i>S. pneumoniae</i> PPCS D93 mutants phosphopantetheine apparent $K_m$ curves	67
2.16	<i>S. pneumoniae</i> PPCS D93 mutants cysteine apparent $K_m$ curves	68
2.17	<i>S. pneumoniae</i> PPCS D93 mutants cytidine triphosphate apparent $K_m$ curves	69
2.18	<i>S. pneumoniae</i> PPCS D93 mutants $MgCl_2$ apparent $K_m$ curves	70
2.19	Active site of bacterial PPCS	71
3.1	Enzymatic activities of LpxA and LpxD in the Raetz pathway	101
3.2	Alanine-substitution effects on RJPXD33 binding to LpxA	102
3.3	Alanine-substitution effects on RJPXD33 binding to LpxD	103
3.4	Alanine-substitution effects on RJPXD33 binding to LpxA and LpxD	104
3.5	Direct binding curve of photopeptides to LpxA	105
3.6	In-gel fluorescence of photocrosslinked LpxA and LpxD	106
3.7	FITC-RJPXD33 titrations of native and iodoacetamide treated LpxD	107
3.8	Structural overlay of LpxA-RJPXD33 onto LpxD-acyl-ACP	108

## List of Tables

Tables	Page
2.1 List of vectors developed for the <i>in vivo</i> and <i>in vitro</i> characterization of bacterial PPCS	48
2.2 List of vectors constructed for active site comparison of <i>E. coli</i> and <i>S. pneumoniae</i> PPCS	49
2.3 List of vectors constructed in the mutagenesis studies of <i>S. pneumoniae</i> PPCS	50
2.4 Phenotypes of <i>S. pneumoniae</i> PPCS mutant	51
2.5 Comparison of apparent Michaelis-Menten constants of <i>S. pneumoniae</i> PPCS mutant	52
3.1 List of vectors constructed for acyltransferases studies	95
3.2 $K_d$ and IC50 values of truncated peptide	96
3.3 Direct binding results of C-terminal carboxylic acid peptide	97
3.4 $K_d$ and IC50 values of alanine-scan peptide	98
3.5 Binding affinity of photopeptides	99
3.6 Binding of FITC-RJPXD33 to various LpxA and LpxD	100



## Abstract

Phosphopantetheine is an essential biomolecule required for life. The enzyme phosphopantothenoylcysteine synthetase (PPCS) incorporates the reactive thiol moiety in the Coenzyme A (CoA) biosynthetic pathway. Two types of PPCS exist in bacteria: bifunctional fusion protein Type 1 and monofunctional Type 3. Previously developed cytidylate mimics were determined to have stronger binding affinity for Type 3 *Streptococcus pneumoniae* PPCS compared to Type 1. To explore the structure activity relationship of Type 3 PPCS, completely conserved residues of bacterial PPCS were probed via saturation mutagenesis in a developed knockout system. Mutagenesis revealed that conserved *S. pneumoniae* PPCS residues K123 and D93 were stringent, as only K123N/R/M and D93E/N were viable mutations. D93 was determined to be responsible for the association of divalent cations and CTP to the active site, as D93E and D93N exhibited a 1.5-2.7 fold (151-267  $\mu\text{M}$  apparent  $K_m$ ) less affinity for CTP and D93N resulted in a 2-fold drop in  $\text{MgCl}_2$  affinity. K123 was identified as catalytically significant to the first half CTP utilizing reaction as the K123M and K123R mutations had 1.4-8.8 fold (142-872  $\mu\text{M}$  apparent  $K_m$ ) loss in the binding affinity for CTP.

Additionally, phosphopantetheine is the essential prosthetic group of acyl carrier protein (ACP), utilized by gram negative specific acyltransferases (LpxA and LpxD) to construct lipopolysaccharide (LPS). Peptide RJPXD33 (TNLYMLPKWDIP) was discovered to bind and inhibit both LpxA and LpxD (binding constants of 22  $\mu\text{M}$  and 6.5  $\mu\text{M}$  respectively), offering a probe for the development of a dual targeting small molecule

inhibitor. The molecular binding mechanism by which RJPXD33 interacts with LpxD was elucidated via fluorescence polarization based binding assays of truncated and alanine-mutated peptide. RJPXD33 P7 was identified to be important to binding LpxD as mutation of the residue to alanine resulted in a binding constant  $>50 \mu\text{M}$ , while similar tests in LpxA had a limited effect on binding ( $9.4 \pm 0.6 \mu\text{M}$ ). Residue K8 appeared inconsequential, as mutation to alanine had little effect on binding to LpxA or LpxD ( $5.1 \mu\text{M}$  and  $3.1 \mu\text{M}$  binding constants, respectively), but essential to inhibition. Photo-labile RJPXD33 probes were implemented for mapping LpxD-RJPXD33 protein-peptide interactions.

## Chapter 1

### Introduction

#### The Essential Biomolecule Phosphopantetheine

Cofactors are non-protein components that are essential for the activity of a multitude of life sustaining enzymes. For metabolism to occur, functional groups must be transferred to and from metabolites, and all of these transfer reactions require a loosely bound cofactor to carry these functional groups between enzymatic reactions (1,2). Broadly, cofactors can be divided into two categories: inorganic cofactors and organic cofactors (3). Inorganic cofactors include metal ions (4), as well as metallo-organic complexes, such as the heme groups (5). Organic cofactors are small organic molecules that directly participate in the enzymatic reaction, and in some cases can be covalently bound as a prosthetic group (6). Several cofactors are derived from vitamins, partially reflecting the essential nature of vitamins, including nicotinamide adenine dinucleotide (7), tetrahydrofolic acid (8), and Coenzyme A (9).

Coenzyme A (CoA) is an organic cofactor utilized in 4% of all enzymatic reactions (10). It consists of the essential biomolecule, phosphopantetheine, linked to an adenylyl group (**Figure 1.1**), and has been discovered as an essential cofactor in all forms of life thus far (10). Fulfilling a multitude of roles, CoA serves as an acyl carrying cofactor in many organisms and is a required cofactor for the oxidation in lipogenesis and pyruvate oxidation in the citric acid cycle, and in certain bacteria is believed to create and

maintain the reductive environment (9,11). Coenzyme A also serves as the biological source of phosphopantetheine for acyl carrier protein (ACP), peptidyl carrier protein (PCP) and aryl carrier protein (ArCP) (9,12,13). In gram-negative bacteria, the formation of lipopolysaccharide (LPS), the outer layer of the outer membrane requires phosphopantetheine as a prosthetic group of acyl-ACP, required for the catalytic acylation of UDP-GlcNAc by LpxA and LpxD (14-16). Low levels of intracellular CoA has been shown to cause slowed growth in *Escherichia coli* (17). Genetic and chemical knockouts of the CoA biosynthetic pathway have been shown to be lethal, further reflecting the essential nature of the cofactor (18-20).

Phosphopantetheine is of particular interest within CoA, as it serves as the active prosthetic group (12). Phosphopantetheine is derived from pantothenate, containing a cystamine/ $\beta$ -alanine dipeptide linked to a phosphorylated pantooyl group (**Figure 1.1**). Most organisms obtain phosphopantetheine via *de novo* synthesis along the Coenzyme A biosynthetic pathway, although not all organisms have the complete pathway (21). Obligate parasites such as those in the *Chlamydia* family appear to have no CoA biosynthetic pathway yet rely on CoA and ACP for LPS and glycerol phosphate biosynthesis for growth (22). It has been proposed that organisms without CoA synthetic pathways are able to transport some phosphopantetheine containing biomolecules and modify them to suit need. Additionally, some bacteria, such as *Escherichia coli*, are able to utilize a salvage pathway wherein the precursor pantetheine can be imported from the environment via a 'pantetheine shunt' and used to generate phosphopantetheine (23). Without the reactive thiol moiety phosphopantetheine introduces, CoA is rendered ineffectual. Thusly, analogs of pantetheine missing the thiol residue have been developed

to utilize the ‘pantetheine shunt’ to become potent antimetabolites of CoA (24-28). The essential nature of the phosphopantetheine thiol in CoA allows for the development of potential antimicrobial agents (29).

The essential nature of phosphopantetheine as well as the divergence in homology between microbial and eukaryotic enzymes that construct this pathway (30), make targeting its synthesis in microbes a novel target for the development of small molecule antimicrobials. Additionally, the gram-negative specific utilization of phosphopantetheine in the acyl transfer reactions of the biosynthesis of LPS offer another unique target for the development of small molecule antibiotics. The work herein focuses on elucidating key target-inhibitor molecular binding mechanisms with enzymes that either produce (phosphopantothenoylcysteine synthetase) or directly interact with (early LPS acyltransferases) the essential biomolecule phosphopantetheine. The goal in doing so is to provide valuable insight for the rational design of potent small molecule antibiotics.

### **Coenzyme A Biosynthesis as a Target for Antimicrobial Development**

The *de novo* synthesis of CoA occurs in nearly all organisms in five highly conserved steps (**Figure 1.2**) (31). Pantothenate (Vitamin B<sub>5</sub>) is first phosphorylated by pantothenate kinase (PanK; EC 2.7.1.33; *coaA*) to 4'-phosphopantothenate. In a two-step reaction, phosphopantothenoylcysteine synthetase (PPCS; EC 6.3.2.5; *coaB*) uses a NTP to form an activated cytidylate intermediate, followed by condensation with cysteine to form phosphopantothenoylcysteine. Following a rare cysteine decarboxylation by phosphopantothenoylcysteine decarboxylase (PPCDC; EC 4.1.1.36; *coaC*),

phosphopantetheine is formed (32,33). Phosphopantetheine adenylyltransferase (PPAT; EC 2.7.7.3; *coaD*) adenylylates phosphopantetheine at the 4'-phosphate to generate dephospho-coenzyme A (deCoA). In the final step, dephospho-CoA kinase (DPCK; EC 2.7.1.24; *coaE*) phosphorylates the 3' hydroxyl of the ribose sugar, forming CoA.

Although enzymes in CoA biosynthesis are highly conserved, there is a great deal of diversity among the enzymes between different species (30). Amino acid sequence similarities between human and bacterial CoA biosynthetic pathways are visualized in **Figure 1.3**. Overall, there is very low sequence similarity between human and bacterial CoA biosynthetic enzymes. Human PPCS shares less than 20% sequence similarity with all of the species listed, except of *Enterococci faecalis* and *Streptococcus pneumoniae*, of which the human PPCS shares a 20-30% sequence similarity. Such low sequence similarity is a good indication that selective inhibition of bacterial Coenzyme A producing enzymes may make good therapeutic targets. Additionally, *E. coli* PPCS shares at least a 20% sequence similarity with other bacterial PPCS, and in several cases a much higher sequence similarity. This suggests that broad spectrum chemotherapeutics can be developed that target bacterial PPCS.

Pantothenate kinase (PanK; EC 2.7.1.33; *coaA*) is expressed in several varieties. Type 1 PanK is expressed in some bacteria, including *Escherichia coli*, and has been determined to be a vital component in the salvage of pantetheine. This PanK is able to phosphorylate extracellular pantetheine to bypass the PPCS/PPCDC enzymatic reactions and produce 4'-phosphopantetheine (24). The pantothenate analog *N*-pentylpantothenamide (N5-Pan) has been determined to be a substrate of Type 1 PanK, but will produce inactive ethyldethia-CoA (27,34). *N*-heptylpantothenamide (N7-Pan) as

a substrate will produce similar results (25). Likewise, Type 2 PanK, expressed in *Staphylococcus aureus* and other gram positive bacteria, is able to utilize N5-Pan and N7-Pan, which act as more potent antimicrobials as a result of inactive CoA formation (35). Type 2 PanK is not feedback inhibited by CoA (11), which is likely why N5 and N7-Pan are much more potent in *S. aureus* than in *E. coli*. A Type 3 PanK, discovered in *Bacillus subtilis*, is present in a majority of bacteria and is expressed by *coaX* (23). Type 3 PanK has been found not to phosphorylate N5-Pan and N7-Pan, due in part to its much smaller active site (36). Type 3 PanK is unable to phosphorylate panthetheine, consistent with the enzyme's inability to utilize alkyl-pantothenamides as alternative substrates to pantothenate (37). Additionally, Type 3 PanK is not feedback inhibited by CoA, and thus it remains uncertain if it plays any role in CoA regulation (38,39).

Phosphopantothenoylcysteine synthetase (PPCS; EC 6.3.2.5; *coaB*) is a critical enzyme in the CoA biosynthetic pathway, as it is responsible for the incorporation of the reactive thiol. As with PanK, PPCS is expressed in three types. Most bacteria express Type 1 PPCS, which is the bifunctional PPCS/PPCDC fusion protein (40,41). In the first half reaction, Type 1 PPCS exclusively utilizes CTP. Higher eukaryotes, including humans, express a monofunctional Type 2 PPCS and a separate monofunctional PPCDC (10). Type 2 PPCS has a much larger nucleotide binding pocket and will utilize ATP or CTP for the first half reaction, however the higher intracellular concentration of ATP make it the more physiologically relevant substrate. *S. pneumoniae* and *E. faecalis* express Type 3 monofunctional PPCS that utilizes CTP in a manner similar to that of Type 1 PPCS (42). Differences in the activity of the PPCS enzyme between human and

bacterial systems and the requisite nature of the enzyme make it a feasible target for the development of small molecule antimicrobial agents.

*In vitro* inhibitors of PPCS have been constructed and characterized by our group (**Figure 1.4**). Cytidylate intermediate mimics of PPCS have been synthesized and characterized as slow on-set, tight-binding inhibitors (43,44). Phosphopantothenate analogs have also been constructed, with phosphopantotheniol determined to be a phosphopantothenate-competitive inhibitor of *E. coli* PPCS with a low  $\mu\text{M}$   $K_i$ . Additionally, *S. pneumoniae* PPCS has previously been screened by our group against 41,000 compounds at the University of Michigan Center for Chemical Genomics. The screening process provided isoxazole-containing compounds that offer low  $\mu\text{M}$  inhibition of the monofunctional PPCS *in vitro* but have limited *in vivo* efficacy (45).

Previous structural studies have revealed that both bacterial and eukaryotic PPCS are active dimers (40,46). Crystal structure of the inactivated *E. coli* Type 1 PPCS(N210D) and human Type 2 PPCS have revealed that a lysine (K123 in *E. coli*) from one monomer completes the active site at the other monomer's asparagine (N210 in *E. coli*). A of native *E. coli* Type 1 PPCS was obtained upon co-crystallization with the cytidylate intermediate **JDP03** (44). This structure revealed that the internal phosphate of the compound makes a salt bridge with *E. coli* Lys341 and binding contact with Lys289, a residue that was previously determined to be critical to the enzymatic catalysis of PPCS (47). This crystal structure gave a wealth of knowledge for improving inhibitors against bacterial Type 1 PPCS; however no structural studies had yet been performed on Type 3 PPCS.



While not all methods of phosphopantetheine acquisition have been fully investigated, it is possible to target specific methods in certain organisms for the purpose of developing selective antimicrobials. Specifically, *de novo* synthesis of phosphopantetheine can be interrupted in bacteria by targeting PanK, PPCS and PPCDC. However, in order to produce compounds which are able to serve as antimicrobials, functional activity of these proteins need to be further investigated. With more knowledge gained, target-based design of potent, cell wall permeable inhibitors of CoA biosynthesis can be achieved. A goal of the research efforts described herein is to determine the residues responsible for the chemistry and unique recognition of substrates in monofunctional PPCS. Our hypothesis is that understanding the role of conserved residues between bacterial bifunctional and monofunctional PPCSs will allow aspects of the molecular basis of catalysis and inhibition to be determined. With a detailed understanding of monofunctional PPCS catalysis and inhibition it will be possible to rationally design more potent small molecules that can selectively inhibit bacterial PPCS to serve as molecular probes in the study of bacterial CoA biosynthesis, as well as antimicrobial leads.

### **Acyl Carrier Protein**

As briefly mentioned earlier, phosphopantetheine also has the essential role as a prosthetic group outside of Coenzyme A; as the active moiety of acyl carrier protein (ACP) (48). ACP is expressed in an inactive apo form, requiring holo-acyl carrier protein synthase to perform a post-translational attachment of phosphopantetheine to a conserved

serine residue, forming active holo-ACP (12). The phosphopantetheine prosthetic group offers chain flexibility and can form covalent bonds with intermediates (49).

ACP is universal and essential to fatty acid synthesis (50). Most bacteria utilize Type II fatty acid synthesis, wherein each step in fatty acid synthesis is performed by a different enzyme, unlike the mammalian Type I fatty acid synthesis wherein one polyprotein performs all of the steps (51,52). Inhibiting the interactions of these fatty acid synthesis enzymes with ACP by the introduction of natural product and small molecules offers significant potential for the development of antimicrobials (53-55). Currently, the drug triclosan is able to inhibit bacterial fatty acid synthesis by forming a ternary complex with enoyl-ACP reductase, no longer allowing it to interact with ACP and participate in fatty acid synthesis (56). However, broad spectrum usage of triclosan offers bacterial resistance concerns (57), and there is still a lack of basic understanding of the diversity in regulation of lipid metabolism in bacteria (53).

ACP also has specialized functions that are specific to bacteria (50). Of particular therapeutic interest are ACP's interactions with the acyltransferases involved in the construction of the cell membrane of gram-negative bacteria (58). The essential nature of ACP makes selectively inhibiting its interactions an intriguing chemotherapeutic target. My research, in part, focuses on ACP's interactions with the early acyl transferases in the Raetz Lipid A biosynthetic pathway of gram negative bacteria.

### **Lipid A Biosynthesis as a Target for Antimicrobial Development**

Lipopolysaccharide (LPS) forms the asymmetrical outermost monolayer of the cell membrane of gram-negative bacteria (**Figure 1.5**) (59,60). Additionally, LPS serves

as a hydrophobic permeability barrier that protects gram negative bacteria from hydrophobic antibiotics (61,62). LPS is composed of three core components: lipid A, a core polysaccharide region, and the outermost repeating *O*-antigen polysaccharide (60). Lipid A is the essential oligosaccharide moiety of LPS, responsible for anchoring the moiety to form the outer monolayer of the outer cell wall membrane of Gram-negative bacteria (59,60,63). Lipid A is essential to growth in most Gram-negative bacteria (64,65) and modification to lipid A plays a role in protecting the bacteria from environmental stress (60).

LPS is also known as endotoxin, and triggers the host-cell response required for bacterial clearance (59). During infection, released lipid A initiates the host-cell immune response via the TLR4-MD-2 complex (66-70). Overstimulation of this complex can occur and lead to septic shock and ultimately death (69,71,72). The requisite nature and toxicity of lipid A make its biosynthetic pathway an optimal target for antimicrobial chemotherapeutic discovery (54,58,65,73,74).

The biosynthesis of lipid A consists of nine consecutive enzymatic processes (**Figure 1.6**) (75). Acyltransferase LpxA performs the first step through a thermodynamically unfavorable reaction, utilizing an acyl carrier protein (ACP) to acylate UDP-*N*-acetylglucosamine (UDP-GlcNAc) at the 3-hydroxyl, producing UDP-3-*O*-(*R*-3-hydroxymyristoyl)-*N*-acetylglucosamine (15,75). Subsequent deacylation of the *N*-acetyl moiety by LpxC provides the first committed step of lipid A biosynthesis and is a key regulatory step in the *E. coli* pathway (76-78). Acyltransferase LpxD utilizes ACP to catalyze the third reaction, acylating the free amine of the glucosamine ring (79). Six

more enzymatic reactions follow to catalyze the formation of hexa-acylated Kdo<sub>2</sub>-lipid A moiety of LPS (59).

Temperature sensitive mutants of the early step of the lipid A biosynthetic pathway have demonstrated that lipid A is required for the viability of the microbe and that the activity of these early steps are required for the maintenance and growth of the microbe (77,79,80). Overexpression of LpxA and LpxD inhibitory peptides has also demonstrated toxicity in *E. coli* (81,82). Synthetic molecules screened against the lipid A biosynthetic pathway yielded small molecule inhibitors of LpxC that exhibited an MIC of 1 µg/ml against *E. coli* (73). These compounds were expanded via crystallographic and structure-activity relationship studies to create a potent, broad spectrum inhibitor of LpxC (58,83,84). Development of such inhibitory compounds chemically validates the early steps of the Raetz pathway as antimicrobial targets.

LPS between different microbes can look very different, with varying external repeating oligonucleotides and varying numbers of Kdo modifications to the lipid A core (59). However, regardless of the diversity of LPS as a whole, the lipid A anchor moiety is relatively conserve. Nearly all lipid A contains the same glucosamine core, although *Leptospira interrogans* will convert the 3'-hydroxyl of UDP-GlcNAc to an amine (85,86). Most of the diversity of lipid A between microbes is a result of the acyl chain lengths that the acyltransferases (LpxA and LpxD) utilize as a substrate (87-90).

LpxA is expressed as a trimeric enzyme, with an active site located at a catalytic histidine on each of the monomers of the trimer (91,92). This histidine deprotonates the 3' hydroxyl of UDP-GlcNAc, which allows for the nucleophilic attack into the phosphopantotheine-acyl thioester of the acyl-ACP substrate (89,93). Crystal structures

have demonstrated that acyl chains are able to bind the hydrophobic pocket located at the intersection of monomeric subunits (85,94). These hydrophobic pockets contain a histidine residue that serves as the ‘hydrocarbon ruler,’ responsible for the selectivity of acyl chains incorporated into the lipid A core by LpxA (95).

In addition to sharing similar enzymatic activity, LpxD also shares a high sequence homology with LpxA (27.2%) (96). Not surprisingly, crystal structures of LpxD demonstrates that it share a similar structure to LpxA, with a left-handed  $\beta$ -helical motif (97). LpxD also contains an  $\alpha$ -helical UDP-binding domain and C-terminal  $\alpha$ -helical extension region. Structural differences in the C-terminus of the L $\beta$ H domain is responsible for the differences in acyl-chain length selectivity between *E. coli* and *C. trachomatis* LpxD (97).

Peptides have provided an invaluable tool in the study of the Raetz pathway acyl-transferases. Phage display was utilized by Benson *et. al.* to identify peptide P920, a 12-mer inhibitory peptide of LpxA (82). As a prelude to the development of rationally designed small molecule inhibitors of LpxD, inhibitory peptide RJPXD33 was identified via phage display by Jenkins *et. al.* (81). A co-crystal structure of RJPXD33 with *E. coli* LpxA demonstrated that the six N-terminal residues of the peptide bind the hydrophobic pocket of the enzyme, within 2.8 Å of the His191 hydrocarbon ruler (14). This site normally is occupied by the substrate acyl-chain of acyl-ACP, suggesting that RJPXD33 binds LpxA and inhibits the enzyme by preventing its association with acyl-ACP. Overlaying the LpxA-RJPXD33 crystal structure with the crystal structure of the LpxD-acyl-ACP complex reveals that peptide likely fills the same space as the phosphopantetheine arm of acyl-ACP (14). However, peptides serve as poor

antimicrobials due to proteolytic cleavage. In order to design potent compounds, extensive characterization of RJPXD33 was required.

## **Thesis Outline**

Antibacterial research has afforded mankind exceptional improvements in the quality of life since the 1930s (98). However, bacterial resistance to currently used therapeutics is increasing at an alarming rate, and the rate that new antibiotics are introduced to the market has slowed dramatically since the 1970s (99,100). As such, there is a call for the design of novel antibacterial chemotherapeutics to combat the rise of resistance. The biomolecule phosphopantetheine is one intriguing target for the development of novel antimicrobial agents, as it is essential across life but there are divergences in its production and utilization between human and bacteria (35,53,54,101,102).

Small molecule probes serve as vital chemical biological tools for the development of antibiotics. They afford a strong platform for evaluating the utility of a chemical space to serve as an inhibitor of target enzymes and allow determination of key molecular binding activity in the inhibitor-enzyme complex. While they themselves cannot directly be utilized as antimicrobial agents, either due to an inability to reach the target within the *in vivo* system or due to chemical instability, the knowledge they afford for the rational development of small molecule antimicrobials is indispensable. The work presented herein both utilizes and characterizes molecular probes to inhibit the production and utilization of phosphopantetheine in bacterial systems, providing key insight to the molecular binding mechanisms of the probes.

The overall goal of the research efforts described herein is to target the production and utilization of phosphopantetheine in bacterial systems as a target of antimicrobial agents. This research was directed along two pathways: 1) PPCS incorporation of the moiety into CoA, and 2) utilization of the moiety by LpxA and LpxD in the formation of lipid A. Our hypothesis is that understanding the role of conserved residues between bacterial bifunctional and monofunctional PPCSs will allow aspects of the molecular basis of catalysis and inhibition to be determined. Among these aspects are phosphopantothenate binding, cysteine selectivity, and inhibitor binding. Additionally, the further characterization and utilization of peptide RJPXD33 will provide essential insight to the molecular binding mechanisms for both LpxA and LpxD, as well as provide a scaffold for the development of small molecule antimicrobial acyltransferases inhibitors.

In Chapter 2, Type 3 *S. pneumoniae* PPCS is evaluated in depth in order to determine the key residues for activity and substrate recognition. A multiple sequence alignment of all bacterial PPCS (both Type 1 and Type 3) was performed to highlight completely conserved residues. Mutagenenic studies were performed in *E. coli* Type 1 PPCS and *S. pneumoniae* Type 3 PPCS to determine if they shared catalytic roles across bacterial PPCS. A double knockout *E. coli* based expression strain was developed in order to quickly verify the PPCS mutants *in vivo*, and follow up *in vitro* characterization was performed via a continuous pyrophosphatase-coupled assay. These studies provided a chemical-biological basis for interactions of previously discovered small molecule inhibitors of PPCS.

In Chapter 3, acyltransferase binding studies utilizing various derivatives of RJPXD33 were undertaken in order to investigate key residues for binding of RJPXD33 to LpxD and discover how the peptide's structure dictates its dual inhibitor nature. Specifically, alanine scanning was performed on RJPXD33 to determine the contribution of each residue to the overall binding of LpxA and LpxD, and the residues important to the binding of both proteins. Additionally, residues responsible for the unique recognition of LpxA or LpxD were identified. Truncations of the RJPXD33 peptide were also made at the C-terminus in order to determine the minimum sequence necessary to inhibit LpxD. Additionally, peptide photo-affinity probes were crosslinked to LpxD in attempts to validate binding model of RJPXD33-LpxD with high resolution mass spectrometry.



## References

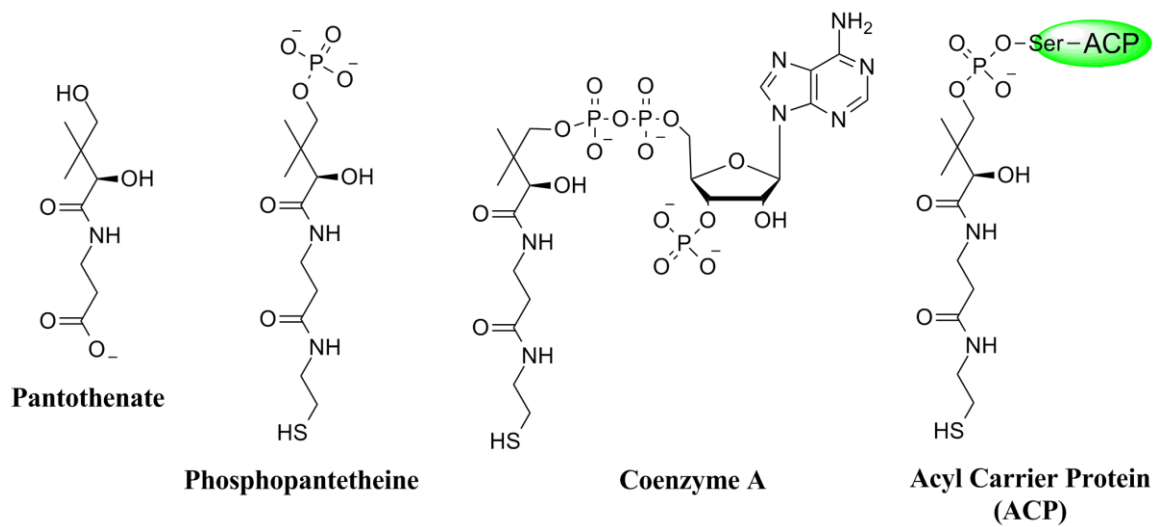
1. Wimmer, M. J., and Rose, I. A. (1978) *Annual Review of Biochemistry* **47**, 1031-1078
2. Tapiero, H., and Tew, K. D. (2003) *Biomedicine & Pharmacotherapy* **57**, 399-411
3. Lehninger, A., Nelson, D., and Cox, M. (2008) *Lehninger Principles of Biochemistry*, W. H. Freeman
4. Aggett, P. J. (1985) *Clinics in Endocrinology and Metabolism* **14**, 513-543
5. Tapiero, H., Townsend, D. M., and Tew, K. D. (2003) *Biomedicine & Pharmacotherapy* **57**, 386-398
6. Joosten, V., and van Berkel, W. J. H. (2007) *Current Opinion in Chemical Biology* **11**, 195-202
7. Pollak, N., Dölle, C., and Ziegler, M. (2007) *Biochemical Journal* **402**, 205-218
8. Donnelly, J. G. (2001) *Critical reviews in clinical laboratory sciences* **38**, 183-223
9. Leonardi, R., Zhang, Y.-M., Rock, C. O., and Jackowski, S. (2005) *Progress in lipid research* **44**, 125-153
10. Daugherty, M., Polanuyer, B., Farrell, M., Scholle, M., Lykidis, A., de Crécy-Lagard, V., and Osterman, A. (2002) *Journal of Biological Chemistry* **277**, 21431-21439
11. Leonardi, R., Chohnan, S., Zhang, Y.-M., Virga, K. G., Lee, R. E., Rock, C. O., and Jackowski, S. (2005) *Journal of Biological Chemistry* **280**, 3314-3322
12. Elovson, J., and Vagelos, P. R. (1968) *Journal of Biological Chemistry* **243**, 3603-3611
13. Vagelos, P. R., and Larrabee, A. R. (1967) *Journal of Biological Chemistry* **242**, 1776-1781
14. Jenkins, R. J., Heslip, K. A., Meagher, J. L., Stuckey, J. A., and Dotson, G. D. (2014) *Journal of Biological Chemistry* **289**, 15527-15535
15. Anderson, M. S., Bull, H. G., Galloway, S. M., Kelly, T. M., Mohan, S., Radika, K., and Raetz, C. R. (1993) *Journal of Biological Chemistry* **268**, 19858-19865
16. Masoudi, A., Raetz, C. R. H., Zhou, P., and Pemble Iv, C. W. (2014) *Nature* **505**, 422-426
17. Jackowski, S., and Rock, C. O. (1986) *Journal of Bacteriology* **166**, 866-871
18. Zhang, Y.-M., Chohnan, S., Virga, K. G., Stevens, R. D., Ilkayeva, O. R., Wenner, B. R., Bain, J. R., Newgard, C. B., Lee, R. E., Rock, C. O., and Jackowski, S. (2007) *Chemistry & Biology* **14**, 291-302
19. Bosveld, F., Rana, A., van der Wouden, P. E., Lemstra, W., Ritsema, M., Kampinga, H. H., and Sibon, O. C. M. (2008) *Human Molecular Genetics* **17**, 2058-2069
20. Spitzer, E. D., and Weiss, B. (1985) *Journal of Bacteriology* **164**, 994-1003
21. Osterman, A., and Overbeek, R. (2003) *Current Opinion in Chemical Biology* **7**, 238-251
22. Azenabor, A., Job, G., and Adedokun, O. (2005) *Molecular and Cellular Biochemistry* **269**, 69-84

23. Moiseenok, A. G., Katkovskaya, I. N., Gurinovich, V. A., Denisov, A. A., Pashkevich, S. G., and Kul'chitskii, V. A. (2010) *Neurochemical Journal* **4**, 257-264
24. Strauss, E., and Begley, T. P. (2002) *Journal of Biological Chemistry* **277**, 48205-48209
25. Zhang, Y.-M., Frank, M. W., Virga, K. G., Lee, R. E., Rock, C. O., and Jackowski, S. (2004) *Journal of Biological Chemistry* **279**, 50969-50975
26. van der Westhuyzen, R., Hammons, Justin C., Meier, Jordan L., Dahesh, S., Moolman, Wessel J. A., Pelly, Stephen C., Nizet, V., Burkart, Michael D., and Strauss, E. (2012) *Chemistry & Biology* **19**, 559-571
27. Meier, J. L., Mercer, A. C., Rivera, H., and Burkart, M. D. (2006) *Journal of the American Chemical Society* **128**, 12174-12184
28. Clarke, K. M., Mercer, A. C., La Clair, J. J., and Burkart, M. D. (2005) *Journal of the American Chemical Society* **127**, 11234-11235
29. Spry, C., Kirk, K., and Saliba, K. J. (2008) *FEMS Microbiology Reviews* **32**, 56-106
30. Genschel, U. (2004) *Molecular Biology and Evolution* **21**, 1242-1251
31. Gerdes, S. Y., Scholle, M. D., D'Souza, M., Bernal, A., Baev, M. V., Farrell, M., Kurnasov, O. V., Daugherty, M. D., Mseeh, F., Polanuyer, B. M., Campbell, J. W., Anantha, S., Shatalin, K. Y., Chowdhury, S. A. K., Fonstein, M. Y., and Osterman, A. L. (2002) *Journal of Bacteriology* **184**, 4555-4572
32. Strauss, E., Zhai, H., Brand, L. A., McLafferty, F. W., and Begley, T. P. (2004) *Biochemistry* **43**, 15520-15533
33. Li, T., Huo, L., Pulley, C., and Liu, A. (2012) *Bioorganic Chemistry* **43**, 2-14
34. Thomas, J., and Cronan, J. E. (2010) *Antimicrobial Agents and Chemotherapy* **54**, 1374-1377
35. Choudhry, A. E., Mandichak, T. L., Broskey, J. P., Egolf, R. W., Kinsland, C., Begley, T. P., Seefeld, M. A., Ku, T. W., Brown, J. R., Zalacain, M., and Ratnam, K. (2003) *Antimicrobial Agents and Chemotherapy* **47**, 2051-2055
36. Paige, C., Reid, S. D., Hanna, P. C., and Claiborne, A. (2008) *Journal of Bacteriology* **190**, 6271-6275
37. Balibar, C. J., Hollis-Symynkywicz, M. F., and Tao, J. (2011) *Journal of Bacteriology* **193**, 3304-3312
38. Yang, K., Eyobo, Y., Brand, L. A., Martynowski, D., Tomchick, D., Strauss, E., and Zhang, H. (2006) *Journal of Bacteriology* **188**, 5532-5540
39. Brand, L. A., and Strauss, E. (2005) *Journal of Biological Chemistry* **280**, 20185-20188
40. Manoj, N., Strauss, E., Begley, T. P., and Ealick, S. E. (2003) *Structure* **11**, 927-936
41. Strauss, E., Kinsland, C., Ge, Y., McLafferty, F. W., and Begley, T. P. (2001) *Journal of Biological Chemistry* **276**, 13513-13516
42. Yao, J., Patrone, J. D., and Dotson, G. D. (2009) *Biochemistry* **48**, 2799-2806
43. Patrone, J. D., Yao, J., Scott, N. E., and Dotson, G. D. (2009) *Journal of the American Chemical Society* **131**, 16340-16341

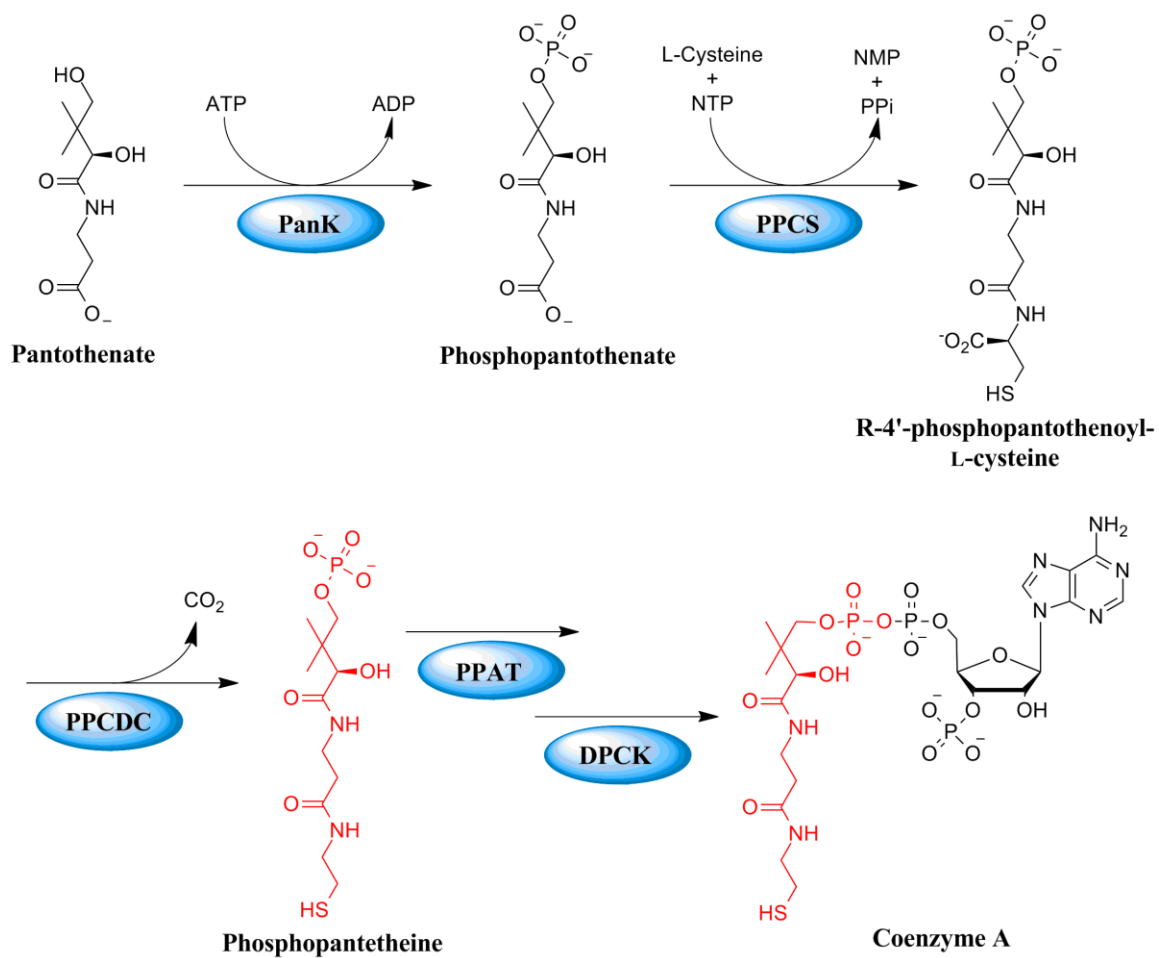
44. Patrone, J. D. (2010) Investigating Phosphopantothienoylcysteine Synthetase as a Potential Antibacterial Target. in *Medicinal Chemistry*, University of Michigan, College of Pharmacy
45. Yao, J. (2010) Exploring the Coenzyme A Biosynthetic Pathway as Novel Antibiotic Target. in *Medicinal Chemistry*, University of Michigan, College of Pharmacy
46. Stanitzek, S., Augustin, M. A., Huber, R., Kupke, T., and Steinbacher, S. (2004) *Structure* **12**, 1977-1988
47. Kupke, T. (2004) *European Journal of Biochemistry* **271**, 163-172
48. Majerus, P. W., Alberts, A. W., and Vagelos, P. R. (1965) *Proceedings of the National Academy of Sciences of the United States of America* **53**, 410-417
49. Johnson, M. N. R., Londergan, C. H., and Charkoudian, L. K. (2014) *Journal of the American Chemical Society* **136**, 11240-11243
50. Byers, D. M., and Gong, H. (2007) *Biochemistry and Cell Biology* **85**, 649-662
51. Marrakchi, H., Zhang, Y. M., and Rock, C. O. (2002) *Biochem Soc Trans* **30**, 1050-1055
52. White, S. W., Zheng, J., Zhang, Y.-M., and Rock, C. O. (2005) *Annual Review of Biochemistry* **74**, 791-831
53. Parsons, J. B., and Rock, C. O. (2011) *Current Opinion in Microbiology* **14**, 544-549
54. Heath, R. J., White, S. W., and Rock, C. O. (2001) *Progress in Lipid Research* **40**, 467-497
55. Heath, R. J., and Rock, C. O. (2004) *Current opinion in investigational drugs (London, England : 2000)* **5**, 146-153
56. Russell, A. D. (2004) *Journal of Antimicrobial Chemotherapy* **53**, 693-695
57. Yazdankhah, S. P., Scheie, A. A., Hoiby, E. A., Lunestad, B. T., Heir, E., Fotland, T. O., Naterstad, K., and Kruse, H. (2006) *Microb Drug Resist* **12**, 83-90
58. Jackman, J. E., Fierke, C. A., Tumey, L. N., Pirrung, M., Uchiyama, T., Tahir, S. H., Hindsgaul, O., and Raetz, C. R. H. (2000) *Journal of Biological Chemistry* **275**, 11002-11009
59. Raetz, C. R. H., and Whitfield, C. (2002) *Annual Review of Biochemistry* **71**, 635-700
60. Raetz, C. R. H., Reynolds, C. M., Trent, M. S., and Bishop, R. E. (2007) *Annual Review of Biochemistry* **76**, 295-329
61. Vuorio, R., and Vaara, M. (1992) *Antimicrobial Agents and Chemotherapy* **36**, 826-829
62. Vaara, M. (1993) *Antimicrobial Agents and Chemotherapy* **37**, 354-356
63. Nikaido, H. (2003) *Microbiology and Molecular Biology Reviews* **67**, 593-656
64. Meredith, T. C., Aggarwal, P., Mamat, U., Lindner, B., and Woodard, R. W. (2006) *ACS Chemical Biology* **1**, 33-42
65. McClerren, A. L., Endsley, S., Bowman, J. L., Andersen, N. H., Guan, Z., Rudolph, J., and Raetz, C. R. H. (2005) *Biochemistry* **44**, 16574-16583
66. Gay, N. J., and Gangloff, M. (2007) *Annual Review of Biochemistry* **76**, 141-165
67. Kim, H. M., Park, B. S., Kim, J.-I., Kim, S. E., Lee, J., Oh, S. C., Enkhbayar, P., Matsushima, N., Lee, H., Yoo, O. J., and Lee, J.-O. (2007) *Cell* **130**, 906-917
68. Beutler, B., and Cerami, A. (1988) *Annual Review of Biochemistry* **57**, 505-518

69. Poltorak, A., He, X., Smirnova, I., Liu, M.-Y., Huffel, C. V., Du, X., Birdwell, D., Alejos, E., Silva, M., Galanos, C., Freudenberg, M., Ricciardi-Castagnoli, P., Layton, B., and Beutler, B. (1998) *Science* **282**, 2085-2088
70. Visintin, A., Halmen, K. A., Latz, E., Monks, B. G., and Golenbock, D. T. (2005) *The Journal of Immunology* **175**, 6465-6472
71. Russell, J. A. (2006) *New England Journal of Medicine* **355**, 1699-1713
72. Lynn, M., Rossignol, D. P., Wheeler, J. L., Kao, R. J., Perdomo, C. A., Noveck, R., Ramon, V., D'Angelo, T., Gotzkowsky, S., and McMahon, F. G. (2003) *The Journal of Infectious Diseases* **187**, 631-639
73. Onishi, H. R., Pelak, B. A., Gerckens, L. S., Silver, L. L., Kahan, F. M., Chen, M.-H., Patchett, A. A., Galloway, S. M., Hyland, S. A., Anderson, M. S., and Raetz, C. R. H. (1996) *Science* **274**, 980-982
74. Vaara, M. (1996) *Science* **274**, 939-940
75. Anderson, M. S., Bulawa, C. E., and Raetz, C. R. (1985) *Journal of Biological Chemistry* **260**, 15536-15541
76. Jackman, J. E., Raetz, C. R. H., and Fierke, C. A. (1999) *Biochemistry* **38**, 1902-1911
77. Young, K., Silver, L. L., Bramhill, D., Cameron, P., Eveland, S. S., Raetz, C. R. H., Hyland, S. A., and Anderson, M. S. (1995) *Journal of Biological Chemistry* **270**, 30384-30391
78. Ogura, T., Inoue, K., Tatsuta, T., Suzaki, T., Karata, K., Young, K., Su, L.-H., Fierke, C. A., Jackman, J. E., Raetz, C. R. H., Coleman, J., Tomoyasu, T., and Matsuzawa, H. (1999) *Molecular Microbiology* **31**, 833-844
79. Kelly, T. M., Stachula, S. A., Raetz, C. R., and Anderson, M. S. (1993) *Journal of Biological Chemistry* **268**, 19866-19874
80. Galloway, S. M., and Raetz, C. R. (1990) *Journal of Biological Chemistry* **265**, 6394-6402
81. Jenkins, R. J., and Dotson, G. D. (2012) *ACS Chemical Biology* **7**, 1170-1177
82. Benson, R. E., Gottlin, E. B., Christensen, D. J., and Hamilton, P. T. (2003) *Antimicrobial Agents and Chemotherapy* **47**, 2875-2881
83. Barb, A. W., Jiang, L., Raetz, C. R. H., and Zhou, P. (2007) *Proceedings of the National Academy of Sciences of the United States of America* **104**, 18433-18438
84. Barb, A. W., Leavy, T. M., Robins, L. I., Guan, Z., Six, D. A., Zhou, P., Bertozzi, C. R., and Raetz, C. R. H. (2009) *Biochemistry* **48**, 3068-3077
85. Robins, L. I., Williams, A. H., and Raetz, C. R. H. (2009) *Biochemistry* **48**, 6191-6201
86. Sweet, C. R., Williams, A. H., Karbarz, M. J., Werts, C., Kalb, S. R., Cotter, R. J., and Raetz, C. R. H. (2004) *Journal of Biological Chemistry* **279**, 25411-25419
87. Sweet, C. R., Lin, S., Cotter, R. J., and Raetz, C. R. H. (2001) *Journal of Biological Chemistry* **276**, 19565-19574
88. Dotson, G. D., Kaltashov, I. A., Cotter, R. J., and Raetz, C. R. H. (1998) *Journal of Bacteriology* **180**, 330-337
89. Wyckoff, T. J. O., and Raetz, C. R. H. (1999) *Journal of Biological Chemistry* **274**, 27047-27055

90. Odegaard, T. J., Kaltashov, I. A., Cotter, R. J., Steeghs, L., van der Ley, P., Khan, S., Maskell, D. J., and Raetz, C. R. H. (1997) *Journal of Biological Chemistry* **272**, 19688-19696
91. Pfitzner, U., Raetz, C. R. H., and Roderick, S. L. (1995) *Proteins: Structure, Function, and Bioinformatics* **22**, 191-192
92. Raetz, C. R. H., and Roderick, S. L. (1995) *Science* **270**, 997-1000
93. Röttig, A., and Steinbüchel, A. (2013) *Microbiology and Molecular Biology Reviews* **77**, 277-321
94. Ulaganathan, V., Buetow, L., and Hunter, W. N. (2007) *Journal of Molecular Biology* **369**, 305-312
95. Allison, H. W., and Raetz, C. R. H. (2007) *Proceedings of the National Academy of Sciences of the United States of America* **104**, 13543-13550
96. Jenkins, R. J. (2013) Phage Display as a Tool for Probing Lipid A Biosynthesis. in *Medicinal Chemistry*, University of Michigan, College of Pharmacy
97. Bartling, C. M., and Raetz, C. R. H. (2009) *Biochemistry* **48**, 8672-8683
98. Cohen, M. L. (1992) *Science* **257**, 1050-1055
99. Neu, H. C. (1992) *Science* **257**, 1064-1073
100. Clatworthy, A. E., Pierson, E., and Hung, D. T. (2007) *Nat Chem Biol* **3**, 541-548
101. Jansen, P. A. M., Hermkens, P. H. H., Zeeuwen, P. L. J. M., Botman, P. N. M., Blaauw, R. H., Burghout, P., van Galen, P. M., Mouton, J. W., Rutjes, F. P. J. T., and Schalkwijk, J. (2013) *Antimicrobial Agents and Chemotherapy* **57**, 4794-4800
102. Zhang, Y.-M., White, S. W., and Rock, C. O. (2006) *Journal of Biological Chemistry* **281**, 17541-17544



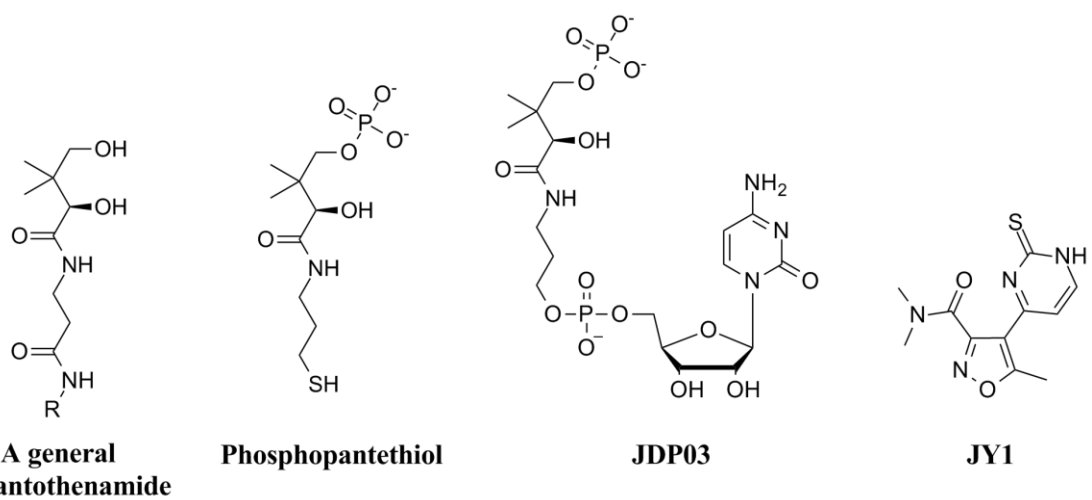
**Figure 1.1:** Structures of essential biomolecules pantothenate, phosphopantetheine, coenzyme A, and acyl carrier protein.



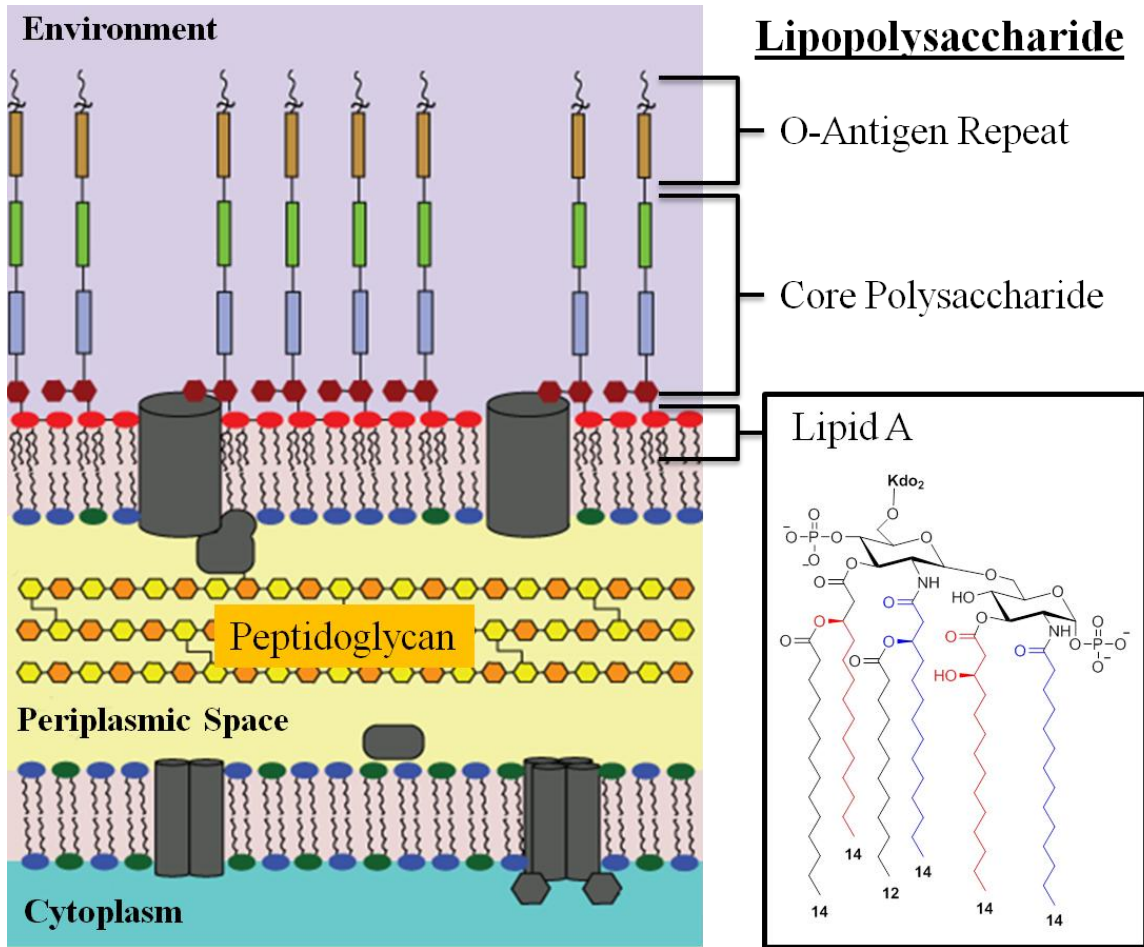
**Figure 1.2:** Biosynthetic pathway of coenzyme A. The five constitutively conserved enzymes are highlighted in blue. Essential biomolecule phosphopantetheine is in red.



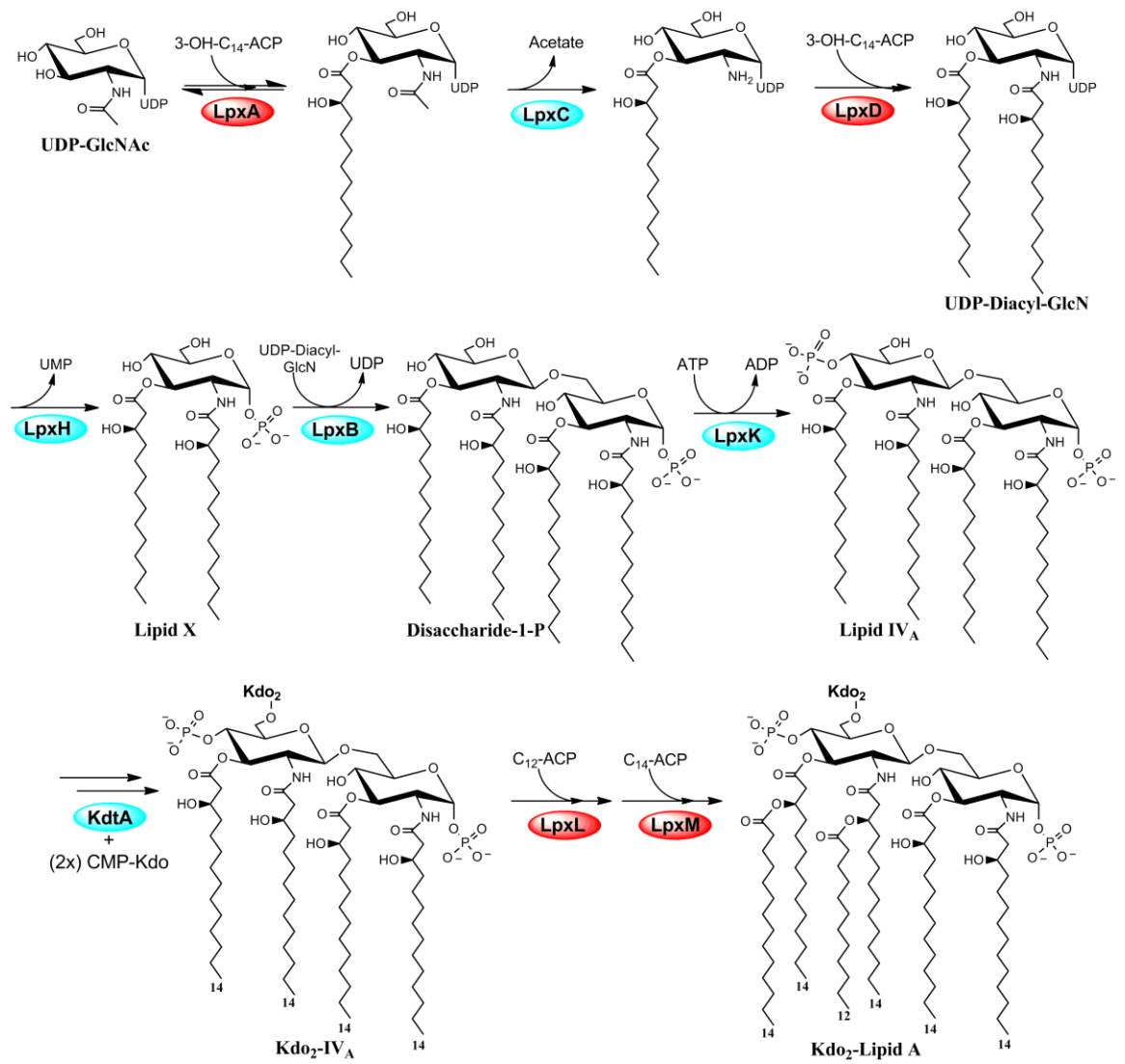




**Figure 1.4:** Selected CoA biosynthetic pathway inhibitors. Phosphopantethiol is a phosphopantothenate mimic (44). JDP03 is a PPCS cytidylate intermediate mimic (44). JY1 is SPB03328, a high throughput screen hit that inhibits PPCS (45).



**Figure 1.5:** The outer membrane of gram-negative bacteria. The lipid A scaffold of *Escherichia coli* is shown in the insert.



**Figure 1.6:** Biosynthesis of lipopolysaccharide.

## Chapter 2

### Activity of the Conserved Residues of *Streptococcus pneumoniae*

#### Phosphopantothenoylcysteine Synthetase

##### Background

Phosphopantetheine is an essential biomolecule that is incorporated as the reactive moiety into several cofactors required in life sustaining processes, including Coenzyme A and the prosthetic group on acyl carrier protein (1-3). Phosphopantothenoylcysteine synthetase (PPCS; EC 6.3.2.5; *coaB*) incorporates the reactive thiol of 4'-phosphopantetheine in a two step reaction, creating a nucleotide activated intermediate followed by a cysteine condensation (**Figure 2.1**). Following cysteine decarboxylation by phosphopantothenoylcysteine decarboxylase (PPCDC; EC 4.1.1.36; *coaC*), 4'-phosphopantetheine is produced. PPCS is found in nature in three types. Most bacteria express Type 1 PPCS as a bifunctional PPCS-PPCDC which exclusively utilizes CTP in the activation step. Higher eukaryotes, including humans, express a monofunctional Type 2 PPCS with a much larger nucleotide binding pocket, allowing for ATP to be utilized as well as CTP in the activation step. *Streptococcus pneumoniae* and *Enterococcus faecalis* express Type 3 monofunctional PPCS that utilizes CTP in a manner similar to that of Type 1 PPCS. The essential nature of phosphopantetheine and different types of PPCS within the Coenzyme A pathway between humans and bacteria make the pathway an intriguing target for antimicrobial development (4,5).

Mutagenesis studies of *E. coli* Type 1 PPCS revealed that point mutations N210D and K289Q led to a complete loss of phosphopantothenoylcysteine synthesis (6). HPLC-based assays of the N210D mutant revealed that the protein utilized all available phosphopantothenate and produce cytidylate intermediate. Thus, Asp210 was determined to mediate the second half cysteine condensation, as mutation of this residue prevents the formation of phosphopantothenoylcysteine (7). From the HPLC-based assay, PPCS(K289Q) appeared to have no activity, as no detectable products were present. This would indicate that Lys289 is key to the first step substrate activation. Crystal structures of *E. coli* PPCS(N210D) with substrates revealed that Lys289 contacts the  $\gamma$ -phosphate oxygen atoms of CTP (8).

*In vitro* inhibitors of PPCS have been constructed and characterized by our group. Cytidylate intermediate mimics of PPCS have been synthesized and characterized as slow on-set, tight-binding inhibitors (9). Phosphopantothenate analogs have also been constructed, with phosphopantothenthioi determined to be a phosphopantothenate-competitive inhibitor of *E. coli* PPCS with a low  $\mu\text{M}$   $K_i$  (10). Additionally, *S. pneumoniae* PPCS has previously been screened by our group against 41,000 compounds at the University of Michigan Center for Chemical Genomics. The screening process provided isoxazole-containing compounds that offer low  $\mu\text{M}$  inhibition of the monofunctional PPCS *in vitro* but have limited *in vivo* efficacy (11). To safely and rapidly evaluate Type 3 PPCS *in vivo*, the knockout strain *E. coli* MG1655::*ApanC,AcoaBC::KanR* was developed. By complementation of the knockout via a transformed low copy number plasmid carrying *coaB* and *coaC* genes, *S. pneumoniae* and *E. faecalis* PPCS proteins could be tested *in vivo* in a system with

controlled levels of cellular pantothenate. Herein, we discuss the development of the knockout strain *MGI655::ΔpanC,ΔcoaBC::KanR*, and the parameters of its growth when complemented with *coaBC* from other organisms.

Currently, there is structural data for Type 1 *E. coli* PPCS, but no crystal structure of Type 3 *S. pneumoniae* PPCS. In order to utilize *E. coli* bifunctional PPCS structural/functional model for *S. pneumoniae* monofunctional PPCS highly conserved proposed active site residues were mapped for both monofunctional and bifunctional PPCS. Multiple sequence alignment of several monofunctional and bifunctional PPCS enzymes revealed several highly conserved residues. These residues also matched residues of high catalytic importance in the *E. coli* PPCS crystal structure. We propose that residues critical for monofunctional PPCS catalysis and specificity for CTP and cysteine are conserved between mono and bifunctional bacterial PPCS. Site-directed mutagenesis was first performed on specific catalytic residues of *E. coli* PPCS as well as at the corresponding sites of *S. pneumoniae* PPCS. Using the developed *in vivo* model system, these mutations were found to have matching phenotypes across *E. coli* and *S. pneumoniae* PPCS, suggesting a validation of our sequence alignment and that the active site of *E. coli* PPCS should share structural similarity. Saturation mutagenesis was then performed on *S. pneumoniae* PPCS at highly conserved residues in order to identify those residues responsible for the substrate recognition and activity of the protein. Through kinetic characterization of active mutants, we were able to elucidate residues vital to the activity of the protein, giving a chemical-biological basis for interactions of previously discovered small molecule inhibitors of PPCS.

## Materials and Methods

*Materials.* All chemicals were used as purchased from Acros, Fisher, Fluka, Sigma-Aldrich, or Specialty Chemicals Ltd. and used without further purification unless otherwise noted. The Mono Q 5/50 GL, Source 15Q, Source 15S, and Superdex 200 resin and columns were purchased from GE Healthcare. Bio-Gel P2 resin was from Bio-Rad. Ni-NTA resin was from Qiagen. Additionally, Qiagen minispin kits were used for DNA purification and cleanup. Ammonium molybdate, ampicillin, L-arabinose, calcium pantothenate, chloramphenicol, L-cysteine, cytidine triphosphate, dithiothreitol, formic acid, concentrated hydrochloric acid, HEPES, imidazole, bacterial inorganic pyrophosphatase, isopropyl  $\beta$ -D-1-thiogalactopyranoside, kanamycin, magnesium chloride, magnesium sulfate, malachite green carbinol hydrochloride, methanol, D-pantethine, pyrophosphate reagent, sodium chloride, sodium hydroxide, sodium pyrophosphate, and Tris HCl, and were purchased from Sigma-Aldrich. Luria-Bertani agar and broth were from Difco. DNA restriction and ligation enzymes and associated reagents were from New England Biolabs. BL21(DE3) *Escherichia coli* cells was purchased from Invitrogen and XL-1 Blue *E. coli* cells were from Stratagene. 384-well polystyrene nonbinding surface plates and 96-well half-area polystyrene nonbinding surface plates were purchased from Corning. Phosphopantetheine was synthesized as previously reported (12). DNA sequencing was performed by the University of Michigan DNA Sequencing Core facility.

*Generating double knockout E. coli  $\Delta$ PanC, $\Delta$ coaBC::*Kan*<sup>R</sup>.* Using P1 phage transduction and our lab's previously generated *E. coli* MG1655  $\Delta$ dfp (coaBC)::*Kan*<sup>R</sup> and *E. coli* MG1655  $\Delta$ PanC::*Kan*<sup>R</sup> mutant knockout strains, a double knockout *E. coli*

*ΔPanC,ΔcoaBC::Kan<sup>R</sup>* strain, designated KH100, was developed (11,13). The temperature sensitive, ampicillin resistance pCP20 vector was transformed into the *ΔPanC::Kan<sup>R</sup>* strain and induced to express a yeast FLP recombinase. Successful recombinants were selected for based on loss of kanamycin resistance and retention of ampicillin resistance selection of pCP20. The plasmid was then removed upon incubation at 42 °C overnight, with loss of vector selected for based on sensitivity to ampicillin. This afforded a *ΔPanC E. coli* strain with no kanamycin resistance that would become the “recipient strain.” Next, P1vir was transduced into the *ΔcoaBC::Kan<sup>R</sup>* “donor strain” by adding 100 μl of 10<sup>9</sup> pfu/ml P1vir to the donor strain growing logarithmically at 37 °C in 5 mL of LB broth containing 0.2% glucose, 100 μM pantetheine and 5 mM CaCl<sub>2</sub>. The culture was incubated for 3 hours at 4 °C until lysis occurred, then the remaining bacteria were killed by the addition of a few drops of CHCl<sub>3</sub> and cellular debris was removed by differential centrifugation. The supernatant containing P1 lysate was stored at 4 °C until use. The *ΔPanC* recipient strain was incubated overnight at 37 °C then 1.5 mL of culture was pelleted and resuspended in 10 mM CaCl<sub>2</sub>/5 mM MgSO<sub>4</sub>. The cells were then mixed with various amounts of the P1 lysate and incubated at room temperature for 30 minutes for phage absorption. The mixtures were then incubated for 1 hour at 37 °C in LB broth containing 200 mM sodium citrate, then plated onto LB plates containing 30 μg/ml kanamycin, 100 μM pantetheine and 5 mM sodium citrate. The plates were incubated overnight at 37 °C, and the plate with the least amount of P1 phage growth, single colonies were streaked onto kanamycin, pantetheine, sodium citrate plates and incubated overnight at 37 °C to remove infective phage. Surviving streaks were then screened for kanamycin resistance and loss of *dfp* (*coaB-coaC*) based on requirement of pantetheine



for growth. Selection screening for growth in the presence of pantetheine and kanamycin, but no growth on media not supplemented with panthetheine resulted in the appropriate phenotype of the  $\Delta PanC, \Delta coaBC::Kan^R$ .

*Cloning of E. coli, E. faecalis, and S. pneumoniae coaBC.* PCR protocols were carried out under standard conditions utilizing *Pfu* DNA Polymerase and DNA obtained from *E. coli* (MG1655), *E. faecalis* (ATCC 700802), and *S. pneumoniae* (TIGR4) and the primers listed in **Table 2.1**. The *coaBC* domains for *E. coli* and *S. pneumoniae* were amplified and cloned into pUMRJ100 using *NdeI* and *HindIII* restriction sites. *E. faecalis coaBC* was amplified and cloned into pUMRJ100 using *NaeI* and *NdeI* restriction sites. The pUMRJ100 plasmid was chosen because it is low copy, L-arabinose inducible, and contains *Cam<sup>R</sup>* for additional chloramphenicol (Cam) resistance selection. Plasmids were transformed into *E. coli* XL-1 Blue cells for amplification. Genetic integrity of plasmids isolated from the cell lines was confirmed by sequencing at the University of Michigan Sequencing Core Facility. The vectors were then transformed into the double knockout cell line and plated onto LB media containing Cam and 1% L-arabinose to create the following strains: KH100/pUMRJ100/*E. coli coaBC*, KH100/pUMRJ100/*E. faecalis*, and KH100/pUMRJ100/*S. pneumoniae coaBC*. Colony growth on unsupplemented LB media proved the functional expression of *coaB* and *coaC* were able to recover the conditionally lethal *coaBC* knockout.

*Growth studies of complemented E. coli  $\Delta PanC, \Delta coaBC::Kan^R$ .* Plasmids containing *coaBC* on arabinose inducible pUMRJ100 were transformed into KH100 cells made chemically competent. Starter cultures (5 mL) of KH100/pUMRJ100/*coaBC* strains in LB (Lennox) containing 100  $\mu$ M pantothenate were allowed to grow overnight at 37

°C. The following day, cells were pelleted by centrifugation at 5000 x g, 4 °C and resuspended in 5 mL fresh minimal salts (Difco) three times in order to remove residual pantothenate. Cell suspensions were then diluted to an OD<sub>600</sub> of 0.01 in 150 ml fresh media that was a 1:1 mixture of minimal salts:pantothenate free media (Difco). These cultures we incubated with aeration at 37 °C for 24 hours. During incubation, 1 ml fractions were removed from each culture and evaluated for absorbance at  $\lambda = 600$  nm.

*Cloning and expression of E. coli, E. faecalis, and S. pneumoniae PPCS.* PCR protocols were carried out under standard conditions utilizing Pfu DNA Polymerase and DNA obtained from *E. coli* (MG1655), *E. faecalis* (ATCC 700802), and *S. pneumoniae* (TIGR4). The *coaB* gene for each bacteria was amplified and cloned into pET23a using *NdeI* and *XhoI* restriction sites and the primers listed in **Table 2.2**. Plasmids were transformed into *E. coli* XL-1 Blue cells for amplification. Genetic integrity of plasmids isolated from the cell lines was confirmed by sequencing at the University of Michigan Sequencing Core Facility. For protein expression, vectors were transformed into BL21-AI, to make the following strains: BL21-AI/pET23a::*E.coli coaB*, BL21-AI/pET23a::*E.faecalis coaB*, BL21-AI/pET23a::*S/ pneumoniae coaB-his<sub>6</sub>* and BL21-AI/pET23a::*S. pneumoniae coaB*. The strains were used to inoculate 500 ml LB (Lennox) media containing 50 µg/ml ampicillin. The culture was incubated at 37 °C with vigorous shaking (250 rpm) until the optical density at 600 nm reached ~0.6. The cultures were induced with 0.2% L-arabinose/1 mM IPTG and allowed to incubate at 37 °C for 4 hours post-induction. Cultures were then cooled and harvested by centrifugation at 5,000 x g, 4 °C for 10 minutes. Cells were resuspended in 10 mL of 10% glycerol, 20 mM HEPES pH 8.0 and stored at -80 °C.

*Purification of E. coli PPCS.* Cell suspension strain BL21-AI/pET23a::*E. coli coaB* was thawed then disrupted by French press at 20,000 psi and the insoluble debris was removed by centrifugation at 20,000 x g, 4 °C for 30 minutes. The resulting crude cytosol (supernatant) was filtered through a 20 micron Millipore syringe filter and then loaded onto a tandem anion exchange column (Source 15Q (GE healthcare); 20 ml) and cation exchange column (Source 15S (GE healthcare); 8 mL) pre-equilibrated in 20 mM HEPES pH 8.0. The column was washed with 3 column volumes (84 mL) of 20 mM HEPES pH 8.0. The anion exchange column was removed and purified *E. coli* PPCS was eluted with a linear gradient of 0-400 mM NaCl in 20 mM HEPES pH 8.0, with a total gradient volume of 80 mL. *E. coli* PPCS elutes as a single peak around 75 mM NaCl and was determined to be greater than 98% pure by SDS-PAGE. Fractions were combined desalted with Bio-Gel P2 column and concentrated using a Centricon 10,000 MW cutoff centrifugal filter unit and protein concentration was determined by absorbance at  $\lambda = 280$  nm ( $\epsilon_{280} = 13,075 \text{ M}^{-1} \text{ cm}^{-1}$ ).

*Purification of E. faecalis PPCS.* Cell suspension strain BL21-AI/pET23a::*E. faecalis coaB* was thawed then disrupted by French press at 20,000 psi and the insoluble debris was removed by centrifugation at 20,000 x g, 4 °C for 30 minutes. The resulting crude cytosol (supernatant) was filtered through a 20 micron Millipore syringe filter and then loaded onto an anion exchange column (Source 15Q (GE healthcare); 8 ml) pre-equilibrated in 20 mM HEPES pH 8.0. The column was washed with 3 column volumes (24 mL) of 20 mM HEPES pH 8.0. Purified *E. faecalis* PPCS was eluted with a linear gradient of 0-500 mM NaCl in 20 mM HEPES pH 8.0, with a total gradient volume of 80 mL. Fraction were analyzed by SDS-PAGE and fractions containing PPCS were pooled

and passed through a 320 mL Superdex 200 prep grade column equilibrated in 20 mM HEPES pH 8.0 containing 150 mM NaCl. Purified fractions were desalted with Bio-Gel P2, subsequently concentrated using a Centricon 10,000 MW cutoff centrifugal filter unit and protein concentration was determined by absorbance at  $\lambda = 280 \text{ nm}$  ( $\epsilon_{280} = 28,415 \text{ M}^{-1} \text{ cm}^{-1}$ ).

*Purification of his<sub>6</sub> tagged S. pneumoniae PPCS.* Cell suspensions were thawed and disrupted by French press at 20,000 psi and the insoluble debris was removed by centrifugation at 20,000 x g, 4 °C for 30 minutes. The resultant crude cytosol was applied to a 2 ml Nickel column (Qiagen), equilibrated with 50 mM Imidazole, 20 mM HEPES pH 8.0. The column was washed with 5 column volumes of 500 mM NaCl, 50 mM Imidazole, 20 mM HEPES pH 8.0 followed by 3 column volumes of 50 mM Imidazole, 20 mM HEPES pH 8.0. Histidine tagged enzyme was eluted from the column with 5 column volumes of 250 mM Imidazole, 20 mM HEPES pH 8.0. The enzyme was then loaded onto a 2 ml Source 15Q column, washed with 3 column volumes of 20 mM HEPES pH 8.0 and eluted over a gradient of 0-500 mM NaCl. Purified PPCS was desalted on a Bio-Gel P2 column and analyzed by SDS-PAGE. Protein concentrations were determined by UV absorbance at  $\lambda = 280 \text{ nm}$  ( $\epsilon_{280} = 12,950 \text{ M}^{-1} \text{ cm}^{-1}$ ).

*Purification of untagged S. pneumoniae PPCS.* Cell suspension strain BL21-AI/pET23a::S. pneumoniae coaB was thawed then disrupted by French press at 20,000 psi and the insoluble debris was removed by centrifugation at 20,000 x g, 4 °C for 30 minutes. The resulting crude cytosol (supernatant) was filtered through a 20 micron Millipore syringe filter and then loaded onto a tandem cation exchange column (Source 15S (GE healthcare); 8 mL) and anion exchange column (Source 15Q (GE healthcare); 8

ml) pre-equilibrated in 20 mM HEPES pH 8.0. The column was washed with 3 column volumes (48 mL) of 20 mM HEPES pH 8.0. The cation exchange column was removed and protein was eluted from the anion exchange column with a linear gradient of 0-500 mM NaCl in 20 mM HEPES pH 8.0, with a total gradient volume of 80 mL. Fractions were analyzed by SDS-PAGE, and those containing PPCS were collected, pooled, and concentrated to 2 mL using a Centricon 10,000 MW cutoff centrifugal filter unit. The protein was passed through a 320 mL Superdex 200 prep grade column equilibrated in 20 mM TrisHCl pH 7.6 containing 10 mM NaCl. Fractions containing *S. pneumoniae* PPCS were combined concentrated using a Centricon 10,000 MW cutoff centrifugal filter unit to a protein concentration of 15 mg/mL. Protein concentration was determined by absorbance at  $\lambda = 280 \text{ nm}$  ( $\epsilon_{280} = 13,075 \text{ M}^{-1} \text{ cm}^{-1}$ ).

*Site directed mutagenesis.* Site-directed mutagenesis was performed on the conserved catalytic residues determined by the multiple sequence alignment of bacterial PPCSs. The general method of mutagenesis followed that of the Quick Change Site-directed Mutagenesis kit (Agilent) by using methylated plasmid DNA as a template. PRC amplification of the entire plasmid was performed using pUMKH7 (the vector containing the *S. pneumoniae coaBC* coding region) or pUMKH5 (the vector containing the *E. coli coaBC* coding region) as a template, and complementary primers (**Table 2.2**). The resultant mixture was then *DpnI* restriction digested which degraded all methylated plasmid. As pUMRJ100 has been introduced to bacteria, it will contain a dam methylated GATC site while the desired mutated DNA will not. The resultant plasmid was then transformed into *E. coli XLI*, which repaired nicks in the mutated plasmid and allowed for

amplification. The resultant plasmids were sequenced to verify that they contained the introduced mutations.

*Saturation mutagenesis and mutant selection criteria.* Saturation mutagenesis was performed on selected conserved *S. pneumoniae* PPCS residues using NNK/MNN codon containing primers **Table 2.3**. PCR amplification of the pUMKH8 vector was performed under standard protocol with *Pfu* polymerase and the primers containing low-fidelity codons. In this process, the entire *coaBC* vector was PCR amplified, creating a pool of vectors containing a wide range of mutations at the single selected residue. This vector pool was transformed directly into the knockout strain KH100 and plated onto media containing 250  $\mu$ M pantethine, allowing for the growth of all non-toxic mutations. Resultant colonies were streaked onto media with and without 250  $\mu$ M pantethine in order to determine the growth phenotype (i.e. whether the mutation no longer was able to support growth without the addition of environmental pantethine). Plasmids were also isolated from these colonies and the specific point mutation was determined by sequencing at the University of Michigan Sequencing Core Facility.

Mutants that were able to sustain cell growth under no pantethine conditions in the knockout model had their *coaB* (i.e. PPCS) domain PCR amplified and inserted into the pET23a vector following an *NdeI*. *XhoI* restriction enzyme digests. This vector was amplified in the XL1-Blue cell line and the sequence was verified at the University of Michigan Sequencing core. The vector was then transformed into the BL21-AI cell line and *his*-tagged protein expression and purification was performed as previously described (follows the *S. pneumoniae* PPCS-*his*<sub>6</sub> protocol).

*Pyrophosphatase assay.* The forward reaction of PPCS was monitored in real-time through utilization of commercially available Pyrophosphate Reagent (Sigma Aldrich), coupling the PPCS production of pyrophosphatase with the oxidation of NADH, monitored by disappearance of absorption  $\lambda = 340$  nm. In UV-visible 96-well half-area plates (Costar UV), 30  $\mu$ L PR, an additional 1 U PPI-PFK, 10 mM DDT, and varying concentrations of cysteine, magnesium chloride, phosphopantetheine, and cytidine triphosphate, were incubated at 37 °C in a final volume of 70  $\mu$ L, buffered with 50 mM Tris-HCl pH 7.6. After 10 minutes, 30  $\mu$ L PPCS in 50 mM Tris-HCl pH 7.6 (pre-incubated at 37 °C) was added and absorbance readings were taken at  $\lambda = 340$  nm for 10 minutes using a SpectraMax M5. Activity of the enzyme was calculated by adjusting for pathlength (0.5 cm) and taking into account that each mole of pyrophosphate produced leads to the oxidation of 2 moles NDAH. Assays were run in triplicate, with average velocities reported.

*Malachite green assay.* Varying concentrations of the mutants and wild-type *S. pneumoniae* PPCS (5.0  $\mu$ M, 2.5  $\mu$ M, 1.0  $\mu$ M, and 0.5  $\mu$ M) we incubated for 15 minutes at 37 °C in 50  $\mu$ M CTP, 50  $\mu$ M MgCl<sub>2</sub>, 150  $\mu$ M phosphopantetheine, 150  $\mu$ M cysteine, 150  $\mu$ M DTT, 20 mM HEPES pH 8.0 in a final volume of 40  $\mu$ L. The reaction was quenched with 40  $\mu$ L malachite green reagent (0.1125% malachite green carbinol hydrochloride, 2.1% ammonium molybdate, in 3 M hydrochloride), allowed to sit at room temperature for 5 minutes, then read at 600 nm in a SpectraMax M5.

*Eikonogen assay.* Metal dependence and pH experiments were performed using the Eikonogen assay, which allows for the direct quantification of pyrophosphate produced from the PPCS reaction. The reaction was quenched by the addition of 50  $\mu$ L of

2.5% w/v ammonium molybdate in 5 N sulfuric acid, followed by the addition of 50  $\mu\text{L}$  of 0.5 M  $\beta$ -mercaptoethanol and 20  $\mu\text{L}$  of Eikonogen solution. The mixture was incubated at 37  $^{\circ}\text{C}$  for 10 minutes, and then absorbance at 580 nm was read to quantify the amount of pyrophosphate produced ( $\epsilon_{580} = 25,000 \text{ M}^{-1} \text{ cm}^{-1}$ ).

## Results and Discussion

*Growth studies of genetically complemented coaBC knockout strain.* Using P1 phage transduction and our lab's previously generated *E. coli* MG1655  $\Delta dfp$  (*coaBC*::*Kan*<sup>R</sup> and *E. coli* MG1655  $\Delta PanC$ ::*Kan*<sup>R</sup> mutant knockout strains, a double knockout *E. coli*  $\Delta PanC, \Delta coaBC$ ::*Kan*<sup>R</sup> strain, designated KH100, was developed. The *dfp* gene is the monofunctional *coaB-coaC* gene in *E. coli*, and thus this knockout allows for the replacement of the *coaB* and *coaC* genes via a transformed vector's expression. The *PanC* knockout allows for the control of cellular pantothenate levels as *de novo* pantothenate synthesis is halted and only environmental pantothenate will be utilized (14,15). Growth rates of pantothenate complemented KH100 are charted in **Figure 2.2**. At concentrations below 250  $\mu\text{M}$  pantothenate, the double knockout exhibited a very long lag phase before entering a much slower logarithmic phase. At concentrations of 250  $\mu\text{M}$  pantothenate and above, KH100 grows at the same rate as wild-type *E. coli* MG1655. Very high concentrations of pantothenate (10 mM) were determined to not be inhibitory to the growth of the double knockout strain.

The genetically complemented *E. coli* model systems were characterized by growth rate in a variety of environments, including analysis of the effects of L-arabinose, dextrose, and pantothenate concentrations on growth. Interestingly, the pUMRJ100



plasmid appears to have loose enough regulation to allow for the expression of *coaB-coaC* to levels necessary for survival, as knockouts containing each vector still grew under high dextrose, no L-arabinose conditions – a scenario which should normally limit the expression of the vector. **Figure 2.3** shows growth curves for the genetically complemented *E. coli*. Growth rates of the genetically complemented knockout strains to wild type MG1655 were comparable.

*Using the knockout system to test MIC of inhibitors.* In a proof of concept experiment, the double knockout model system KH100 was utilized in an MIC study against compound JY1 (ChemDiv SPB03328), the small molecule isoxazole discovered to inhibit PPCS in a previous high throughput screen (11). In an overnight study, the MIC50 for JY1 against *E. coli*, *E. faecalis*, and *S. pneumoniae* complemented double knockout was determined to be approximately 300 µg/ml (**Figure 2.4**). This shows that the compound is able to inhibit the growth of the complemented double knockouts *in vivo* in a concentration dependent manner.

Further, a disc diffusion experiment was performed with JY1 against *S. pneumoniae coaBC* complemented KH100 and *E. coli ΔtolC* to give a more visual representation of the inhibitory activity of JY1 (**Figure 2.5**). With dextrose present to suppress plasmid expression, JY1 exhibited a zone of inhibition against both the supplemented knockout and *ΔtolC* cell line at 150 and 300 µg JY1. The addition of 100 µM pantethine provided an environmental source of pantetheine for the knockout, and limited the zone of inhibition caused by JY1, indicating that antimicrobial activity of JY1 is due to PPCS inhibition, further verifying the enzyme as a therapeutic target. In this manner, it would be possible to utilize KH100 in whole cell screens for antimicrobial

inhibitors of PPCS-PPCDC. The ability to rescue the knockout strain with pantetheine adds the element of rapid target validation.

*Multiple sequence alignment.* To determine which residues are conserved among bacterial PPCS, several known bifunctional PPCS sequences were aligned with those of the three known bacterial monofunctional PPCS (Type 3) expressed in *S. pneumoniae*, *E. faecalis*, and *Bacillus anthracis*. Based on the moderate sequence homology of the proteins, it was possible to construct the alignment and quickly determine which residues are conserved and to what extent (**Figure 2.6**). A handful of residues were completely conserved across bacterial PPCS, including the N210 and K289 residues that were previously found to be essential to the catalytic activity of PPCS (6).

In order to examine these residues in a structural sense they were mapped onto the *E. coli* PPCS structure, which was the only structure solved for bacterial PPCS. **Figure 2.7** shows the alignment of residues of the putative pockets of PPCS, and **Figure 2.8** shows these residues mapped onto the native *E. coli* crystal structure. Residues in *E. coli* that form the putative oxyanion hole, the divalent metal binding residue, and the CTP alpha phosphate binding residue (Asn210, Asp279, and Lys289 respectively) are highly conserved across all PPCS. Residues that make binding contacts with a divalent metal ion and the CTP alpha phosphate, important in the first half reaction of PPCS, are also conserved (6). While Gly214 and Lys385 in the phosphopantothenate phosphate binding pocket are conserved across all bacterial PPCS, residues Ser212 and Ser213 are not conserved in the monofunctional enzymes. However, the activity of conserved residues between the mono and bifunctional enzymes remained to be determined.

*In vivo model system for the evaluation of monofunctional PPCS.* In order to quickly evaluate the viability of sited-directed mutants of *S. pneumoniae* PPCS, a model system needed to be established. Using *E. coli* as the model organism would also confirm the validity of assumptions made from the multiple sequence alignment and the crystal structure of *E. coli* PPCS. By performing site directed mutagenesis on *coaB* of the *coaB-coaC* containing vectors and transforming them into the double knockout KH100 strain, genetic mutants could be screened very quickly for their ability to support growth in a pantothenine-free environment.

In a proof of concept experiment, vectors for *E. coli* PPCS(N210D)-PPCDC, PPCS(K289Q)-PPCDC, and PPCS(S212A)-PPCDC were generated. As mentioned earlier, Kupke identified the PPCS(N210D) mutation in *E. coli* as inactivating the first step cysteine condensation of PPCS (16). Additionally, the *E. coli* PPCS(K289Q) mutation inactivates the first step reaction, causing a build-up of phosphopantothenoyl cytidylate (16). The *E. coli* PPCS(S212A) mutation had no effect on catalysis and was selected as a control. These vectors were each separately transformed into KH100 and streaked onto media with and without pantothenine. As expected, both *E. coli* PPCS(N210D)-PPCDC and PPCS(K289Q)-PPCDC resulted in a lethal phenotype without the presence of environmental pantothenine (**Figure 2.9**). This experiment was repeated with *S. pneumoniae* PPCS vectors PPCS(N22D)-PPCDC, PPCS(S24A)-PPCDC, and PPCS(K123Q)-PPCDC (which align with *E. coli* PPCS mutations N210D, S212A, and K289Q). These vectors were also transformed into KH100 and streaked onto media with and without pantothenine. *S. pneumoniae* PPCS(N22D)-PPCDC and PPCS(K123Q)-PPCDC expressed lethal phenotypes without the presence of

environmental pantethine. The matched phenotype of these point mutations in *E. coli* Type 1 PPCS and *S. pneumoniae* Type 3 suggest that these residues perform similar enzymatic roles. Initial mutagenesis performed on both *E. coli coaB-coaC* and *S. pneumoniae coaB-coaC* determined previously characterized mutations in *E. coli* PPCS have the same effect in the context of the bifunctional enzyme and the monofunctional enzyme. With a functioning model system, saturation mutagenesis could then be performed in *S. pneumoniae* for *in vivo* phenotypic evaluation of the mutants.

To determine if *S. pneumoniae* PPCS residue is responsible for the second half cysteine condensation (as it is in *E. coli*), *S. pneumoniae* PPCS(N22D), PPCS(S24A), and PPCS(K123Q) were overexpressed and purified. Varying concentrations of the mutant and wild-type *S. pneumoniae* PPCS (5.0  $\mu$ M, 2.5  $\mu$ M, 1.0  $\mu$ M, and 0.5  $\mu$ M) were assayed using the malachite green dye to calculate the pyrophosphate released in the first half of the PPCS reaction (**Figure 2.1**). Wild-type *S. pneumoniae* PPCS produced approximately 10  $\mu$ M pyrophosphate regardless of the amount of enzyme in the assay, which would mean that the wild-type PPCS would have to perform multiple turnovers in order to produce more pyrophosphate than enzyme present (**Figure 2.10**). PPCS(S24A) produced approximately the same amount of pyrophosphate as the wild-type enzyme, further suggesting that the S22 residues doesn't play a major role in catalysis. PPCS(K123Q) produced no pyrophosphate regardless of the amount of enzyme present, further verifying that the K123Q mutant completely inactivates *S. pneumoniae* PPCS as the first half reaction did not occur. PPCS(N22D) produced an amount of pyrophosphate roughly equivalent to the amount of enzyme present in the assay. This approximately 1:1 molar ratio of PPCS(N22D) present:pyrophosphate produced suggests a that each PPCS mutant

was able to perform a single turnover of the first half reaction. This would match with previous mutagenesis studies with *E. coli* PPCS(N210D), wherein PPCS(N210D) was able to produce the cytidylate intermediate but not phosphopantethoylecysteine (16). While not as robust at an HPLC aggregate study, this assay gave a quick indication that *S. pneumoniae* PPCS(N22D) could perform enough activity to produce some pyrophosphate, but not enough to complement the *in vivo* double knockout system.

*Saturation mutagenesis of highly conserved bacterial PPCS residues.* To continue investigating the conserved residues of *S. pneumoniae* PPCS, several conserved residues were targeted for saturation mutagenesis to determine their utility. These residues (Glu12, Asp15, Asp93, Lys123, Ser125, Ser126 and Lys213) were subjected to saturation mutagenesis in the *S. pneumoniae* PPCS-PPCDC vector (pUMKH7), transformed into KH100 and streaked onto pantethine-free media in order to determine their growth phenotype (**Table 2.4**).

Residues 123, 125 and 126 compose a KxKK domain in Type I PPCS that is conserved as KxSS in the Type III enzyme. Lys125 aligns with the catalytic Lys289 of Type I PPCS that is responsible for the first half reaction (6). *In vivo* results support that this residue has a similar conserved role in *S. pneumoniae* PPCS, as only the K123M, K123N, and K123R mutations were viable. Residue 125 does not support mutations to other polar uncharged residues, but mutations to positively charged polar residues or hydrophobic residues are viable. The S125C mutation may be lethal due to cysteine interacting preferentially over Lys123, not allowing for catalysis of the first half reaction.

Residue Asp93 of *S. pneumoniae* PPCS aligns with Asp279, which appears to coordinate with the divalent cation  $Mg^{2+}$  in the active site of *E. coli* PPCS crystal

structures (**Figure 2.9**) (8,10). *In vivo* analysis supports that Asp93 plays an important role in the activity of *S. pneumoniae* PPCS, as only D93E and D93N were able to complement the double knockout model system (**Table 2.4**). A polar or negative charge is likely required at this position to coordinate with  $Mg^{2+}$ , which is in turn coordinating with the phosphate backbone of CTP,

Other residues probed by saturation mutagenesis include to the completely conserved acidic residues Glu12 and Asp15. These residues supported a wide array of mutations. Glu12 can be substituted with any residue, and thus has no direct role on activity and is likely conserved as an optimized residue for structural stability. Asp15 supported several diverse mutations, including arginine, glycine and cysteine. However, bulky residues (such as tryptophan) and hydrophobic residues (such as valine) were lethal, likely as a result of the mutation causing a protein misfolding rather than interfering directly with the catalysis of enzyme. Mapping these residues onto the *E. coli* PPCS crystal structure (**Figure 2.6**) shows that both E12 and D15 are closer to the dimer interface of PPCS and away from the cytidylate in the active site.

The completely conserved Lys213 was probed by saturation mutagenesis due to its close proximity to the pantothenoyl arm of the **JDP03** in the *E. coli* crystal structure. Mutagenesis results revealed that K213 plays a minor role in activity. Of the residues that were found in the mutant pool, all of them were able to support growth of the knockout model. K213 supported both large and small hydrophobic residues, as well as aromatics. Residues that were not found in the mutant pool could be either to not enough coverage or due to toxicity of the mutation, but the high number of viable mutants suggests that the residue is more important structurally and not catalytic.

*In vitro* analysis of *S. pneumoniae* PPCS mutants. To further characterize the activities of the selected conserved residues, *in vitro* analysis was performed by determining the enzymatic activity of each mutant. Following steady state Michaelis-Menten kinetics, apparent Michaelis constants ( $K_m$ ) were determined for each mutant to each substrate. Wild-type *S. pneumoniae* PPCS was first characterized with the continuous pyrophosphatase assay as a reference point for the mutant apparent  $K_m$ 's (**Figure 2.11**). The wild-type enzyme had a  $K_m$  for CTP of 98.7  $\mu\text{M}$ ,  $K_m$  for cysteine of 391  $\mu\text{M}$ , and a  $K_m$  for phosphopantetheine (PPA) of 98.7  $\mu\text{M}$  (**Table 2.5**).

The K123M, K123N, and K123R mutants were tested in the pyrophosphatase assay to determine apparent  $K_m$  values for each substrate, and thus estimate the impact of K123 on substrate binding (**Table 2.5**). There appeared to me no significant trend of mutant effects with phosphopantetheine (**Figure 2.12**) and cysteine binding (**Figure 2.13**). The Lys123 residue of Type 3 *S. pneumoniae* was believed to be responsible for mediating the phosphate activation of phosphopantothenate as Lys289 does in the *E. coli* enzyme. *In vitro* analysis supports this as the K123M and K123R mutations had huge loss in the binding affinity of CTP (**Figure 2.14**), which is utilized in the first step activation. Additionally, all three viable Lys123 mutations exhibited a large loss in the overall efficiency of the enzyme.

The D93E and D93N mutants were also tested with the *in vitro* pyrophosphatase assay for substrate apparent  $K_m$  values (**Table 2.5**). Residue Asp93 of *S. pneumoniae* Type 3 PPCS was believed to be largely responsible for coordinating  $\text{Mg}^{2+}$  into the active site to assist with the activation step from the crystal data. *In vitro* analysis supported this claim, as the D93E and D93N mutants had a 1.5-2.7 fold less affinity for CTP (**Figure**

**2.17).** Additionally, the Eikonogen assay was used to determine apparent  $K_m$  values for the D93 mutants to  $MgCl_2$  (**Figure 2.18**). D93E was on par with wild-type *S. pneumoniae* PPCS, however D93N mutation had a much lower affinity for  $MgCl_2$ . This is likely due to the long amino acid chain of asparagine compared to aspartate or glutamate to coordinate the  $Mg^{2+}$  thus hindering the activity of the enzyme.

## Conclusion

This work represents the first molecular characterization of Type 3 PPCS. Through a novel multiple sequence alignment of strictly Type 1 and Type 3 PPCS, we were able to identify residues conserved completely across bacterial PPCS. The residues were mapped onto the available *E. coli* crystal structure, and highly conserved residues aligned with the active site (**Figure 2.19**).

To probe these conserved residues for their roles in *S. pneumoniae* Type 3 PPCS, a double knockout system was developed which allowed for the rapid *in vivo* characterization of saturation mutant pools. Follow up *in vitro* characterization was performed on residues of interest to estimate the role of the residue based on its effect on substrate apparent Michaelis-Menten constants.

Point mutation of N22 and K123 confirmed that they share the activities of N210 and K289 in *E. coli* (**Figure 2.19**). K123 plays a catalytic role in the first half activation step, mediating the phosphate activation of pantetheine. N22 is believed to interact with cysteine and mediate the condensation in the second half reaction. Additionally, mutagenesis studies of D93 revealed that the residue plays an important role in associating the divalent cation,  $Mg^{2+}$ , with the active site.



## REFERENCES

1. Anderson, M. S., Bulawa, C. E., and Raetz, C. R. (1985) *Journal of Biological Chemistry* **260**, 15536-15541
2. Brozek, K. A., and Raetz, C. R. (1990) *Journal of Biological Chemistry* **265**, 15410-15417
3. Spry, C., Kirk, K., and Saliba, K. J. (2008) *FEMS Microbiology Reviews* **32**, 56-106
4. Gerdes, S. Y., Scholle, M. D., D'Souza, M., Bernal, A., Baev, M. V., Farrell, M., Kurnasov, O. V., Daugherty, M. D., Mseeh, F., Polanuyer, B. M., Campbell, J. W., Anantha, S., Shatalin, K. Y., Chowdhury, S. A. K., Fonstein, M. Y., and Osterman, A. L. (2002) *Journal of Bacteriology* **184**, 4555-4572
5. Zhang, Y.-M., White, S. W., and Rock, C. O. (2006) *Journal of Biological Chemistry* **281**, 17541-17544
6. Kupke, T. (2002) *Journal of Biological Chemistry* **277**, 36137-36145
7. Kupke, T., Hernández-Acosta, P., and Culiáñez-Macià, F. A. (2003) *Journal of Biological Chemistry* **278**, 38229-38237
8. Stanitzek, S., Augustin, M. A., Huber, R., Kupke, T., and Steinbacher, S. (2004) *Structure* **12**, 1977-1988
9. Patrone, J. D., Yao, J., Scott, N. E., and Dotson, G. D. (2009) *Journal of the American Chemical Society* **131**, 16340-16341
10. Patrone, J. D. (2010) Investigating Phosphopantothencysteine Synthetase as a Potential Antibacterial Target. in *Medicinal Chemistry*, University of Michigan, College of Pharmacy
11. Yao, J. (2010) Exploring the Coenzyme A Biosynthetic Pathway as Novel Antibiotic Target. in *Medicinal Chemistry*, University of Michigan, College of Pharmacy
12. Yao, J., Patrone, J. D., and Dotson, G. D. (2009) *Biochemistry* **48**, 2799-2806
13. Datsenko, K. A., and Wanner, B. L. (2000) *Proceedings of the National Academy of Sciences* **97**, 6640-6645
14. MIYATAKE, K., NAKANO, Y., and KITAOKA, S. (1976) *Journal of Biochemistry* **79**, 673-678
15. Brown, G. M. (1982) *Advances in enzymology and related areas of molecular biology* **53**, 345-381
16. Kupke, T. (2004) *European Journal of Biochemistry* **271**, 163-172

Vector	Insert	Plasmid	Digest	Forward Primer (Top), Reverse Primer (Bottom)
pUMKH5	<i>E. coli</i> PPCS-PPCDC	pUMRJ100	<i>NdeI</i> <i>HindIII</i>	CGG <u>C</u> CATATGTCGCCCCTCAACGACCTGAAACATCTG CGG <u>A</u> AGCTTTTTTAACGTCGATTTTTTTCATCATAACGGG
pUMKH6	<i>E. faecalis</i> PPCS-PPCDC	pUMRJ100	<i>NdeI</i> <i>NaeI</i>	GCG <u>C</u> CATATGGATGTTTTAGTTACTGCTGGCGG ATATG <u>C</u> CGGCTTACTCCTTGTTATCAGATGC
pUMKH7	<i>S. pneumoniae</i> PPCS-PPCDC	pUMRJ100	<i>NdeI</i> <i>HindIII</i>	GCG <u>C</u> CATATGAGCCTGGCCGGTAAAAAATCGTTCTCGGCG CGG <u>A</u> AGCTTTTTAGAGCGTTTTTTCATCGATAGTTTCC
pUMKH32	<i>H. sapien</i> PPCS, <i>S. pneumoniae</i> PPCDC	pUMRJ100	<i>NdeI</i> <i>HindIII</i>	CGG <u>C</u> CATATGGCAGAAATGGATCCGGTTGC CGG <u>A</u> AGCTTTTTAGAGCGTTTTTTCATCGATAGTTTCC
pUMDOT3	<i>E. coli</i> PPCS	pET23a	<i>NdeI</i> <i>XhoI</i>	CGG <u>C</u> CATATGTCGCCCCTCAACGACCTGAAACATCTG GCG <u>C</u> CTCGAGACGTCGATTTTTTTCATCATAACGGG
pUMGD1	<i>E. faecalis</i> PPCS	pET23a	<i>NdeI</i> <i>XhoI</i>	GCG <u>C</u> CATATGGATGTTTTAGTTACTGCTGGCGG GCG <u>C</u> CTCGAGTCATTGTTGTTCTCTCCATTTCTTTTC
pUMKH8	<i>S. pneumoniae</i> PPCS	pET23a	<i>NdeI</i> <i>XhoI</i>	GCG <u>C</u> CATATGAAAATTTTAGTTACATCGGGCG GCG <u>C</u> CTCGAGTTAAGAATGATAGGCTTGAATTTTTTC
pUMKH9	<i>S. pneumoniae</i> PPCS- <i>his</i> <sub>6</sub>	pET23a	<i>NdeI</i> <i>XhoI</i>	GCG <u>C</u> CATATGAAAATTTTAGTTACATCGGGCG GCG <u>C</u> CTCGAGAGAATGATAGGCTTGAATTTTTTC

**Table 2.1:** List of vectors developed for the *in vivo* and *in vitro* characterization of bacterial PPCS. The parent plasmid and restriction digest sites used to construct the vector are also listed. The underlined portion of the primer is the recognition sequence for the corresponding restriction enzyme.

Vector	Insert	Plasmid	Forward Primer (Top), Reverse Primer (Bottom)
pUMKH10	<i>E. coli</i> PPCS(N210D)-PPCDC	pUMRJ100	CGGTGCGTTATATCTCT <b>GAT</b> CACAGCTCCGGCAAG CTTGCCGGAGCTGT <b>GAT</b> CAGAGATATAACGCACCG
pUMKH11	<i>E. coli</i> PPCS(S212A)-PPCDC	pUMRJ100	CGTTATATCTCTAATCAC <b>GC</b> CTCCGGCAAGATGGGTTTTG CAAAACCCATCTTGCCGG <b>AGG</b> CGTGATTAGAGATATAACG
pUMKH12	<i>E. coli</i> PPCS(K289Q)-PPCDC	pUMRJ100	GCTACCGTGGCCCCAGAG <b>CAG</b> ATCAAAAAGCAGGCCAC GTGGCCTGCTTTTTG <b>ATCTG</b> CTCTGGGGCCACGGTAGC
pUMKH13	<i>S. pneumoniae</i> PPCS(N22D)-PPCDC	pUMRJ100	GCGTCCGCTCTATCACT <b>GAT</b> CATTCTACAGGTCAC GTGACCTGTAGAAT <b>GAT</b> CAGTGATAGAGCGGACGC
pUMKH14	<i>S. pneumoniae</i> PPCS(S24A)-PPCDC	pUMRJ100	CGCTCTATCACTAACC <b>ATG</b> CCACAGGTCACCTGGGG CCCCAAGTGACCTGT <b>GGC</b> ATGGTTAGTGATAGAGCG
pUMKH15	<i>S. pneumoniae</i> PPCS(K123Q)-PPCDC	pUMRJ100	GCAAGCAAAATCATCAGGCC <b>AG</b> ATTTCTTCAACTGATG CATCAGTTGAAGAA <b>ATCTG</b> GGCCTGATGATTTTGCTTGC
pUMKH16	<i>E. coli</i> PPCS(N210D)- <i>his</i> <sub>6</sub>	pET23a	CGGTGCGTTATATCTCT <b>GAT</b> CACAGCTCCGGCAAG CTTGCCGGAGCTGT <b>GAT</b> CAGAGATATAACGCACCG
pUMKH17	<i>E. coli</i> PPCS(S212A)- <i>his</i> <sub>6</sub>	pET23a	CGTTATATCTCTAATCAC <b>GC</b> CTCCGGCAAGATGGGTTTTG CAAAACCCATCTTGCCGG <b>AGG</b> CGTGATTAGAGATATAACG
pUMKH18	<i>E. coli</i> PPCS[K289Q]- <i>his</i> <sub>6</sub>	pET23a	GCTACCGTGGCCCCAGAG <b>CAG</b> ATCAAAAAGCAGGCCAC GTGGCCTGCTTTTTG <b>ATCTG</b> CTCTGGGGCCACGGTAGC
pUMKH19	<i>S. pneumoniae</i> PPCS(N22D)- <i>his</i> <sub>6</sub>	pET23a	GCGTCCGCTCTATCACT <b>GAT</b> CATTCTACAGGTCAC GTGACCTGTAGAAT <b>GAT</b> CAGTGATAGAGCGGACGC
pUMKH20	<i>S. pneumoniae</i> PPCS(S24A)- <i>his</i> <sub>6</sub>	pET23a	CGCTCTATCACTAACC <b>ATG</b> CCACAGGTCACCTGGGG CCCCAAGTGACCTGT <b>GGC</b> ATGGTTAGTGATAGAGCG
pUMKH21	<i>S. pneumoniae</i> PPCS(K123Q)- <i>his</i> <sub>6</sub>	pET23a	GCAAGCAAAATCATCAGGCC <b>AG</b> ATTTCTTCAACTGATG CATCAGTTGAAGAA <b>ATCTG</b> GGCCTGATGATTTTGCTTGC

**Table 2.2:** List of vectors constructed for active site comparison of *E. coli* and *S. pneumoniae* PPCS. Codons used to insert the mutation are in bold on the listed primers.

Vector	Insert	Plasmid	Forward Primer (Top), Reverse Primer (Bottom)
pUMKH25	<i>S. pneumoniae</i> PPCS(E12L)-PPCDC	pUMRJ100	CATCGGGCGGTACCAGT <b>CTGG</b> CTATCGATAGCGTCCG CGGACGCTATCGATAGCCAGACTGGTACCGCCCGATG
pUMKH26	<i>S. pneumoniae</i> PPCS(D15A)-PPCDC	pUMRJ100	GTACCAGTGAAGCTAT <b>CGCG</b> AGCGTCCGCTCTATCAC GTGATAGAGCGGACGCT <b>CGC</b> GATAGCTTCACTGGTAC
pUMKH27	<i>S. pneumoniae</i> PPCS(D93N)-PPCDC	pUMRJ100	CACTCAATGGCTGTTTCT <b>AACT</b> ACTACTCCTGTTTATATG CATATAAACAGGAGTGTAG <b>TT</b> AGAAACAGCCATTGAGTG
pUMKH28	<i>S. pneumoniae</i> PPCS(E12L)- <i>his</i> <sub>6</sub>	pET23a	CATCGGGCGGTACCAGT <b>CTGG</b> CTATCGATAGCGTCCG CGGACGCTATCGATAGCCAGACTGGTACCGCCCGATG
pUMKH29	<i>S. pneumoniae</i> PPCS(D15A)- <i>his</i> <sub>6</sub>	pET23a	GTACCAGTGAAGCTAT <b>CGCG</b> AGCGTCCGCTCTATCAC GTGATAGAGCGGACGCT <b>CGC</b> GATAGCTTCACTGGTAC
pUMKH30	<i>S. pneumoniae</i> PPCS(D93N)- <i>his</i> <sub>6</sub>	pET23a	CACTCAATGGCTGTTTCT <b>AACT</b> ACTACTCCTGTTTATATG CATATAAACAGGAGTGTAG <b>TT</b> AGAAACAGCCATTGAGTG
pUMKH31	<i>S. pneumoniae</i> PPCS(E12X)-PPCDC	pUMRJ100	CATCGGGCGGTACCAGT <b>NNK</b> GCTATCGATAGCGTCCG CGGACGCTATCGATAGCMN <b>N</b> ACTGGTACCGCCCGATG
pUMKH32	<i>S. pneumoniae</i> PPCS(D15X)-PPCDC	pUMRJ100	GTACCAGTGAAGCTAT <b>CNNK</b> AGCGTCCGCTCTATCAC GTGATAGAGCGGACGCT <b>MNN</b> GATAGCTTCACTGGTAC
pUMKH33	<i>S. pneumoniae</i> PPCS(D93X)-PPCDC	pUMRJ100	CACTCAATGGCTGTTTCT <b>NNK</b> TACTACTCCTGTTTATATG CATATAAACAGGAGTGTAM <b>NN</b> NAGAAACAGCCATTGAGTG
pUMKH34	<i>S. pneumoniae</i> PPCS(K123X)-PPCDC	pUMRJ100	GCAAATCATCAGGCC <b>NNK</b> ATTTCTTCAACTGATGAGG CCTCATCAGTTGAAGAAAT <b>MNN</b> GGCCTGATGATTTTGC
pUMKH35	<i>S. pneumoniae</i> PPCS(S125X)-PPCDC	pUMRJ100	CAAATCATCAGGCCAAGATT <b>NNK</b> TCAACTGATGAGGTT <b>CAG</b> CTGAACCTCATCAGTTGAM <b>NN</b> AATCTTGGCCTGATGATTTT <b>G</b>
pUMKH36	<i>S. pneumoniae</i> PPCS(S126X)-PPCDC	pUMRJ100	CATCAGGCCAAGATTTCT <b>NNK</b> ACTGATGAGGTT <b>CAG</b> GTTT <b>G</b> CAAACCTGAACCTCATCAGT <b>MNN</b> NAGAAATCTTGGCCTGATG
pUMKH37	<i>S. pneumoniae</i> PPCS(K213X)-PPCDC	pUMRJ100	GCTTCAAACAGTCCAGACT <b>NNK</b> GAAGAAATTGCAGAACTCC GGAGTTCTGCAATTTCT <b>TCMNN</b> AGTCTGGACTGTTTGAAGC

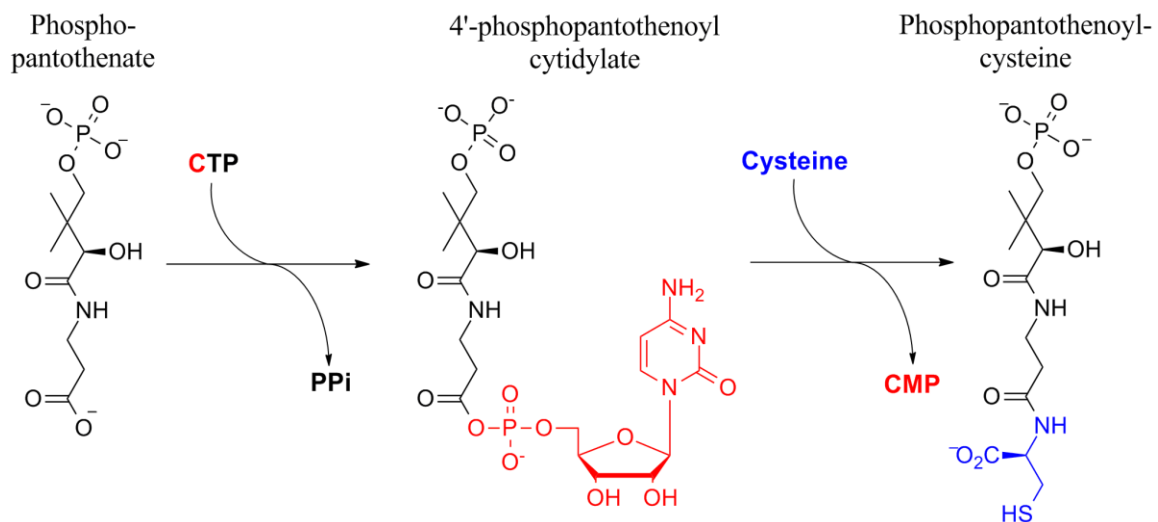
**Table 2.3:** List of vectors constructed in the mutagenesis studies of *S. pneumoniae* PPCS. Codons used to insert the mutation are in bold on the listed primer.

<b>Residue</b>	<b>E12</b>	<b>D15</b>	<b>D93</b>	<b>K123</b>	<b>S125</b>	<b>S126</b>	<b>K213</b>
Alanine (A)	Grow	Grow	NG	NG	Grow	-	Grow
Arginine (R)	Grow	Grow	NG	Grow	Grow	Grow	-
Asparagine (N)	Grow	-	Grow	Grow	NG	Grow	Grow
Aspartate (D)	Grow	<b>Native</b>	<b>Native</b>	NG	NG	Grow	-
Cysteine (C)	Grow	Grow	NG	NG	NG	Grow	-
Glutamate (E)	<b>Native</b>	Grow	Grow	NG	-	Grow	-
Glutamine (Q)	Grow	-	NG	NG	NG	-	-
Glycine (G)	Grow	Grow	NG	NG	-	-	Grow
Histidine (H)	Grow	NG	NG	NG	Grow	Grow	Grow
Isoleucine (I)	Grow	-	NG	NG	Grow	Grow	Grow
Leucine (L)	Grow	Grow	NG	NG	Grow	NG	Grow
Lysine (K)	Grow	-	NG	<b>Native</b>	-	-	<b>Native</b>
Methionine (M)	Grow	-	NG	Grow	Grow	-	-
Phenylalanine (F)	Grow	-	NG	NG	Grow	Grow	Grow
Proline (P)	Grow	NG	NG	NG	Grow	-	-
Serine (S)	Grow	Grow	NG	NG	<b>Native</b>	<b>Native</b>	Grow
Threonine (T)	Grow	NG	NG	NG	NG	NG	Grow
Tryptophan (W)	Grow	NG	NG	NG	Grow	-	-
Tyrosine (Y)	Grow	Grow	NG	NG	NG	Grow	Grow
Valine (V)	Grow	NG	NG	NG	Grow	Grow	Grow

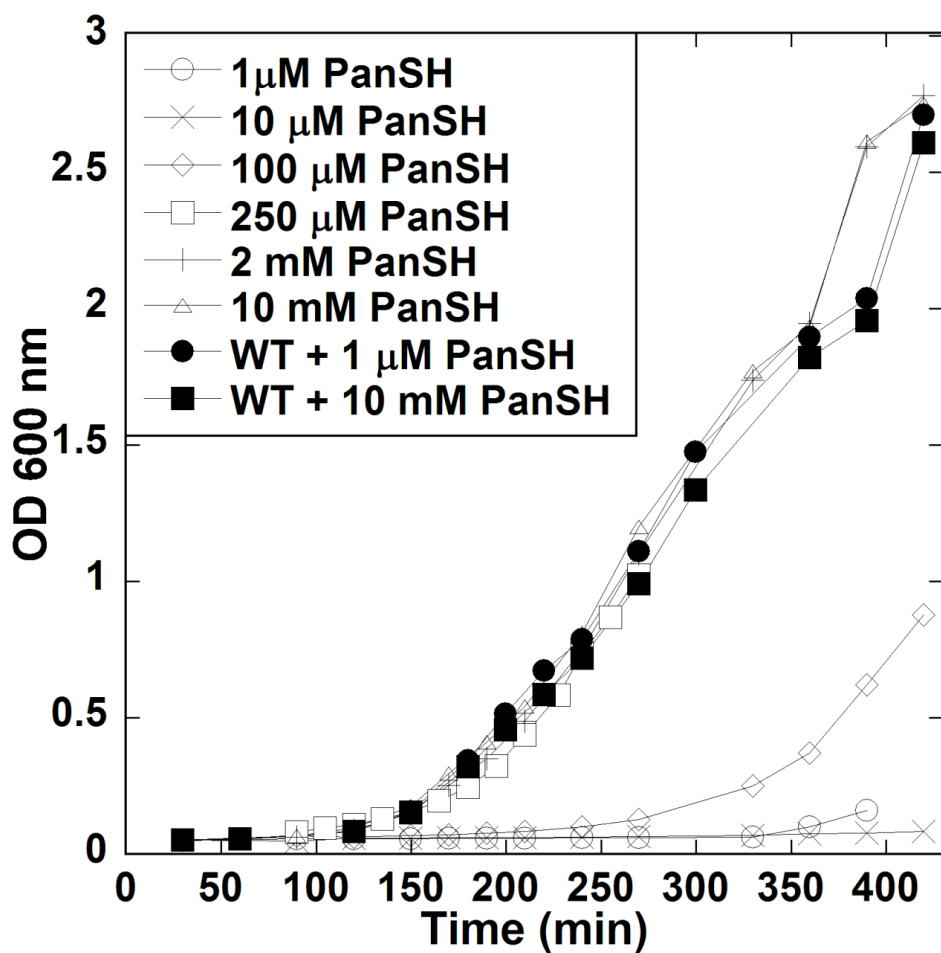
**Table 2.4:** Phenotypes of *S. pneumoniae* PPCS mutants. Dashes indicate mutants not found in the pool of saturation mutagenesis.

<b>PPCS Mutant</b>	<b><math>K_m(\text{CTP})</math>, <math>\mu\text{M}</math></b>	<b><math>K_m(\text{cysteine})</math>, <math>\mu\text{M}</math></b>	<b><math>K_m(\text{PPA})</math>, <math>\mu\text{M}</math></b>	<b><math>k_{\text{cat}}^{\text{app}}(\text{PPA})</math> (<math>\text{s}^{-1}</math>)</b>	<b><math>k_{\text{cat}}^{\text{app}}(\text{PPA})/</math> <math>K_m(\text{PPA})</math> (<math>\text{s}^{-1}</math>)</b>
Wild Type	98.7 ± 18.7	391 ± 17.8	99.3 ± 10.3	132	1.33
D93E	151.0 ± 28.5	197.0 ± 18.1	150.1 ± 6.4	124	0.824
D93N	266.5 ± 27.1	234.4 ± 11.8	247.9 ± 15.7	3.1	0.012
K123M	142 ± 16.1	448 ± 23.0	181 ± 11.4	0.41	0.0022
K123N	99.7 ± 12.3	305 ± 37.6	145 ± 17.2	0.22	0.0015
K123R	872 ± 108	53.2 ± 9.0	211 ± 12.6	0.86	0.0040

**Table 2.5:** Comparison of apparent Michaelis-Menten constants of *S. pneumoniae* PPCS mutants.

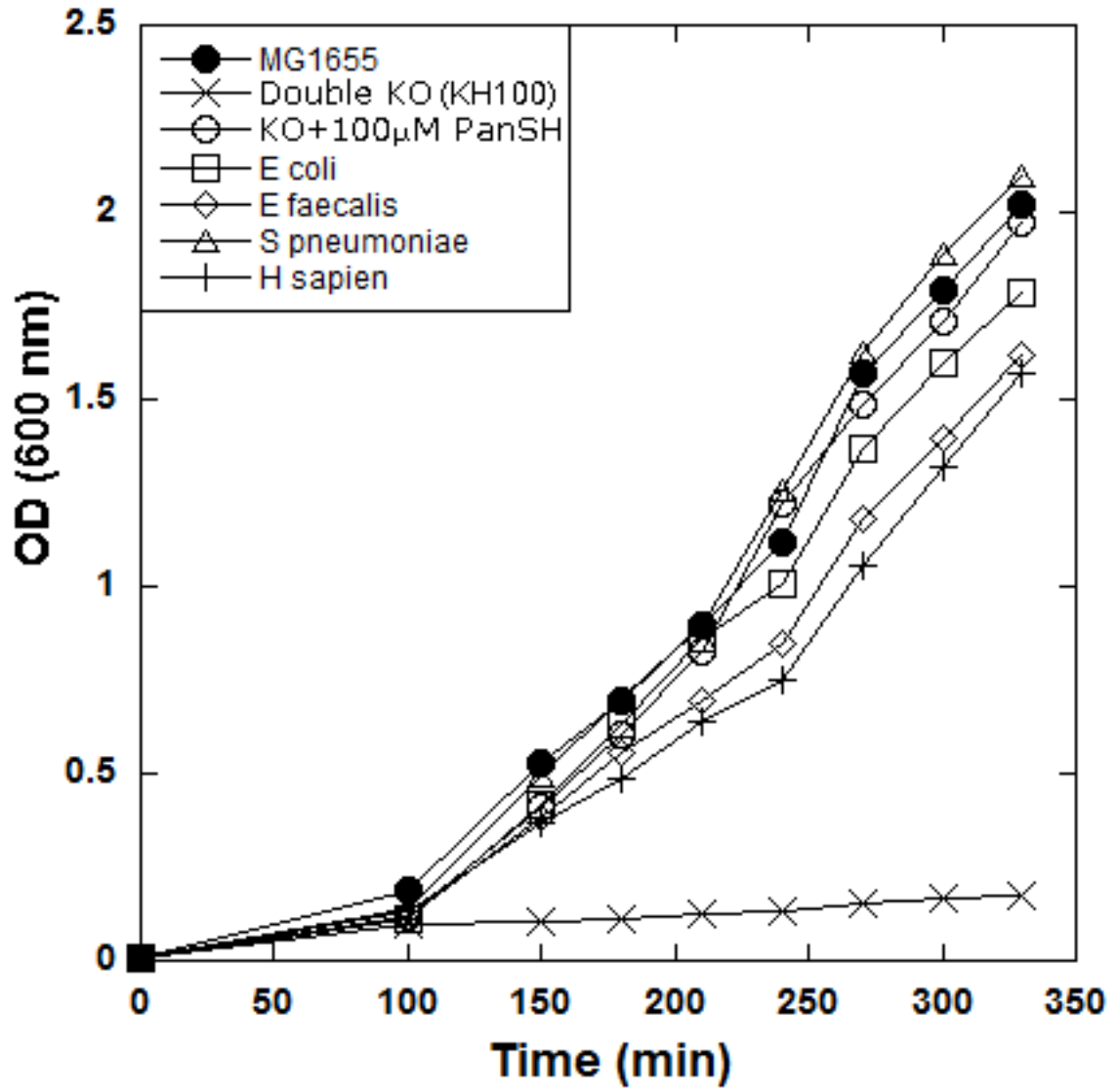


**Figure 2.1:** Two step reaction of PPCS. Bacterial PPCS utilize strictly CTP in the first step activation, whereas eukaryotic systems utilize ATP in addition to CTP.

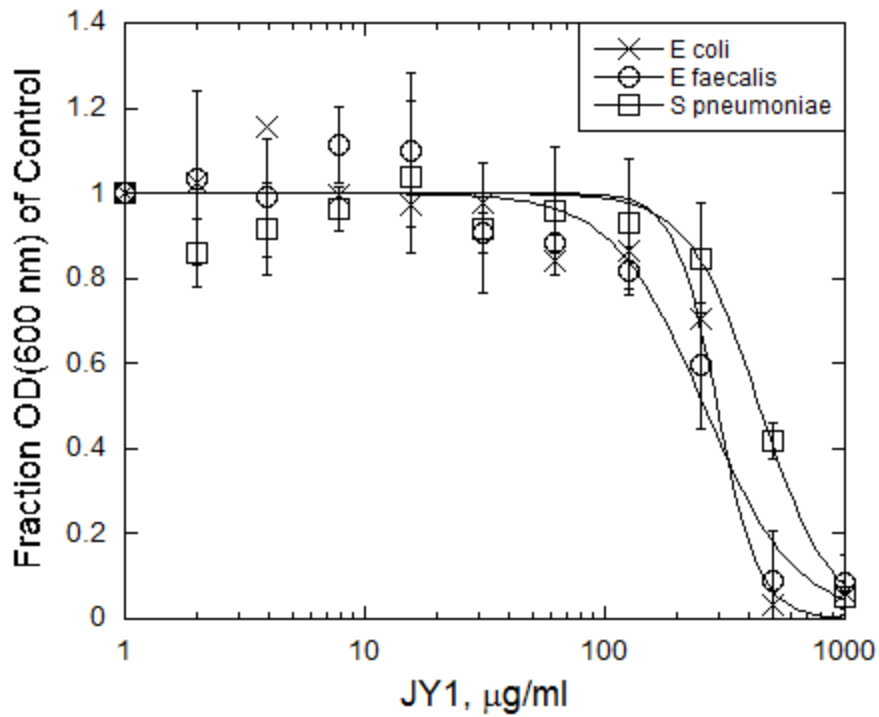


**Figure 2.2:** Growth curve of knockout strain KH100 (*E. coli* MG1655  $\Delta$ PanC, $\Delta$ coaBC::*Kan<sup>R</sup>*) supplemented with various amounts of environmental pantetheine.

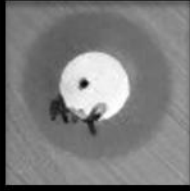
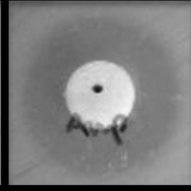
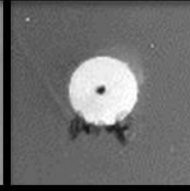
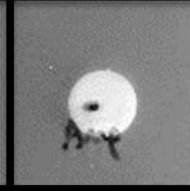
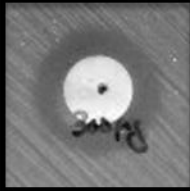
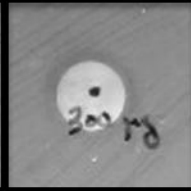
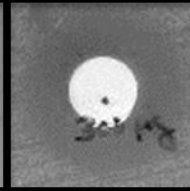
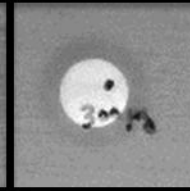

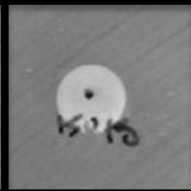
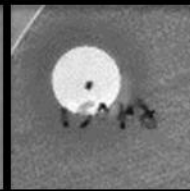
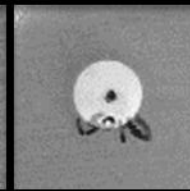


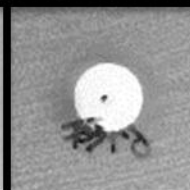
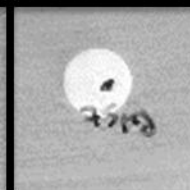



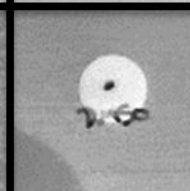




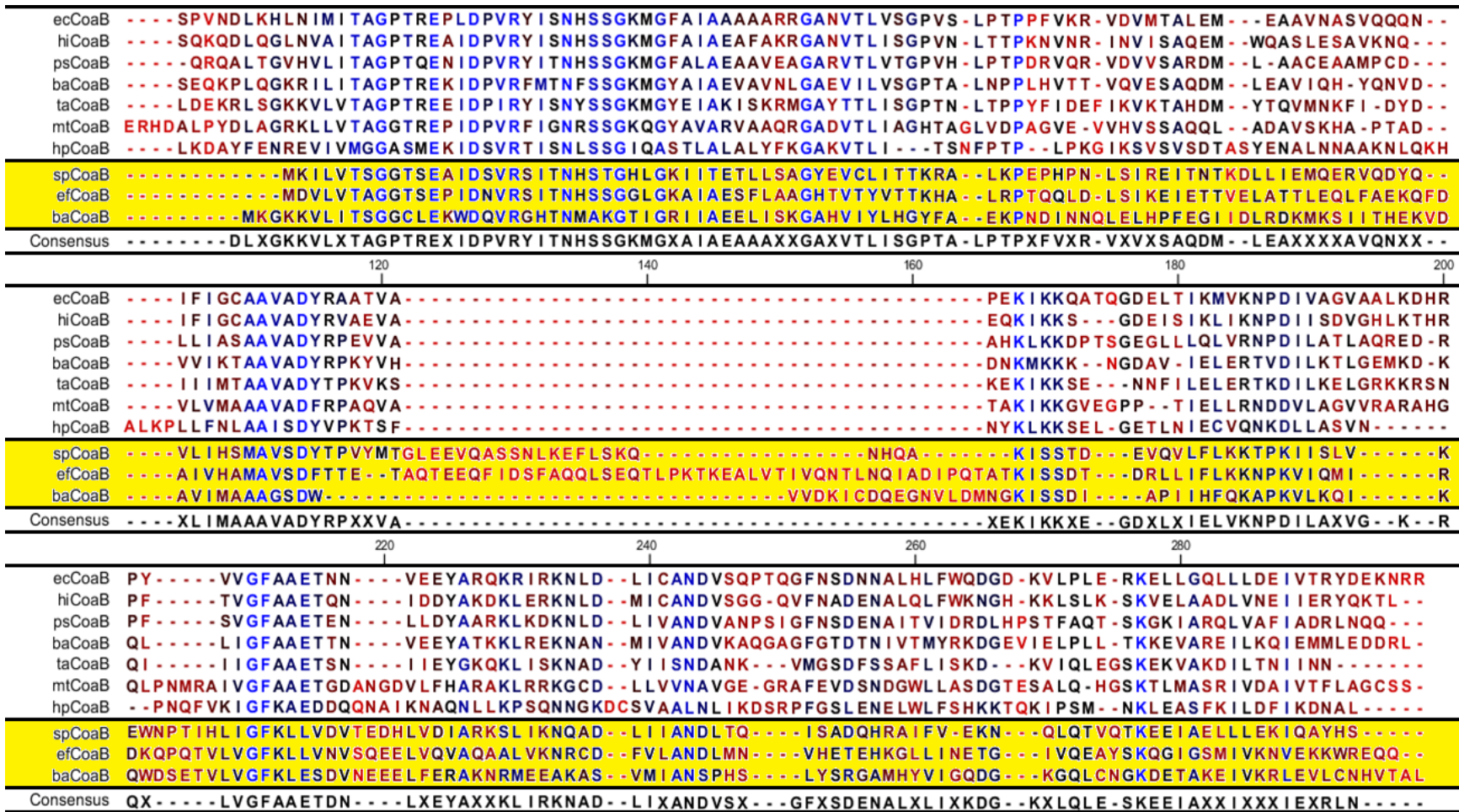
**Figure 2.3:** Growth curve of knockout strain KH100 genetically complemented with plasmid based *coaBC* domains from other organisms. Wild-type *E. coli* MG1655 and the uncomplemented knockout strain are also shown as controls.



**Figure 2.4:** MIC test of JY1 (SPB03328) against *coaBC* complemented KH100. Compound JY1 was tested in an MIC study against the double knockout strain complemented with the *coaBC* domains of *E. coli*, *E. faecalis*, and *S. pneumoniae*. The compound exhibited comparable Minimal Inhibitory Concentration against each of the three complements.

<i>ΔpanCΔcoaBC</i> + <i>S. pneu. coaBC</i>		<i>E. coli ΔtolC</i> ( <i>E. coli coaBC</i> )		Strain
10% Dextrose	100 μM Pantethine	10% Dextrose	100 μM Pantethine	
				Ampicillin 50 μg
				<b>JY1</b> 300 μg
				<b>JY1</b> 150 μg
				<b>JY1</b> 75 μg
				DMSO (no compd)

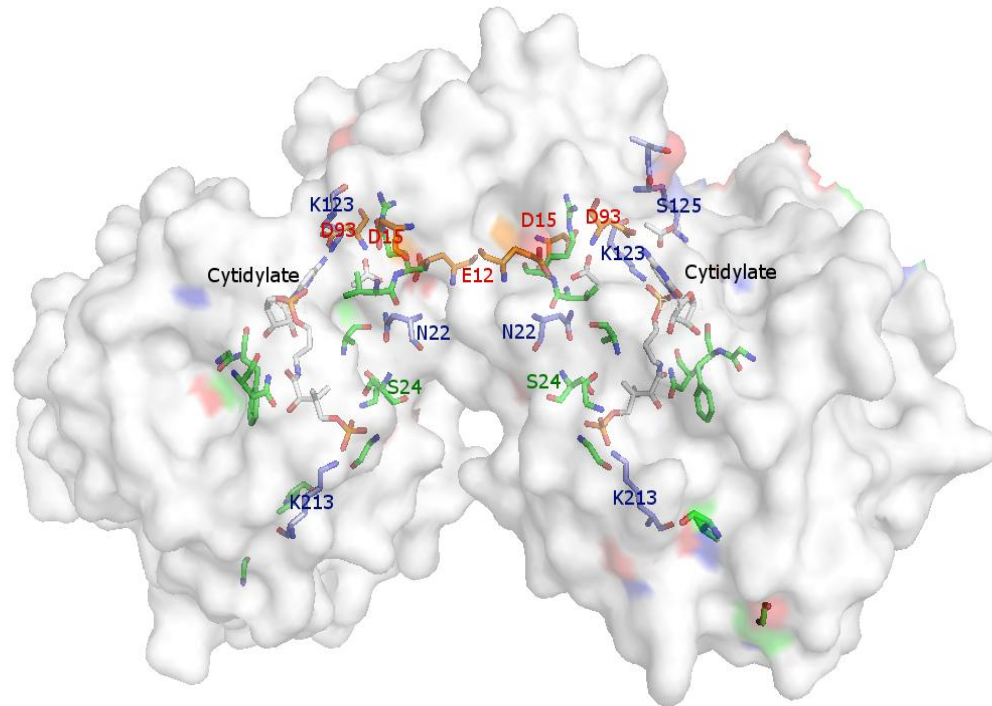
**Figure 2.5:** Disc diffusion of JY1 against KH100 and *E. coli ΔtolC*. JY1 was tested against *S. pneumoniae coaBC* complemented double knockout on the two left columns, with and without supplemented pantethine. JY1 300 μg exhibited a ring of inhibition that was rescued by the addition of pantethine. JY1 was tested against *tolC* knockout (missing efflux pump) strain on the right two columns. The ring of inhibition is much larger, but still recovered by the addition of pantethine, indicating that JY1 is targeting the desired PPCS in its antimicrobial activity.



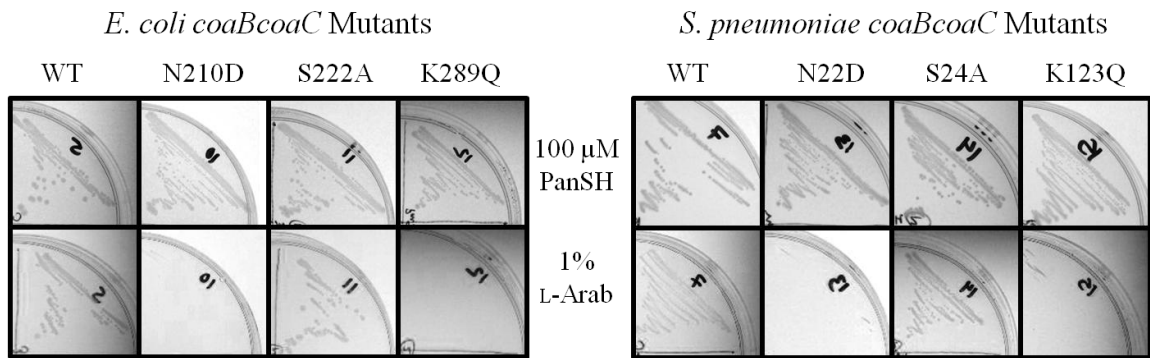
**Figure 2.6:** Full multiple sequence alignment of bacterial PPCS. Boxed and highlighted sequences represent the monofunctional Type 3 PPCS enzymes. The Type 1 PPCS are from the following species (in order top to bottom): *Escherichia coli*, *Haemophilus influenzae*, *Pseudomonas aeruginosa*, *Bacillus anthracis* Type 1 PPCS, *Thermus aquaticus*, *Mycobacterium tuberculosis*, and *Helicobacter pylori*. The Type 3 PPCS are highlighted in yellow and are from species as follows (in order from top to bottom): *Streptococcus pneumoniae*, *Enterococcus faecalis*, and *Bacillus anthracis* Type 3 PPCS. *Bacillus anthracis* contains both genes for Type 1 and Type 3 PPCS.

		196	205	214	385	270	276	284	289	292
		8	17	26	213	84	90	98	123	126
		↓	*	↓	↓	↓	*	↓	↓	↓
BIFUNCTIONAL	ecCoaB	GP	TREPLDPVRY	ISNHSSG	K	IFIGCAAVADYRAAT	PEKIKKQA			
	hiCoaB	GP	TREAIDPVRY	ISNHSSG	K	IFIGCAAVADYRVAE	EQKIKKS-			
	psCoaB	GP	TQENIDPVRY	ITNHSSG	K	LLIASAAVADYRPEV	AHKLKKDP			
	baCoaB	GP	TREKIDPVRFMTNFSSG	K	VVIKTAAVADYRPKY	DNKMKKK-				
	taCoaB	GP	TREEIDPIRYISNYSSG	K	IIIMTAAVADYTPKV	KEKIKKSE				
	mtCoaB	GG	TREPIDPVRFIGNRSSG	K	VLVMAAAVADFRPAQ	TAKIKKGV				
hpCoaB	GASMEK	IDSVRTISNLSGG	K	LLFNLAASIDYVPKT	NYKLKKSE					
MONO	spCoaB	GGTSEA	IDSVRSITNHSTG	K	VLIHSMVSDYTPVY	--KISSTD				
	efCoaB	GGTSEP	IDNVRSITNHSSG	K	AIVHAMAVSDFTTE-	ATKISSDT				
	baCoaBmono	GGCLEKWDQVRGHTNMAKG	K	AVIMAAAGSDW----	NGKISSDI					
Consensus		GP	TREXIDPVRYITNHSSG	K	XLIMAAAVADYRPXX	XEKIKKXE				
			Oxyanion	PPA Phos		Mg <sup>2+</sup>	CTP α-Phos			
		301	311	324	329	333	350	355	362	367
		132	145	154	159	163	184	189	192	197
		↓	↓	↓	*	↓	↓	*	*	↓
BIFUNCTIONAL	ecCoaB	T	IKMVKNPDI	V	VVGFAAETNN	I	CANDVSQPTQGFNSDNN			
	hiCoaB	S	IKLIKNPDI	I	TVGFAAETQN	I	CANDVSGG-QVFNADEN			
	psCoaB	L	LQLVRNPDI	L	SVGFAAETEN	I	VANDVANPSIGFNSDEN			
	baCoaB	-	I E L E R T V D I L	L	I G F A A E T T N	I	VANDVKAQGAGFGDTN			
	taCoaB	I	L E L E R T K D I L	I	I G F A A E T S N	I	I S N D A N K - - - V M G S D F S			
	mtCoaB	T	I E L L R N D D V L	I	V G F A A E T G D	L	V V N A V G E - G R A F E V D S N			
hpCoaB	N	I E C V Q N K D L L	K	I G F K A E D D Q	V	A A L N L I K D S R P F G S L E N				
MONO	spCoaB	V	LFLKKTPKII	L	LIGFKLLVDV	I	IANDLTQ----ISADQH			
	efCoaB	L	I FLKKNPKVI	L	LVGFKLLVNV	V	LANDLMN----VHETEH			
	baCoaBmono	I	I HFQKAPKVL	L	LVGFKLESDV	M	IANSPPHS----LYSRGA			
Consensus		X	I E L V K N P D I L	L	V G F A A E T D N	I	X A N D V S X - - - G F X S D E N			
			Cytidine							

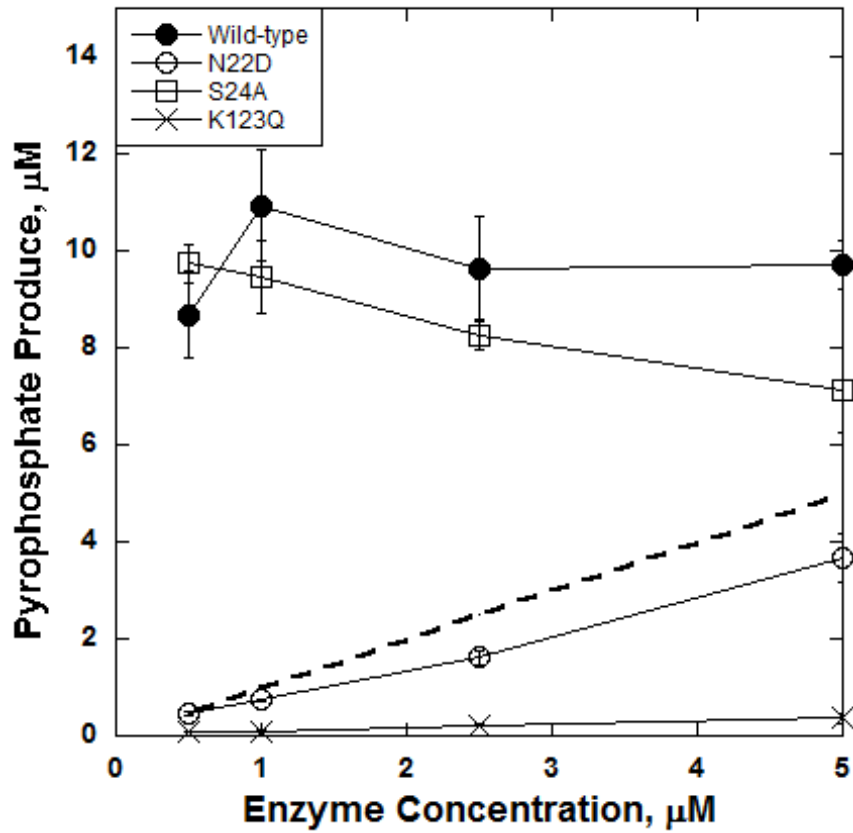
**Figure 2.7:** Selected conserved sequences found in the multiple sequence alignment between bacterial mono and bifunctional PPCS. Blue residues are highly conserved. Asterisks indicate residues that are part of the putative hydrophobic substrate cysteine pocket. Lines labeled in red represents the role those residues fulfill in *E. coli* according to structural data. Residues are labeled based on their position in *E. coli* in black and their position in *S. pneumoniae* PPCS in red.



**Figure 2.8:** Crystal structure of *E. coli* PPCS dimer (2.37 Å resolution) bound to cytidylate intermediate mimic. Highly conserved residues among all bacterial PPCS are rendered as stick figures. Residues of particular interest for mutagenesis probing are labeled with their equivalent residue number as expressed in *S. pneumoniae* PPCS.



**Figure 2.9:** Streaks of plasmid-based PPCS-PPCDC point mutations complementing KH100. *E. coli* PPCS mutants are listed on the left, and the corresponding *S. pneumoniae* PPCS mutation is listed on the right.



**Figure 2.10:** Results of single turnover assay in selected *S. pneumoniae* PPCS point mutations. The bold dotted line represents 1:1 enzyme to pyrophosphate concentration, indicating that the enzyme is performing single turnover.



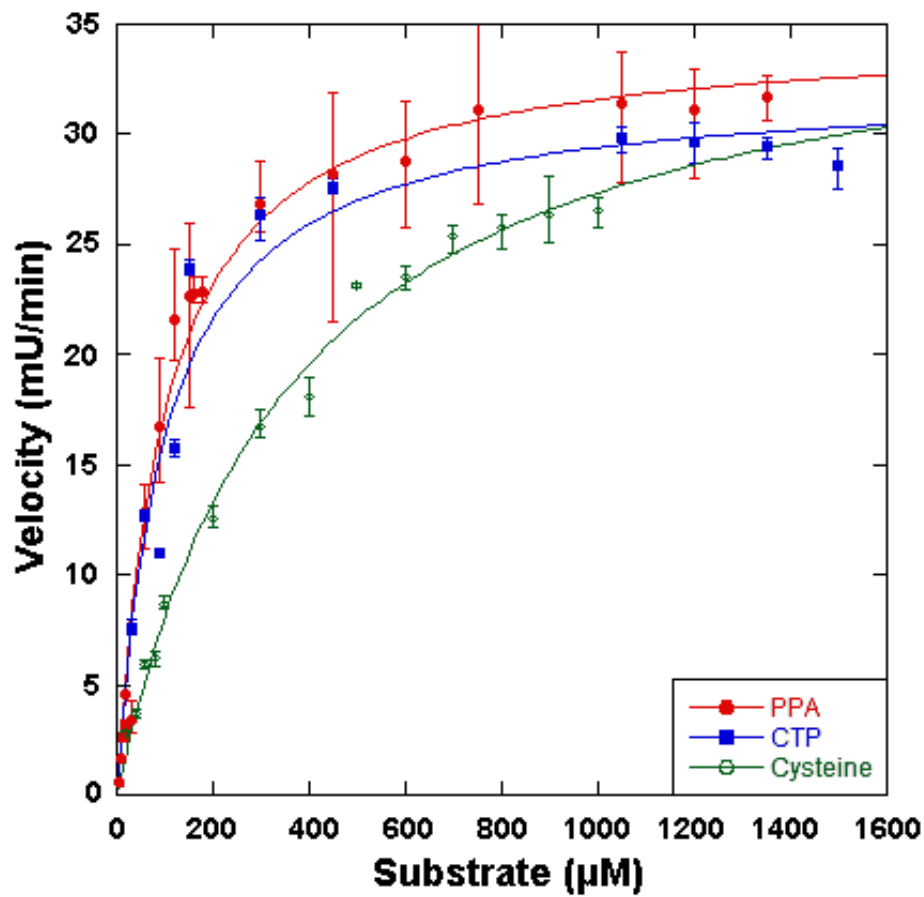


Figure 2.11: *S. pneumoniae* substrates  $K_m$  curves.

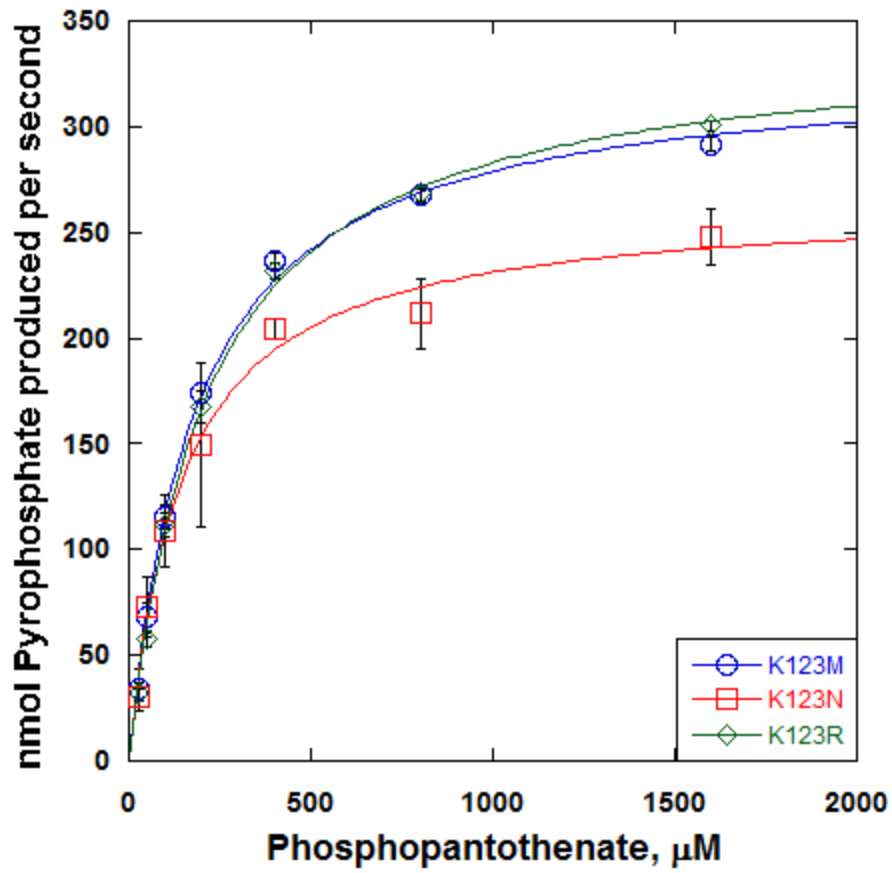


Figure 2.12: *S. pneumoniae* PPCS K123 mutants phosphopantothenate apparent Km curves.

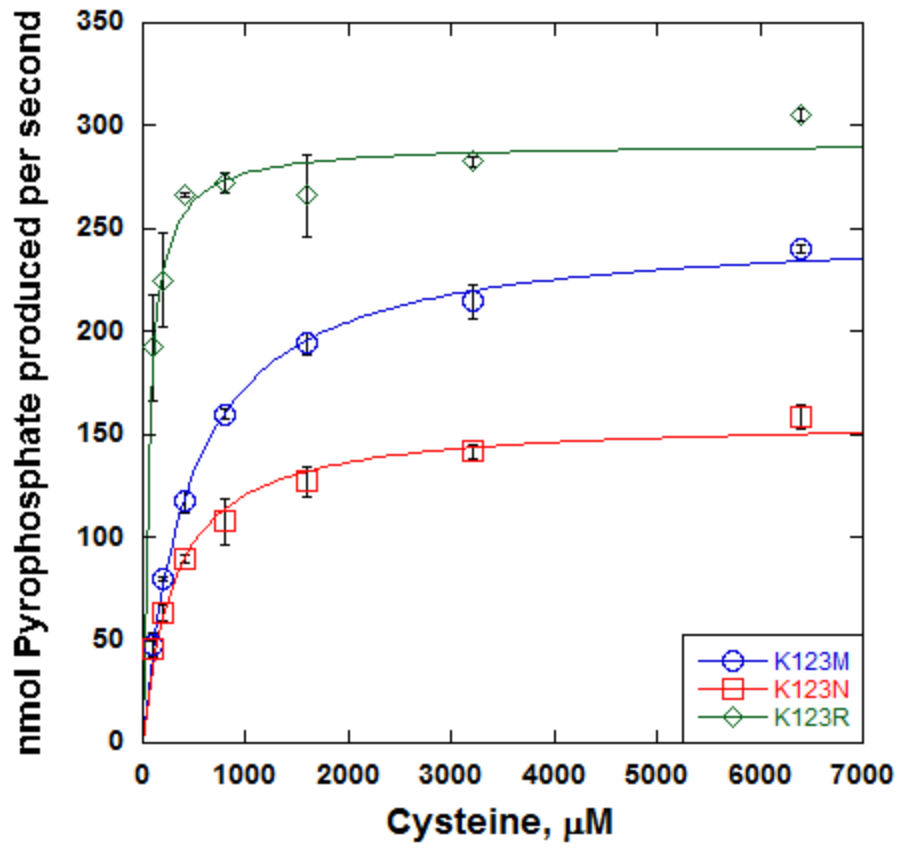


Figure 2.13: *S. pneumoniae* PPCS D93 mutants cysteine apparent Km curves.

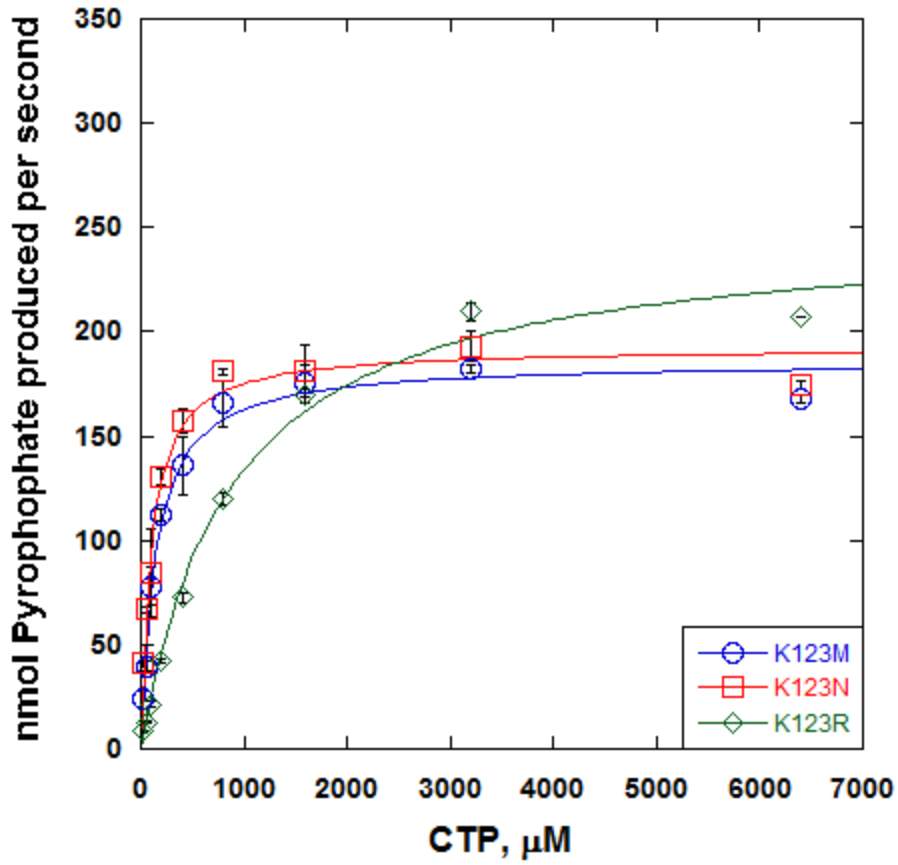


Figure 2.14: *S. pneumoniae* PPCS K123 mutants cytidine triphosphate apparent  $K_m$  curves.

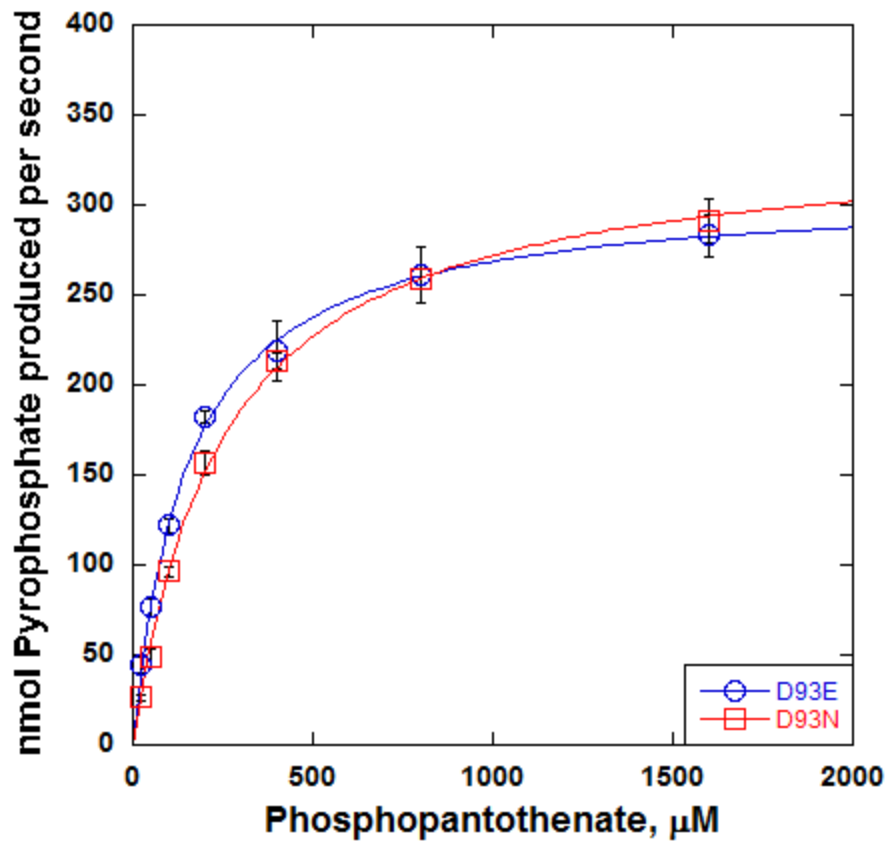


Figure 2.15: *S. pneumoniae* PPCS D93 mutants phosphopantothenate apparent Km curves.

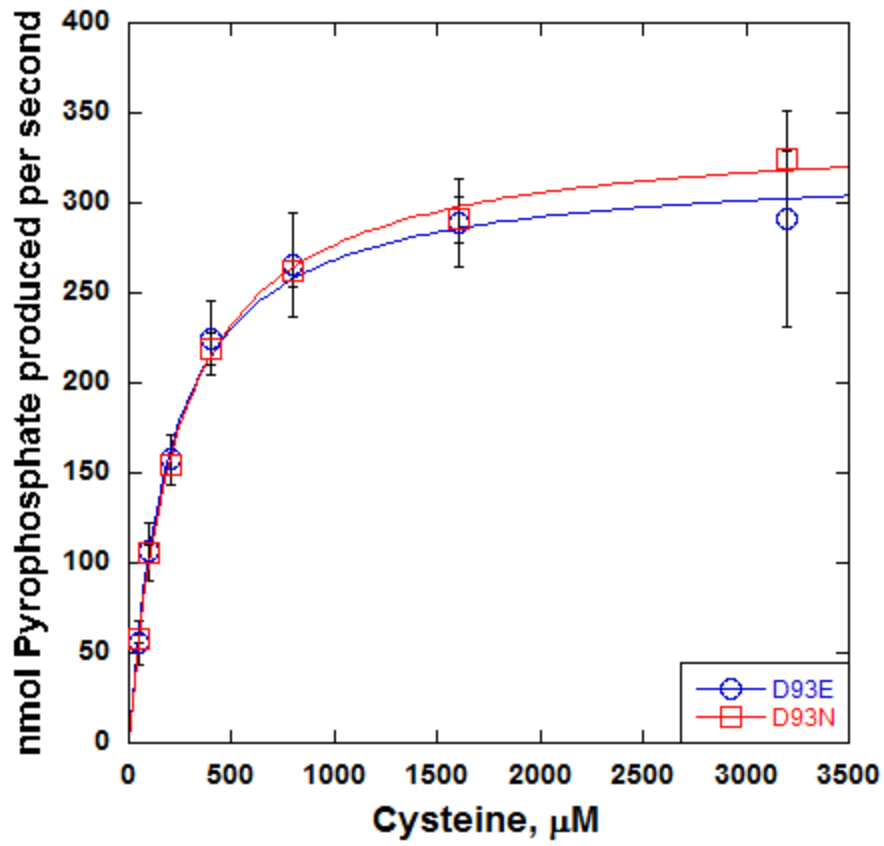


Figure 2.16: *S. pneumoniae* PPCS D93 mutants cysteine apparent Km curves.

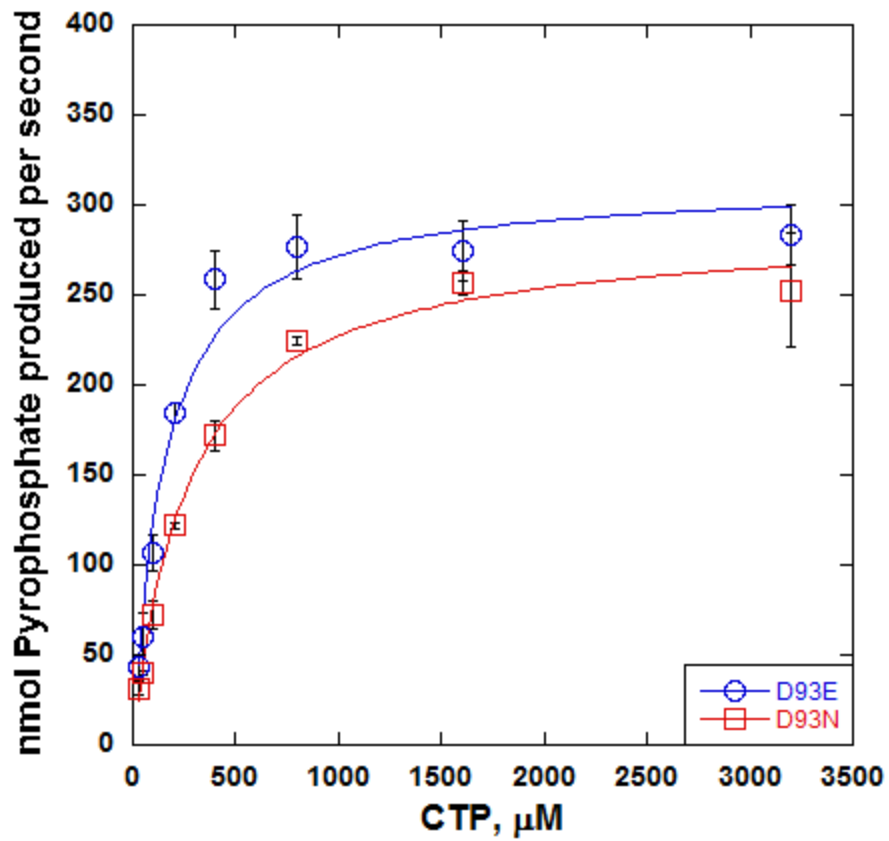


Figure 2.17: *S. pneumoniae* PPCS D93 mutants cytidine triphosphate apparent Km curves.

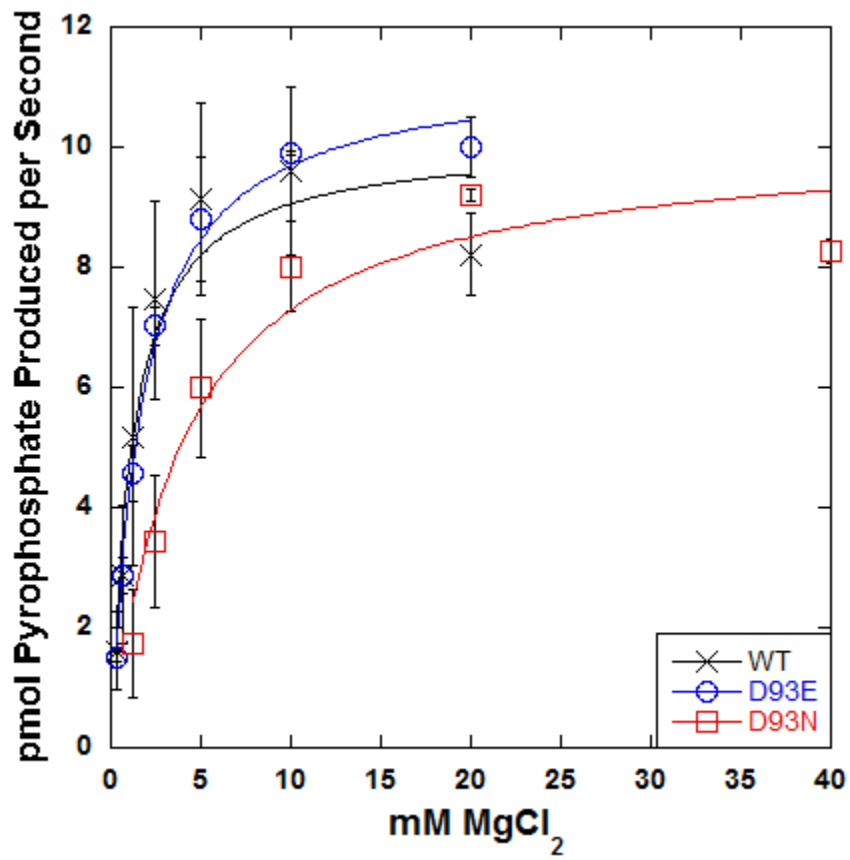
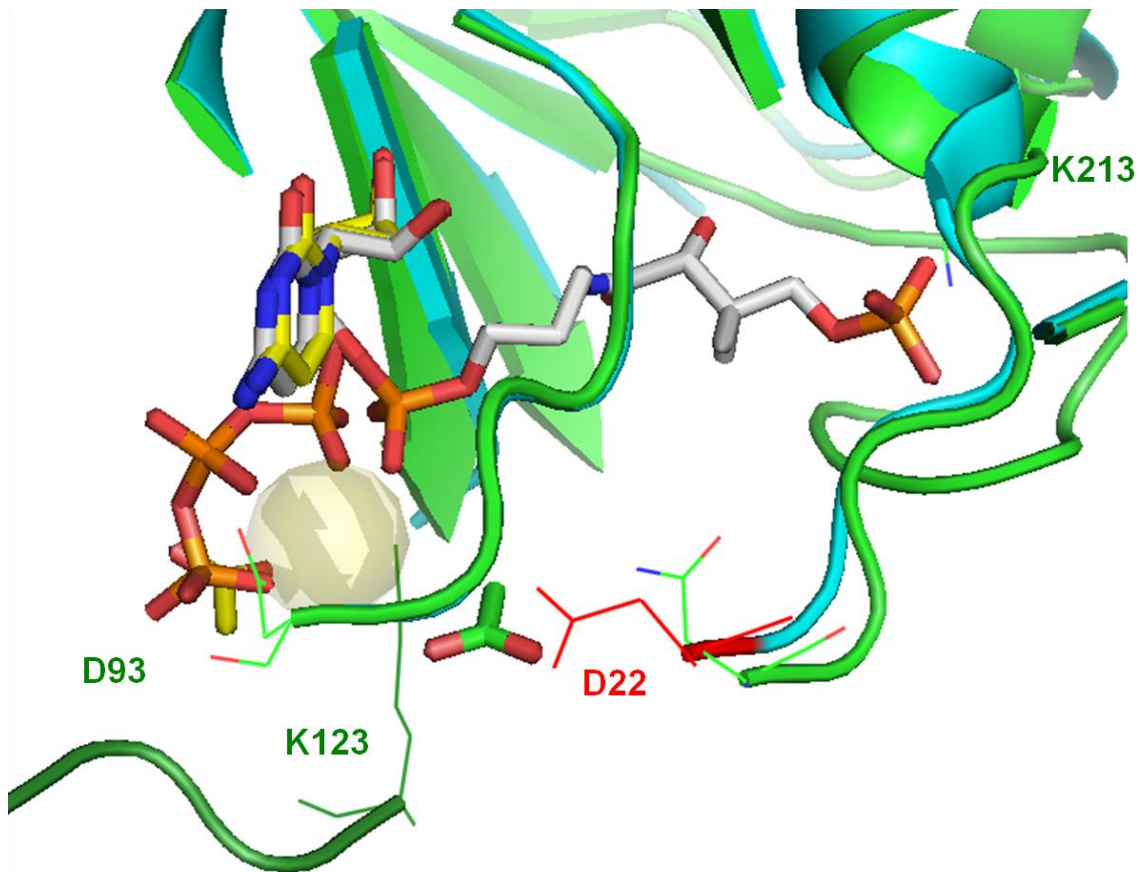


Figure 2.18: *S. pneumoniae* PPCS D93 mutants MgCl<sub>2</sub> apparent Km curves.





**Figure 2.19** Active site of bacterial PPCS. In green is the co-crystal structure of native *E. coli* PPCS with **JDP03** (in white) overlaid with 1U7W (teal), the structure of *E. coli* PPCS(N210D) in complex with CTP (yellow and orange). Residues highlighted are the conserved residues from *S. pneumoniae* PPCS.

## Chapter 3

### Molecular binding mechanism of RJPXD33 to early Raetz pathway acyltransferases

#### Background

An underexplored area in the arena of novel therapeutics advancement is in the research and development of single antimicrobials which are able to act upon multiple essential subcellular targets. Dual-targeting antimicrobial agents have been shown to reduce the frequency of selection of resistant mutants mediated by target mutation, due to the requirement of an organism to obtain multiple mutations in several targets in order to display clinically relevant resistance. One group of enzymes with very strong structural and functional relationships, and therefore amenable to a dual-targeting strategy, are acyltransferases found in bacterial lipopolysaccharide (LPS) biosynthesis.

Lipid A is the essential oligosaccharide moiety of lipopolysaccharide (LPS), responsible for anchoring the moiety to form the outer monolayer of the outer cell wall membrane of Gram-negative bacteria (1-3). Lipid A is essential to growth in most Gram-negative bacteria(4,5) and modification to lipid A plays a role in protecting the bacteria from environmental stress (2). During infection, released lipid A initiates the host-cell immune response via the TLR4-MD-2 complex (6-10). Overstimulation of this complex can occur and lead to septic shock and ultimately death (9,11,12). The requisite nature and toxicity of lipid A make its biosynthetic pathway an optimal target for antimicrobial chemotherapeutic discovery (5,13-16) .

The biosynthesis of lipid A consists of nine consecutive enzymatic processes. Acyltransferase LpxA performs the first step through a thermodynamically unfavorable reaction, utilizing an acyl carrier protein (ACP) to acylate UDP-*N*-acetylglucosamine (UDP-GlcNAc) at the 3-hydroxyl, producing UDP-3-*O*-(*R*-3-hydroxymyristoyl)-*N*-acetylglucosamine (**Figure 3.1**) (17,18). Subsequent deacylation of the *N*-acetyl moiety by LpxC provides the first committed step of lipid A biosynthesis and is a key regulatory step in the *E. coli* pathway (19-21). Acyltransferase LpxD utilizes ACP to catalyze the third reaction, acylating the free amine of the glucosamine ring (22). A peptide inhibitor (RJPXD33; TNLYMLPKWDIP-NH<sub>2</sub>) was recently identified and demonstrated affinity for both LpxD and LpxA. Crystal structures have been solved of the LpxA-RJPXD33 complex; however no structure has been solved for the LpxD-RJPXD33 complex. Both LpxA and LpxD are essential, cytosolic enzymes that contain significant sequence, structural, and functional homology with one another.

The nine enzymatic steps of Lipid A are constitutive. The glucosamine core of lipid A tends to be conserved across Gram-negative organisms though there is a high variability in the length of acyl chains incorporated by LpxA and LpxD. Differences in these acyl chain lengths play an integral role in the recognition by the host-immune system. In several species of LpxA, single amino acid residues have been identified as “hydrocarbon rulers,” limiting the length of acyl chains allowed to bind and be utilized by the enzyme (23). Recently our lab obtained a crystal structure of RJPXD33 bound to *E. coli* LpxA, wherein L6 of the peptide is within 2.8 Å of LpxA histidine 191, which has previously been identified as the hydrocarbon ruler.

Herein, acyltransferase binding studies utilizing various derivatives of RJPXD33 were undertaken in order to investigate key residues for binding of RJPXD33 to LpxD and discover how the peptide's structure dictates its dual inhibitor nature. Specifically, alanine scanning was performed on RJPXD33 to determine the contribution of each residue to the overall binding of LpxA and LpxD, and the residues important to the binding of both proteins. Additionally, residues responsible for the unique recognition of LpxA or LpxD were identified. Truncations of the RJPXD33 peptide were also made at the C-terminus in order to determine the minimum sequence necessary to inhibit LpxD. Additionally, peptide photo-affinity probes were crosslinked to LpxD in attempts to validate binding model of RJPXD33-LpxD with high resolution mass spectrometry.

RJPXD33 and RJPXD33c $\Delta$ 6 provide for a direct and competitive binding assay that has been tested in *E. coli* acyltransferases thus far. Through characterization of these peptides ability to bind non-*E. coli* acyltransferases, it may be possible to extend fluorescence polarization competitive assays as a viable high throughput method for the rapid identification of broad spectrum LpxA and LpxD inhibitors.

## **Materials and Methods**

*Materials.* LB (Lennox) broth and agar were purchased from Difco. Benzoylase was purchased from Novagen. Sephadex G-10 gel filtration media was purchased from MP Biomedicals. Bio-Rad Protein assay and BioGel P2 size exclusion gel was purchased from Bio-Rad. Ellman's Reagent and Streptavidin-coated resin were purchased from Thermo Fisher/Pierce. All buffers and antibiotics were purchased in the highest grade from Sigma Aldrich or Fisher Scientific.

*Cloning of E.coli lpxC, acpP, acpS, Vibrio harveyi aasS, and lpxA and lpxD from various bacterial species.* PCR protocols were carried out under standard conditions utilizing Pfu DNA Polymerase and DNA obtained from *Acinetobacter baumannii*, *Chlamydomophila pneumoniae*, *Chlamydia trachomatis*, *Escherichia coli*, *Helicobacter pylori*, *Neisseria meningitidis*, *Porphyromonas gingivalis*, and *Pseudomonas aeruginosa*. To perform the amplifications of the individual genes, primers used are found in **Table 3.1**. Amplified PCR products for *lpxA*, and *acpP* were cloned into pET24a using *NdeI* and *XhoI* restriction sites. Vectors containing a *his<sub>6</sub>-lpxD* were inserted into a pET23a plasmid that was modified with the addition of a his-tag encoding region with a *PmeI* (CACGTG) site inserted into the original *NdeI/HincII*. Plasmids were transformed into *E. coli* XL-1 Blue cells for amplification and plasmids isolated from these cells were sequenced at the University of Michigan Sequencing Core Facility. Plasmids with confirmed sequences were transformed to create the *E.coli* expression strains found in **Table 3.1**.

Proposed *lpxA* and *lpxD* were PCR amplified and individually cloned into pET23a using *NdeI* and *XhoI* restriction sites. All plasmids were transformed into *E. coli* XL-1 Blue cells for amplification and plasmids were isolated from these cell lines were sequenced at the University of Michigan Sequencing Core Facility. To construct expression strains, confirmed *lpxA* plasmids were transformed into BL21-AI and confirmed *lpxD* plasmids were transformed into Rosetta (DE3)/pLysS.

*Purification of holo-ACP.* Following a modified protocol from Broadwater and Fox, as published by Jenkins et. al. (24), holo-ACP was prepared. An overnight starter culture of BL21-AI/pET24a::*acpP*/pET23a::*acpS-his<sub>6</sub>* was used to inoculate 500 ml LB

media containing 50 µg/ml Ampicillin, 35 µg/ml Kanamycin. The cell culture was incubated at 37 °C with shaking at 250 rpm until an OD<sub>600</sub> of approximately 0.6 was reached. Protein expression was then induced by quickly cooling the culture to 18 °C, then adding 1 mM IPTG, 0.07% L-arabinose. The culture was allowed to grow overnight (at least 14 hours) at 18 °C with shaking at 250 RPM. Cultures were then cooled and harvested by centrifugation at 5,000 x g, 4 °C for 10 minutes. Cells were resuspended in 20 ml of 20 mM HEPES pH 8.0, 1mM TCEP and then disrupted by French press at 20,000 psi. To the cellular lysate, 20 ml of cold isopropanol was slowly added while gently mixing at 4 °C for 1 hour. The resulting suspension was centrifuged at 20,000 x g, 4 °C for 30 minutes. The supernatant was collected and gently mixed with 40 ml of 20 mM HEPES pH 8.0, 1 mM TCEP and then loaded onto a Source 15Q column (8 ml) pre-equilibrated with 20 mM HEPES pH 8.0, 1 mM TCEP. A 100 ml gradient of 20 mM HEPES pH 8.0, 1 mM TCEP containing 0-500 mM NaCl was performed and holo-ACP eluted at approximately 300 mM NaCl as determined by SDS-PAGE. The protein was then desalted on a P2 Bio-Gel column in 20 mM HEPES pH 8.0, 1 mM TCEP. Purified holo-ACP was lyophilized and stored at -20 °C. Protein concentrations were measured via BioRad protein assay.

*Purification of E. coli LpxA-his<sub>6</sub>.* An overnight starter culture of BL21-AI/pET23a::*lpxA-his<sub>6</sub>* was used to inoculate 2x250 ml LB (Lennox) media containing 50 µg/ml Ampicillin. The culture was incubated at 37 °C with shaking at 250 rpm until an OD<sub>600</sub> of approximately 0.6 was reached. The culture was induced with 1 mM IPTG, 0.07% L-Arabinose and allowed to further incubate at 37 °C for 4 hours post-induction. Cultures were then cooled and harvested by centrifugation at 5,000 x g, 4 °C for 10

minutes. Cells were resuspended in 10 ml of 10% glycerol, 20 mM HEPES pH 8.0 and stored at -80 °C. Cell suspensions were thawed and disrupted by French press at 20,000 psi and the insoluble debris was removed by centrifugation at 20,000 x g, 4 °C for 30 minutes. The resultant crude cytosol was applied to a 2 ml Nickel column (Qiagen), equilibrated with 50 mM Imidazole, 20 mM HEPES pH 8.0. The column was washed with 5 column volumes of 500 mM NaCl, 50 mM Imidazole, 20 mM HEPES pH 8.0 followed by 3 column volumes of 50 mM Imidazole, 20 mM HEPES pH 8.0. Histidine tagged enzyme was eluted from the column with 5 column volumes of 250 mM Imidazole, 20 mM HEPES pH 8.0. The enzyme was then loaded onto a 2 ml Source 15Q column, washed with 3 column volumes of 20 mM HEPES pH 8.0 and eluted over a gradient of 0-500 mM NaCl. Purified LpxA was desalted on a Bio-Gel P2 column and analyzed by SDS-PAGE. Protein concentration was determined by Biorad Protein Assay via the microplate protocol and reconfirmed based on UV absorbance at 280 nm ( $\epsilon = 9190 \text{ M}^{-1} \text{ cm}^{-1}$ ).

*Purification of E. coli his<sub>6</sub>-LpxD.* Previously generated *E. coli* expression strain Rosetta (DE3)/pLysS/pET23d::*his<sub>6</sub>-LpxD* were used to inoculate 500 ml TB media containing 50 µg/ml Ampicillin. The culture was incubated while shaking (250 rpm) at 37 °C until an OD<sub>600</sub> of 0.6-1.0 was reached. The culture was induced with 1 mM IPTG and allowed to incubate at 37 °C for 4 hours post-induction. The culture was then cooled and harvested by centrifugation at 5,000 x g, 4 °C for 10 minutes. Cells were resuspended in 10 ml of 10% glycerol, 20 mM HEPES pH 8.0 and stored at -80 °C. Cell suspensions were thawed and disrupted by French press at 20,000 psi and incubated on ice with 25 U/ml benzonase for 30 minutes. Insoluble debris was removed by centrifugation at

20,000 x g, 4 °C for 30 minutes. The resultant crude cytosol was applied to a 3 ml Nickel column (Qiagen), equilibrated with 50 mM Imidazole, 20 mM HEPES pH 8.0. The column was washed with 5 column volumes of 500 mM NaCl, 50 mM Imidazole, 20 mM HEPES pH 8.0 followed by 3 column volumes of 50 mM Imidazole, 20 mM HEPES pH 8.0. Histidine tagged enzyme was eluted from the column with 5 column volumes of 250 mM Imidazole, 20 mM HEPES pH 8.0. The enzyme was then loaded onto a 2 ml Source 15Q column, washed with 3 column volumes of 20 mM HEPES pH 8.0 and eluted over a gradient of 0-500 mM NaCl. Purified LpxD was desalted on a Bio-Gel P2 column and analyzed by SDS-PAGE. Protein concentrations were determined by Biorad Protein Assay via the microplate protocol and reconfirmed based on UV absorbance at 280 nm ( $\epsilon = 27,305 \text{ M}^{-1} \text{ cm}^{-1}$ ).

*Purification of E. coli LpxC.* An overnight starter culture of Rosetta (DE3)/pLysS/pET23a::lpxC-his<sub>6</sub> was used to inoculate 2x250 ml TB media containing 50 µg/ml Ampicillin, 20 µg/ml Chloramphenicol. The culture was incubated at 37 °C with shaking at 250 rpm until an OD<sub>600</sub> of approximately 0.6 was reached. The culture was induced with 1 mM IPTG and allowed to further incubate at 37 °C for 4 hours post-induction. Cells were cooled on ice, and then harvested by centrifugation at 5,000 x g for 10 min at 4 °C. The cells were then resuspended in 10 ml of 20 mM HEPES pH 8.0, 10 % glycerol, and either immediately lysed or frozen and stored at -80 °C until ready for lysis. The cell suspension was disrupted by at 20,000 psi, then incubated on ice for 30 minutes with 25 U/ml benzonase. Insoluble cell debris was then removed by centrifugation at 20,000 x g, 4 °C for 30 minutes. Soluble protein was loaded onto a 3 ml Ni-NTA (Qiagen) column pre-equilibrated in 20 mM HEPES pH 8.0, 50 mM imidazole. The



column was washed with 10 column volumes of 20 mM HEPES pH 8.0, 50 mM imidazole, 500 mM NaCl followed by 3 column volumes of 20 mM HEPES pH 8.0, 50 mM imidazole. Purified protein was then eluted with 20 mM HEPES pH 8.0, 250 mM imidazole, desalted on a Gio-Gel P2 column, and analyzed by SDS-PAGE. Concentration of *E. coli* LpxC-his<sub>6</sub> was determined by UV absorbance at 280 nm ( $\epsilon = 22,920 \text{ M}^{-1} \text{ cm}^{-1}$ ).

*Purification of V. harvey AasS-his<sub>6</sub>.* A 2 ml overnight starter culture of BL21-AI/pET23a::*aasS-his<sub>6</sub>* was used to inoculate 2x250 ml LB media containing 50 µg/ml Ampicillin. The cells were incubated at 37 °C with shaking at 250 rpm until an OD<sub>600</sub> of approximately 0.6 was reached. Cultures were induced with 1 mM IPTG and 0.07% L-arabinose and allowed to incubate at 37 °C for 4 hours post-induction. Cells were cooled on ice, and then harvested by centrifugation at 5,000 x g for 10 min at 4 °C. The cells were then resuspended in 10 ml of 20 mM HEPES pH 8.0, 10 % glycerol, and either immediately lysed or frozen and stored at -80 °C until ready for lysis. The cell suspension was disrupted by at 20,000 psi, then incubated on ice for 30 minutes with 25 U/ml benzonase. Insoluble cell debris was then removed by centrifugation at 20,000 x g, 4 °C for 30 minutes. Soluble protein was loaded onto a 3 ml Ni-NTA (Qiagen) column pre-equilibrated in 20 mM HEPES pH 8.0, 50 mM imidazole. The column was washed with 10 column volumes of 20 mM HEPES pH 8.0, 50 mM imidazole, 500 mM NaCl followed by 3 column volumes of 20 mM HEPES pH 8.0, 50 mM imidazole. Protein was then eluted with 20 mM HEPES pH 8.0, 250 mM imidazole, and analyzed by SDS-PAGE. Purified protein was desalted on a Bio-Gel P2 column in 20 mM Tris-HCl pH 7.5, 10% glycerol, 1 mM EDTA, 0.1 mM TCEP, 0.002% Triton-X100, aliquoted into

microfuge tubes and stored at -80 °C for optimal storage (25). Concentration for *V. harvey* AasS-his<sub>6</sub> was determined by UV absorbance at 280 nm ( $\epsilon = 65,780 \text{ M}^{-1} \text{ cm}^{-1}$ ).

*Fmoc-Photoleucine.* Fmoc-PhotoLeu was synthesized as previously described (26). A 100 ml round bottom flask was covered with aluminum foil and kept on ice. In the flask, 200 mg PhotoLeu (1.4 mmol) and 236 mg sodium bicarbonate (2.8 mmol) were dissolved in 20 ml H<sub>2</sub>O. In 10 ml of THF, 708 mg Fmoc-OSu (2.1 mmol) was dissolved and added dropwise over 15 minutes into the PhotoLeu solution. The slurry was allowed to stir on ice for 10 minutes, and then stirred at room temperature for 8 hours. The flask was then placed on ice and the reaction quenched by adding 75 ml of 1:2 water:ethyl acetate followed by acidification to pH 2 with the dropwise addition of HCl. The product was extracted three times with 50 mL ethyl acetate. The organic layer was collected and applied to a rotary evaporator in order to concentrate the product. Resulting white solid was purified by flash chromatography with 1% methanol (v/v) and 1% acetic acid (v/v) in dichloromethane. The product was obtained as a white solid (440 mg, 86%). <sup>1</sup>H NMR (400 MHz, DMSO)  $\delta$  12.70 (s, 1H), 7.87 (d, J = 7.5, 2H), 7.71 (dd, J = 7.6, 4.4, 3H), 7.39 (t, J = 7.4, 2H), 7.30 (t, J = 7.4, 2H), 4.38 - 4.16 (m, 3H), 3.89 - 3.76 (m, 1H), 1.93 - 1.81 (m, 1H), 1.63 (dd, J = 14.8, 10.8, 1H), 0.99 (s, 3H). HRMS ESI<sup>+</sup>: calculated for [M+Na]<sup>+</sup>, 388.1278; observed 388.1276.

*Fluorescence Polarization (FP) Assay.* Peptides were synthesized as previously reported for solid phase peptide synthesis (2). The FP assay was performed as previously described (3). In 384-well black Costar plates, His<sub>6</sub>-LpxD and iodoacetamide treated His<sub>6</sub>-LpxD were serially diluted while holding FITC-RJPXD33 at 20 nM in a final volume of 50  $\mu$ L in 20 mM HEPES pH 8.0, 0.01% Triton-X100. The wells were gently mixed and

incubated in the dark at 30 °C for 15 minutes in a SpectraMax M5 plate reader.

Polarization was measured by the plate reader in triplicate with readings taken at  $\lambda_{\text{ex}} = 485 \text{ nm}$  and  $\lambda_{\text{em}} = 525 \text{ nm}$ . The binding data was first fit to a standard binding isotherm (eq 1) with KaleidaGraph:

$$mP = mP_f + \left[ (mP_b - mP_f) \left( \frac{[P]}{[P] + K_d} \right) \right]$$

where  $mP$  is the experimentally determined polarization,  $mP_f$  is the polarization of free FITC-RJPXD33,  $[P]$  is the total acyltransferase concentration,  $K_d$  is the dissociation constant of peptide-protein complex, and  $mP_b$  is the polarization value of the fully bound fluorescent peptide. The calculated  $mP_b$  was used to normalize the experimental data in order to fit the binding curves to the Hill equation (eq. 2):

$$\alpha = \frac{\left( \frac{[P]}{K_d} \right)^h}{1 + \left( \frac{[P]}{K_d} \right)^h}$$

where  $\alpha$  is the fraction of bound fluorescent peptide,  $[P]$  is the concentration of acyltransferase,  $K_d$  is the dissociation constant of the protein-peptide complex, and  $h$  is the Hill coefficient.

*Competitive Binding Assay.* Varying concentrations of unlabeled peptides were incubated for 10 minutes at 30 °C with 220-660 nM acyltransferase (concentration held at the  $K_d$  determined for the fluorescent tracer). Fluorescent tracer was then added to a final concentration of 20 nM, and the mixture was further incubated for 10 minutes.

Polarization was then measured by the SpectraMax M5 plate reader in triplicate with readings taken at  $\lambda_{\text{ex}} = 485 \text{ nm}$  and  $\lambda_{\text{em}} = 525 \text{ nm}$ . The  $[I]_{50}$  was determined from the

competition binding curve and the dissociation constant of the unlabeled ligand was calculated as previously described using eq. 3:

$$K_i = \frac{[I]_{50}}{\frac{[L]_{50}}{K_d} + \frac{[P]_0}{K_d} + 1}$$

where  $[I]_{50}$  is the unlabeled peptide concentration at 50% inhibition,  $[L]_{50}$  is the free ligand (fluorescent tracer) concentration at 50% inhibition,  $[P]_0$  is the free protein concentration at 0% inhibition,  $K_d$  is the dissociation constant of the fluorescent tracer, and  $K_i$  is the calculated dissociation constant for the unlabeled ligand.

*Iodoacetamide Modification.* Iodoacetamide (10 mM) was incubated in the dark at room temperature with LpxD (150  $\mu$ M) in 20 mM HEPES pH 8.0 at a final volume of 500  $\mu$ L for 45 minutes. The reaction was subsequently loaded onto a 3 ml BioGel P2 size exclusion column equilibrated with 0.1 M Tris-HCl pH 7.5. The acylated protein was eluted with 0.1 M Tris-HCl pH 7.5, collected in 50  $\mu$ L fractions, and monitored by the Bio-Rad Protein Reagent. Protein fractions were combined and concentrated via ultrafiltration in a Microcon YM-10 concentrator (Millipore) to a final concentration of 244  $\mu$ M and kept on ice until use in the assays.

*Ellman's Assay.* In a polystyrene semi-micro cuvette (Brandtech), 0.12 mg of LpxD or iodoacetamide treated LpxD was diluted to a final volume of 980  $\mu$ L in 0.1 M Tris-HCl pH 7.5. with or without 5.3 M urea. The protein was incubated at room temperature for 5 minutes then 20  $\mu$ L of 10 mM Ellman's reagent in 50 mM HEPES pH 7.0 and mixed by inversion. Subsequently, the absorbance of the solution was read at 412 nm, blanked against the solution containing no protein, in a SpectraMax M5 for 10 minutes. The absorbance readings plateaued by 10 minutes and the max absorbance

reading was used to determine the number of modified sulfhydryls using Beer-Lambert's Law and a molar extinction coefficient of  $13,600 \text{ M}^{-1} \text{ cm}^{-1}$ .

*Covalent Crosslinking of Photoaffinity Probes to LpxA and LpxD.* On ice in clear 96-well half-area plates, 24  $\mu\text{M}$  photoactivatable peptides were incubated with 10  $\mu\text{M}$  acyltransferase in the presence or absence of 150  $\mu\text{M}$  unlabeled peptide in a final volume of 30  $\mu\text{L}$  in 20 mM HEPES pH 8.0 (DMSO 1% v/v). Plates, remaining on ice, were irradiated at  $\lambda = 365 \text{ nm}$  for 10 minutes using a UV lamp (UVP model UVGL-58) at a distance of  $\sim 2 \text{ cm}$ . Gel loading buffer was added directly to the samples, which were subsequently loaded and run on a 12% Tris-glycine SDS-PAGE gel. Gels were washed three times for 20 minutes at room temperature with deionized water to remove SDS. Fluorescein-labeled peptides were analyzed for in-gel fluorescence using a Typhoon 9400 imaging system set to fluorescein wavelength ( $\lambda_{\text{ex}} = 485 \text{ nm}$  and  $\lambda_{\text{em}} = 525 \text{ nm}$ ), PMT sensitivity at 500 and pixel size at 50 microns. Resulting data was visualized using ImageQuant 5.2 software (RSBS-ANU). Following in-gel fluorescence, analysis, gels were stained using SimplyBlue SafeStain (Invitrogen).

*Identification of crosslinked photoaffinity probes to LpxD protein fragments.* On ice in clear 96-well half-area plates, 10  $\mu\text{M}$  photoactivatable peptides were incubated with 10  $\mu\text{M}$  acyltransferase in a final volume of 4 aliquots of 30  $\mu\text{L}$  in 20 mM HEPES pH 8.0 (DMSO 1% v/v). Plates, remaining on ice, were irradiated at  $\lambda = 365 \text{ nm}$  for 15 minutes using a UV lamp (UVP model UVGL-58) at a distance of  $\sim 2 \text{ cm}$ . Following irradiation, these aliquots were loaded and run on a 12% Tris-Glycine SDS-PAGE gel. Gels were washed 3 times with water and the protein band was stained with Coomassie Brilliant Blue. The single protein bands were isolated, excised, and transferred to a

microcentrifuge tube that was pretreated with 0.1 % TFA in 50% Acetonitrile. In-gel Trypsin digest was performed using the Sigma protocol: Gel pieces were washed twice at 37 C for 30 minutes with 200  $\mu$ L of 20 mM ammonium bicarbonate in 40% acetonitrile. Gel pieces were dried in a Speed Vac, then digested overnight at 37 C by the addition of 0.4  $\mu$ g of Tryptsin in 70  $\mu$ L 40 mM ammonium bicarbonate in 9% acetonitrile. Protein fragments were loaded directly onto an HPLC column and separated on a gradient of 5-95% acetonitrile over 35 minutes at a flow rate of 1 ml/min. Fractions were monitored at  $\lambda = 490$  nm and peaks were lyophilized, resuspended in 20  $\mu$ L deionized water, and submitted for LC-UV-MS. Concentrations of the peaks estimated based on the absorbance of fluorescein at  $\lambda = 490$  nm ( $\epsilon = 8300 \text{ M}^{-1} \text{ cm}^{-1}$ ).

## Results and Discussion

*Activity of truncated RJPXD33.* Determining the shortest chain length of the peptide is important for peptidomimetics as it provide the smallest scaffold with highest potency. To accomplish this, a series of C and N-terminally truncated peptides were synthesized and tested for binding to *E. coli* LpxA and LpxD.

Previously, Ronald Jenkins performed N-terminal truncations of RJPXD33 (**Table 3.2**) (27,28). From his findings, RJPXD33(N $\Delta$ 1) caused a complete loss of binding to LpxA. Thus, it was determined that residue Thr1 is essential to the binding of the peptide to the acyltransferase. As such, it was not necessary to test the remaining peptide series against LpxA, as none contained the essential Thr1. N-terminal truncations of RJPXD33 had a much less dramatic impact on LpxD binding. Loss of the N-terminal TN had little impact on binding. Truncation of Leu3 caused a 7.5-fold decrease in

binding affinity to LpxD, and truncation of Tyr4 resulted in a complete loss of binding to LpxD.

To complete the peptide truncations study, C-terminal truncations were synthesized and tested for binding potency to *E. coli* LpxA and LpxD (**Table 3.2**). Unlike the N-terminal truncations, C-terminal truncations of RJPXD33 had little overall effect on the binding of the peptide to LpxA. Truncations up to RJPXD33(CΔ3) had had similar binding affinity (5.7 μM) as the full length peptide (4.4 μM). Peptide RJPXD44(CΔ4) exhibited a 3-fold loss in potency, which could be a result of unfavorable interactions of the exposed basic Lys8. Truncation to RJPXD33(CΔ5) exhibited a further loss of binding affinity to LpxA, which may be a result of the placement of the exposed Pro7, because truncation to RJPXD33(CΔ6) increased potency, back to a 10.5 μM  $K_d$  to LpxA. This minor loss in overall binding affinity to LpxA indicates that only the six N-terminal residues of RJPXD33, equivalent to RJPXD33(CΔ6), are required for binding.

C-terminally truncated peptides were also tested against *E. coli* LpxD. Initial C-terminal truncations had a beneficial impact on affinity to LpxD, as RJPXD33(CΔ3) bound 4-fold more tightly (0.5 μM) to the acyltransferase than the full length peptide. This is an indication that Asp10 isn't forming any major interaction in the peptide-LpxD complex, as loss of Asp10 increased binding affinity. Truncations past Trp9 demonstrated a decrease in binding to LpxD, with RJPXD33(CΔ6), exhibiting a  $K_d$  greater than 50 μM. From these truncation studies, it appears that the shortest peptide to exhibit high affinity to LpxD would be RJPXD33(NΔ2, CΔ3): YMLPKW. The shortest peptide to exhibit dual affinity to LpxA and LpxD would be RJPXD33(CΔ3): TNLYMLPKW.

*Effects of C-terminal carboxylic acid on the binding of FITC-RJPXD33*

*truncations*. Through the utilization of Wang resin rather than Rink amide resin, it was possible to synthesize a series of FITC-labeled peptides with a C-terminal carboxylic acid. In this manner, it is possible to test the effects of a negative charge being moved through the RJPXD33 binding site. Thus, direct binding studies would highlight positions where the addition (or omission) of an acidic moiety would be beneficial in the rational design of a small molecule inhibitor of LpxA and LpxD.

**Table 3.3** lists the direct binding results of these carboxylate-capped peptides against *E. coli* LpxA. Overall, this series of peptides bound slightly tighter to LpxA than FITC-RJPXD33 with the C-terminal amide, with the exception of FITC-RJPXD33(C $\Delta$ 4)-COOH. This drop in affinity could be due to the C-terminal carboxylic acid being adjacent to the basic Lys8, causing instability to the structure of the peptide as a whole, as this peptide had a similar loss in affinity to LpxD. FITC- $\beta$ -TNLYML-COOH afforded the highest affinity to LpxA, with a 2.3-fold increase in affinity compared to FITC-RJPXD33. The addition of the C-terminal carboxylic acid had an adverse effect on the affinity of FITC-RJPXD33 to LpxD. This would corroborate that RJPXD33 is binding to a hydrophobic region of LpxD, as the addition of an acidic moiety anywhere along the 6 C-terminal residues of LpxD caused a loss in affinity.

*Alanine-scan of RJPXD33*. To further characterize the binding of RJPXD33, it was essential to determine which residues are responsible for binding to the acyltransferases and selectivity between LpxA and LpxD. By systematically replacing each residue of the 12-mer RJPXD33 peptide with alanine and determining its new binding capacity to the acyltransferases, we obtain an estimation of how valuable the mutated residue is to the overall binding of the peptide. The results of these binding assays are presented in **Table 3.4**.



A graphical representation of the affinity of the alanine series of peptides against *E. coli* LpxA is presented in **Figure 3.2**. Supporting the truncation studies, swapping Thr1 to and alanine caused a complete loss of affinity to LpxA. RJPXD33(L3A) and RJPXD33(Y4A) also exhibited complete loss of affinity for LpxA. RJPXD33(N2A) also exhibited a nearly 20-fold drop in binding affinity to LpxA. The large to complete loss of binding affinity from swapping these 4 C-terminal residues to alanine further highlights the essentiality of these residues in the RJPXD33-LpxA binding complex.

Interestingly, Thr1 and Asn2 had little impact on the binding RJPXD33 to LpxD (**Figure 3.3**); however mutation of Leu3 caused a 7-fold drop in binding capacity. Moreover, Tyr4 is essential for the binding of the peptide to both LpxA and LpxD, as mutation of this residue to alanine caused the peptide to no longer bind either acyltransferase. The alanine mutations showed that each individual component of the YML motif is essential to the binding of the entire RJPXD33 peptide to LpxD. Additionally, mutation of Pro7 caused a nearly 45-fold drop in the binding efficiency to LpxD while having a nominal effect on the binding to LpxA.

Mutation of Trp9 appeared to have a large impact on the binding of the peptide to both LpxA and LpxD (**Figure 3.4**), however this could be that the swapping of the bulky tryptophan to a much smaller alanine side chain places Lys8 and Asp10 into much closer proximity, allowing them to interact and develop secondary structure that would impede the binding of the peptide to the acyltransferases.

*Inhibitory effects of truncated and alanine-substituted peptides.* In order to validate the binding of these peptides correlated with inhibition of the acyltransferases, the IC<sub>50</sub> of each peptide was determined against both LpxA and LpxD. For this, the

forward direction of the acyltransferase was monitored using a previously developed continuous fluorescent assay (24).

C-terminal truncations of RJPXD33 against both LpxA and LpxD caused a decrease in the potency of the peptide (**Table 3.2**) However, RJPXD33(CΔ3) had no decrease on potency when compared to the full length peptide. Thus, the C-terminal DIP are not required for activity of the peptide.

Alanine-scan peptides further verified that the 6 N-terminal residues of RJPXD33 are required for inhibitory activity against LpxA. Mutation of any of these residues to alanine resulted in at least a 5-fold drop in potency, though most caused the peptide to be completely ineffective. Interestingly, Trp9 is required for inhibitory activity of the full length peptide against LpxA. Additionally, Lys8 and Asp10 had little overall impact on inhibitory activity of RJPXD33.

The alanine-scan peptides also highlighted the essential nature of the YML motif in binding and inhibiting LpxD, as mutation of any of these residues caused the peptide to be ineffective. Pro7 and Trp9 are integral to the potency of RJPXD33, as mutations of these residues cause a 20-fold loss of inhibition. Overlays of the LpxA and LpxD crystal structures suggest that Pro7 is important in bending the peptide into the groove toward the C-terminal  $\alpha$ -helical extension of LpxD (28).

From the truncation and alanine studies, we have learned that Trp9 is interacting with LpxA and LpxD in a manner integral to inhibitory activity, which is significant as the 6 C-terminal residues of RJPXD33 did not have a density in the RJPXD33-LpxA crystal structure. In **Figure 3.4**, we have an overlay of the residue activities of RJPXD33 against both LpxA and LpxD. It is quickly apparent that Lys8 has little impact on the

binding or inhibition of the overall peptide. Going forward, the shortest length, most potent peptide to inhibit both LpxA and LpxD is TNLYMLPAW.

*Crosslinking of Photopeptides to LpxD.* Crystallographic data is available for RJPXD33-LpxA, but we were unable to obtain a structure of RJPXD33-LpxD. As an alternative to obtaining a crystal structure, a series of FITC-labeled photopeptides were synthesized. This series of peptides introduced a diazine-containing leucine residue in place of Leu3 (Photo 1), Leu6 (Photo3), or Ile11 (Photo 4). By incubating the photopeptides with LpxA and LpxD and adding UV light to mixture, photo-leucine activates and forms a covalent bond with the protein, near the normal binding location of the peptide. From this FITC-photopeptide-protein linkage, the enzyme can be digested and the segment of enzyme linked to the FITC-photopeptide can be recollected and submitted to MALDI-MS. In doing so, we can identify the location the peptide binds the protein, and thus identify key residues in the molecular binding mechanism of the peptide.

The first step in this endeavor was to test that the photopeptides could still bind LpxA and LpxD. Thus, direct bind FP assays were performed (**Figure 3.5**). These peptides were able to bind to LpxA and LpxD with similar affinity to that of RJPXD33 (**Table 3.5**). As these peptides were able to bind LpxA and LpxD, they were tested for in-gel fluorescence following crosslinking and SDS-PAGE. Photopeptides 1, 3, and 4, were all able to crosslink both LpxA and LpxD and exhibit in-gel fluorescence (**Figure 3.6**). These photopeptides bound in the same location as RJPXD33, as addition of the unlabeled peptide to the mixture was able to compete with the photopeptide crosslinking.

*Iodoacetamide Modification of LpxD.* To limit the amount of off target crosslinking of the photopeptides, acylation of cysteine residues of LpxD by iodoacetamide modification was investigated. First, the number of solvent exposed cysteine moieties of LpxD could be determined from Ellman's Assay. For unmodified LpxD, the ratio in absorbance between denatured and native protein was calculated to be approximately 7:2. As there are 7 cysteine residues in LpxD, there are thus 2 solvent exposed cysteine residues that are open to sulfhydryl modification by DTNB in the native protein. From the Ellman's Assay of the urea denatured iodoacetamide treated LpxD, it was determined that approximately 5 of the 7 cysteine residues of LpxD were acylated.

The FP assay was performed on iodoacetamide treated LpxD to determine if acylation of the 5 exposed cysteines affected RJPXD33 binding (**Figure 3.7**). These residues do not appear to effect RJPXD33 binding, as the peptide was able to bind both native and acylated LpxD with roughly the same affinity ( $K_d = 2.8 \mu\text{M}$  for native LpxD,  $K_d = 3.1 \mu\text{M}$  for iodoacetamide treated LpxD).

FITC-Photopeptides were crosslinked to both native and iodoacetamide modified LpxD. Excess peptide was washed away and the covalent photopeptide-LpxD complex underwent protein digest. The digested protein mixture submitted to HPLC, and the fraction containing the crosslinked photopeptide was collected by monitoring at 490 nm for the FITC moiety. These collected fragments were submitted to collaborators at the University of Michigan Biomedical Mass Spectrometry Facility for MALDI MS in order to determine the mass of these fragments. They were unable to obtain a mass for the first round of fragments. The process was scaled up and we are currently awaiting results.

*Binding of RJPXD33 to acyltransferases from other organisms.* In order to further utilize RJPXD33 as a chemical biological probe, the binding affinity of RJPXD33 was determined against a wide spectrum of gram negative bacteria, including *Acinetobacter baumannii*, *Chlamydia pneumoniae*, *Chlamydia trachomatis*, *Helicobacter pylori*, *Neisseria meningitides*, *Porphyromonas gingivalis*, and *Pseudomonas aeruginosa*. These represent LpxA and LpxD that incorporate varying length acyl chains into the glucosamine core. By testing RJPXD33 against this array, we can determine how broad spectrum the peptide scaffold offers and also the utility of RJPXD33 in screens for compounds against a wider array of bacterial species.

There appeared to be no connection between the acyl-chain preference of the enzyme and the affinity of FITC-RJPXD33 to the enzyme, as both *A. baumannii* and *N. meningitidis* LpxA incorporate OH-C12 acyl chains, yet FITC-RJPXD33 a  $K_d$  3.01  $\mu$ M against *A. baumannii* LpxA and a  $K_d >100$   $\mu$ M against *N. meningitidis* LpxA. Additionally, the ability of RJPXD33 to bind the LpxA of a species does not guarantee it also binds the LpxD of that species. For example, FITC-RJPXD33 has a  $K_d$  17.8  $\mu$ M against *P. aeruginosa* LpxA, and a  $K_d >100$   $\mu$ M against *P. aeruginosa* LpxD. Overall, RJPXD33 does appear to be a useful broad spectrum chemical biological probe of Raetz acyltransferases, as it was able to bind most of the explored enzymes.

## **Conclusion**

Through binding and inhibition studies of LpxA and LpxD with peptide RJPXD33 analogs, we were able to determine the key residues in the molecular binding mechanism of the peptide to the proteins. Through N-terminal truncations, we determined

that T1 is essential to binding to LpxA, and that the first N-terminus residue essential to LpxD recognition is M5. C-terminal truncations revealed that the 6 C-terminal residues have little impact on LpxA recognition, but loss of W9 causes a drop in IC<sub>50</sub> from 27.4 μM to 66.6 μM, against LpxA and a drop in IC<sub>50</sub> from 3.2 μM to >100 μM against LpxD. This is likely due to the loss of a large, bulky group to assist in preventing the acyl-phosphopantetheine prosthetic arm of acyl-ACP from associating with the acyltransferase. **Figure 3.8** are the crystal structures of LpxA-RJPXD33 (28) overlaid with that of LpxD-acyl-ACP (29), illustrating this space. This structural overlay also gives insight to the significance of P7, as substitution of the proline to alanine resulted in a 44-fold drop in affinity to LpxD (2.03 μM to 89.6 μM) and a 20-fold loss in inhibition of LpxD (3.2 μM to 64 μM). The proline is likely creating a vital hairpin turn in the peptide secondary structure, allowing W9 to occupy a more structurally relevant space.

While TNLYML has been identified as the shortest peptide to bind both LpxA and LpxD with high affinity, TNLYMLPKW has been identified as the optimal peptide for high affinity binding and inhibition of both acyltransferases, with a sub 6 μM binding affinity to both LpxA (5.7 μM) and LpxD (0.5 μM), and inhibit LpxA with an IC<sub>50</sub> of 26.7 μM and LpxD with an IC<sub>50</sub> of 2.4 μM. Alanine substitution elucidated that K8 resulted in a slight improvement of inhibition of the full length peptide to LpxA (20.6 μM IC<sub>50</sub>). As a basic residue at this position appears to be of little inhibitory or binding consequence to either acyltransferase, TNLYMLPAW would be the best peptidic scaffold to begin rational design of small molecule dual targeting inhibitors.

Additionally, FITC-RJPXD33 proved to be useful probe in investigating a broader spectrum of bacterial Raetz pathway acyltransferases. Interestingly, these

peptides appeared to be more useful as LpxA probes than LpxD, those this may have been in part due to difficulties in the expression and purification of *Chlamydia* and *Helicobacter* LxpD.

## REFERENCES

1. Nikaido, H. (2003) *Microbiology and Molecular Biology Reviews* **67**, 593-656
2. Raetz, C. R. H., Reynolds, C. M., Trent, M. S., and Bishop, R. E. (2007) *Annual Review of Biochemistry* **76**, 295-329
3. Raetz, C. R. H., and Whitfield, C. (2002) *Annual Review of Biochemistry* **71**, 635-700
4. Meredith, T. C., Aggarwal, P., Mamat, U., Lindner, B., and Woodard, R. W. (2006) *ACS Chemical Biology* **1**, 33-42
5. McClerren, A. L., Endsley, S., Bowman, J. L., Andersen, N. H., Guan, Z., Rudolph, J., and Raetz, C. R. H. (2005) *Biochemistry* **44**, 16574-16583
6. Gay, N. J., and Gangloff, M. (2007) *Annual Review of Biochemistry* **76**, 141-165
7. Kim, H. M., Park, B. S., Kim, J.-I., Kim, S. E., Lee, J., Oh, S. C., Enkhbayar, P., Matsushima, N., Lee, H., Yoo, O. J., and Lee, J.-O. (2007) *Cell* **130**, 906-917
8. Beutler, B., and Cerami, A. (1988) *Annual Review of Biochemistry* **57**, 505-518
9. Poltorak, A., He, X., Smirnova, I., Liu, M.-Y., Huffel, C. V., Du, X., Birdwell, D., Alejos, E., Silva, M., Galanos, C., Freudenberg, M., Ricciardi-Castagnoli, P., Layton, B., and Beutler, B. (1998) *Science* **282**, 2085-2088
10. Visintin, A., Halmen, K. A., Latz, E., Monks, B. G., and Golenbock, D. T. (2005) *The Journal of Immunology* **175**, 6465-6472
11. Russell, J. A. (2006) *New England Journal of Medicine* **355**, 1699-1713
12. Lynn, M., Rossignol, D. P., Wheeler, J. L., Kao, R. J., Perdomo, C. A., Noveck, R., Ramon, V., D'Angelo, T., Gotzkowsky, S., and McMahon, F. G. (2003) *The Journal of Infectious Diseases* **187**, 631-639
13. Heath, R. J., White, S. W., and Rock, C. O. (2001) *Progress in Lipid Research* **40**, 467-497
14. Jackman, J. E., Fierke, C. A., Tumey, L. N., Pirrung, M., Uchiyama, T., Tahir, S. H., Hindsgaul, O., and Raetz, C. R. H. (2000) *Journal of Biological Chemistry* **275**, 11002-11009
15. Onishi, H. R., Pelak, B. A., Gerckens, L. S., Silver, L. L., Kahan, F. M., Chen, M.-H., Patchett, A. A., Galloway, S. M., Hyland, S. A., Anderson, M. S., and Raetz, C. R. H. (1996) *Science* **274**, 980-982
16. Vaara, M. (1996) *Science* **274**, 939-940
17. Anderson, M. S., Bull, H. G., Galloway, S. M., Kelly, T. M., Mohan, S., Radika, K., and Raetz, C. R. (1993) *Journal of Biological Chemistry* **268**, 19858-19865
18. Anderson, M. S., Bulawa, C. E., and Raetz, C. R. (1985) *Journal of Biological Chemistry* **260**, 15536-15541
19. Jackman, J. E., Raetz, C. R. H., and Fierke, C. A. (1999) *Biochemistry* **38**, 1902-1911
20. Young, K., Silver, L. L., Bramhill, D., Cameron, P., Eveland, S. S., Raetz, C. R. H., Hyland, S. A., and Anderson, M. S. (1995) *Journal of Biological Chemistry* **270**, 30384-30391
21. Ogura, T., Inoue, K., Tatsuta, T., Suzaki, T., Karata, K., Young, K., Su, L.-H., Fierke, C. A., Jackman, J. E., Raetz, C. R. H., Coleman, J., Tomoyasu, T., and Matsuzawa, H. (1999) *Molecular Microbiology* **31**, 833-844



22. Kelly, T. M., Stachula, S. A., Raetz, C. R., and Anderson, M. S. (1993) *Journal of Biological Chemistry* **268**, 19866-19874
23. Wyckoff, T. J. O., and Raetz, C. R. H. (1999) *Journal of Biological Chemistry* **274**, 27047-27055
24. Jenkins, R. J., and Dotson, G. D. (2012) *Analytical Biochemistry* **425**, 21-27
25. Jiang, Y., Chan, C. H., and Cronan, J. E. (2006) *Biochemistry* **45**, 10008-10019
26. Chan, W., and White, P. (2000) *Fmoc Solid Phase Peptide Synthesis: A Practical Approach*, OUP Oxford
27. Jenkins, R. J. (2013) Phage Display as a Tool for Probing Lipid A Biosynthesis. in *Medicinal Chemistry*, University of Michigan, College of Pharmacy
28. Jenkins, R. J., Heslip, K. A., Meagher, J. L., Stuckey, J. A., and Dotson, G. D. (2014) *Journal of Biological Chemistry* **289**, 15527-15535
29. Masoudi, A., Raetz, C. R. H., Zhou, P., and Pemble Iv, C. W. (2014) *Nature* **505**, 422-426

Gene	Plasmid	Digest	Forward Primer (Top), Reverse Primer (Bottom)
<i>E. coli</i> <i>LpxA-his6</i>	pET23a	<i>NdeI</i> <i>XhoI</i>	GCGCCATATGATTGATAAAATCCGCCTTTGTGCATCCAACCGC ATATCTCGAGACGAATCAGACCGCGCGTTGAGCGTGC
<i>E. coli</i> <i>LpxC-his6</i>	pET23a	<i>NdeI</i> <i>XhoI</i>	GCGCCATATGATGATCAAACAAAGGACACT GCGCCTCGAGTGCCAGTACAGCTGAAGGCG
<i>E. coli</i> <i>his6-LpxD</i>	pET24d	<i>NcoI</i> <i>XhoI</i>	CATCACCATCACCATCACGCTCAATTCGACTGGCTGATTTAGCG CGCGCTCGAGTTAGTCTTGTTGATTAACCTTGCGCTC
<i>E. coli</i> <i>AcpP</i>	pET23a	<i>NdeI</i> <i>XhoI</i>	GCGCCATATGAGCACTATCGAAGAACGCGTTAAGAAAATTATC CGCGCTCGAGCGCCTGGTGGCCGTTGATGTAATCAATG
<i>E. coli</i> <i>AcpS-his6</i>	pET24a	<i>NdeI</i> <i>XhoI</i>	GCGCCATATGGCAATATTAGGTTTAGGCACGGATATTG GCGCCTCGAGACTTTCAATAATTACCGTGGCACAAGC
<i>V. harveyi</i> <i>aasS-his6</i>	pET23a	<i>NdeI</i> <i>XhoI</i>	GCGCCATATGAACCAGTATGTAAAT GCGCCTCGAGCAGATGAAGTTTACGCGAG
<i>A. baumannii</i> <i>LpxA-his6</i>	pET23a	<i>NdeI</i> <i>XhoI</i>	GCGCCATATGAGCAATCACGATTTAATCC GCGCCTCGAGGCGCACAATCCACGCTCTG
<i>A. baumannii</i> <i>his6-LpxD</i>	pET23a	<i>PmlI</i> <i>XhoI</i>	GCGCCACGTGCAACAATATCGTTTAGATGAATTAGC GCGCCTCGAGTTATTTACGCAAATTAAGTTGATTC
<i>C. pneumoniae</i> <i>LpxA-his6</i>	pET23a	<i>NdeI</i> <i>XhoI</i>	GCGCCATATGGCGAGCATTACCCAACTGC GCGCCTCGAGAGATTCAATCAAACTCCTTC
<i>C. pneumoniae</i> <i>his6-LpxD</i>	pET23a	<i>PmlI</i> <i>XhoI</i>	GCGCCACGTGTCTTAAACAGTTAGCTGAGC GCGCCTCGAGTTAGATCTCTGAAGGAATCTCAGC
<i>C. trachomatis</i> <i>LpxA-his6</i>	pET23a	<i>NdeI</i> <i>XhoI</i>	GCGCCATATGACCAACATTCATCCTACAGCG GCGCCTCGAGTTAAGACTCAACGAAAGCTCCTTC
<i>C. trachomatis</i> <i>his6-LpxD</i>	pET23a	<i>NdeI</i> <i>HindIII</i>	GCGCCATATGATTGATAAAATCCGCCTTTGTGCATCCAACCGC GCGCAAGCTTAATGTTGTTCTGAGAGAGC
<i>H. pylori</i> <i>LpxA-his6</i>	pET23a	<i>NdeI</i> <i>XhoI</i>	GCGCCATATGAGTAAGATTGCAAAAACAGCC GCGCCTCGAGTTCCTCTTGTTTTTCTTCGC
<i>H. pylori</i> <i>his6-LpxD</i>	pET23a	<i>PmlI</i> <i>XhoI</i>	GCGCCACGTGTTAAGCGAATTGTTGAGCGCC GCGCCTCGAGTTAAGACTTAAAAAACCTTTAGC
<i>N. meningitidis</i> <i>LpxA-his6</i>	pET23a	<i>NdeI</i> <i>XhoI</i>	GCGCCATATGACCCTCATCCACCCGACCG GCGCCTCGAGGCGGATGATGCCGCGCGCCG
<i>N. meningitidis</i> <i>his6-LpxD</i>	pET23a	<i>PmlI</i> <i>XhoI</i>	GCGCCACGTGATTCCGGCCACCTACACCCTG GCGCCTCGAGTTATTTGCTGTCTTGACCGGCATC
<i>P. gingivalis</i> <i>LpxA-his6</i>	pET23a	<i>NdeI</i> <i>XhoI</i>	GCGCCATATGATGTCAGAGACAAAAATCAG GCGCCTCGAGCTCCATGGTTCCGCGGACAATGC
<i>P. gingivalis</i> <i>his6-LpxD</i>	pET23a	<i>PmlI</i> <i>XhoI</i>	GCGCCACGTGGAATTTACAGCCCAACAGATAGC GCGCCTCGAGTTAGTGTGTTGTTTTCATATTC
<i>P. aeruginosa</i> <i>LpxA-his6</i>	pET23a	<i>NdeI</i> <i>XhoI</i>	GCGCCATATGAGTTTGATCGATCCTCGCG GCGCCTCGAGGCGGGTGATGCCGCGGGTTGCGC
<i>P. aeruginosa</i> <i>his6-LpxD</i>	pET23a	<i>PmlI</i> <i>XhoI</i>	GCGCCACGTGATGAGTACCTTGTCCTACACCCTGG GCGCCTCGAGTTACGCATCAGATGAAGCGTCACC

**Table 3.1:** List of vectors constructed for acyltransferases studies.

Peptide	Sequence	LpxA $K_d$ ( $\mu$ M)	LpxA IC50	LpxD $K_d$ ( $\mu$ M)	LpxD IC50
RJPXD33	TNLYMLPKWDIP	$4.4 \pm 0.4$	$27.4 \pm 4.4$	$2.0 \pm 0.3$	$3.2 \pm 0.08$
RJPXD33(N $\Delta$ 1)	NLYMLPKWDIP	DNB	N/A	$1.6 \pm 0.2$	N/A
RJPXD33(N $\Delta$ 2)	LYMLPKWDIP	N/A	N/A	$2.8 \pm 0.4$	N/A
RJPXD33(N $\Delta$ 3)	YMLPKWDIP	N/A	N/A	$15.3 \pm 1.5$	N/A
RJPXD33(N $\Delta$ 4)	MLPKWDIP	N/A	N/A	DNB	N/A
RJPXD33(C $\Delta$ 1)	TNLYMLPKWDI	$4.0 + 0.2$	$79.0 \pm 2.9$	$1.3 + 0.1$	$5.3 \pm 0.6$
RJPXD33(C $\Delta$ 2)	TNLYMLPKWD	$4.2 \pm 0.2$	$151 \pm 1.4$	$1.2 + 0.1$	$10.8 \pm 1.7$
RJPXD33(C $\Delta$ 3)	TNLYMLPKW	$5.7 \pm 0.4$	$26.7 \pm 1.2$	$0.5 + 0.1$	$2.4 \pm 0.1$
RJPXD33(C $\Delta$ 4)	TNLYMLPK	$12.7 \pm 0.8$	$66.6 \pm 5.8$	$6.8 + 0.5$	> 100
RJPXD33(C $\Delta$ 5)	TNLYMLP	$14.5 \pm 1.7$	>200	$14.6 + 1.3$	>100
RJPXD33(C $\Delta$ 6)	TNLYML	$10.5 \pm 1.1$	$123 \pm 26$	> 50 $\mu$ M	>100

**Table 3.2:**  $K_d$  and IC50 values of truncated peptides.

<b>Sequence</b>	<b>C-Term</b>	<b>LpxA <math>K_d</math> (<math>\mu</math>M)</b>	<b>LpxD <math>K_d</math> (<math>\mu</math>M)</b>
FITC- $\beta$ -TNLYMLPKWDIP	CONH	$12.6 \pm 0.5$	$0.66 \pm 0.10$
FITC- $\beta$ -TNLYMLPKWDI	COOH	$6.8 \pm 0.9$	$3.8 \pm 1.0$
FITC- $\beta$ -TNLYMLPKWD	COOH	$7.8 \pm 0.2$	$5.2 \pm 0.3$
FITC- $\beta$ -TNLYMLPKW	COOH	$11 \pm 1.0$	$2.4 \pm 0.1$
FITC- $\beta$ -TNLYMLPK	COOH	$42.7 \pm 2.6$	$62 \pm 8.9$
FITC- $\beta$ -TNLYMLP	COOH	$6.2 \pm 0.1$	$18 \pm 2.3$
FITC- $\beta$ -TNLYML	COOH	$5.4 \pm 0.3$	$36 \pm 3.5$

**Table 3.3:** Direct binding results of C-terminal carboxylic acid peptides.

Peptide	Sequence	LpxA $K_d$ ( $\mu$ M)	LpxA IC50	LpxD $K_d$ ( $\mu$ M)	LpxD IC50
RJPXD33	TNLYMLPKWDIP	4.35 $\pm$ 0.42	27.4 $\pm$ 4.4	2.03 $\pm$ 0.26	3.2 $\pm$ 0.08
RJPXD33(T1A)	<b>A</b> NLYMLPKWDIP	DNB	D.N.I.	12.8 $\pm$ 0.6	3.8 $\pm$ 0.3
RJPXD33(N2A)	T <b>A</b> LYMLPKWDIP	81.3 $\pm$ 19.4	>200	17.0 $\pm$ 2.9	11.2 $\pm$ 1.7
RJPXD33(L3A)	TN <b>A</b> YMLPKWDIP	DNB	D.N.I.	78.9 $\pm$ 24.3	18.3 $\pm$ 2.5
RJPXD33(Y4A)	TNL <b>A</b> MLPKWDIP	DNB	D.N.I.	DNB	D.N.I.
RJPXD33(M5A)	TNLY <b>A</b> LPKWDIP	23.9 $\pm$ 3.4	106 $\pm$ 32	DNB	D.N.I.
RJPXD33(L6A)	TNLYM <b>A</b> PKWDIP	26.2 $\pm$ 4.3	>200	DNB	D.N.I.
RJPXD33(P7A)	TNLYML <b>A</b> KWDIP	9.4 $\pm$ 0.6	59.7 $\pm$ 9.6	89.6 $\pm$ 33.7	63.7 $\pm$ 7.7
RJPXD33(K8A)	TNLYMLP <b>A</b> WDIP	5.1 $\pm$ 0.4	20.6 $\pm$ 3.4	3.1 $\pm$ 0.2	9.8 $\pm$ 1.8
RJPXD33(W9A)	TNLYMLPK <b>A</b> DIP	43.6 $\pm$ 5.2	D.N.I.	DNB	78.6 $\pm$ 26.9
RJPXD33(D10A)	TNLYMLPKW <b>A</b> IP	1.8 $\pm$ 0.7	39.4 $\pm$ 12.3	1.6 $\pm$ 0.7	1.52 $\pm$ 0.04
RJPXD33(I11A)	TNLYMLPKWD <b>A</b> P	2.3 $\pm$ 0.4	68.8 $\pm$ 19.4	4.3 $\pm$ 0.3	18.2 $\pm$ 3.0
RJPXD33(P12A)	TNLYMLPKWDI <b>A</b>	58.0 $\pm$ 3.5	>200	13.0 $\pm$ 1.7	16.7 $\pm$ 2.4

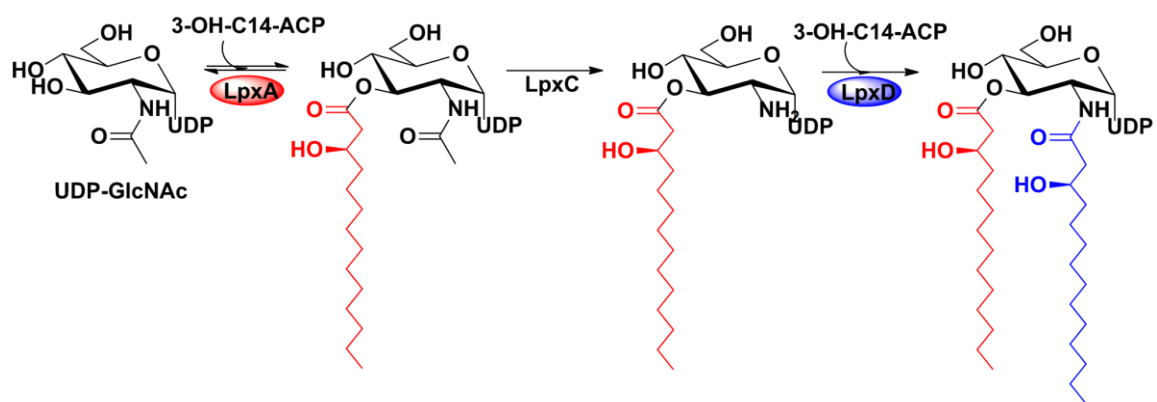
**Table 3.4:**  $K_d$  and IC50 values of alanine-scan peptides. D.N.B. indicates the peptide did not exhibit binding, D.N.I. indicates that the peptide did not exhibit inhibition.

Peptide	Sequence	LpxA $K_d$ ( $\mu$ M)	LpxD $K_d$ ( $\mu$ M)
Photo 1	TN <u>X</u> YMLPKWDIP	$37.4 \pm 2.42$	$2.07 \pm 0.30$
Photo 3	TNLYM <u>X</u> PKWDIP	$32.1 \pm 3.28$	$1.09 \pm 0.11$
Photo 4	TNLYMLPKWD <u>X</u> P	$20.3 \pm 1.75$	$0.80 \pm 0.15$
FITC-RJXD33	TNLYMLPKWDIP	$20.0 \pm 1.5$	$0.60 \pm 0.04$

**Table 3.5:** Binding affinity of photopeptides.

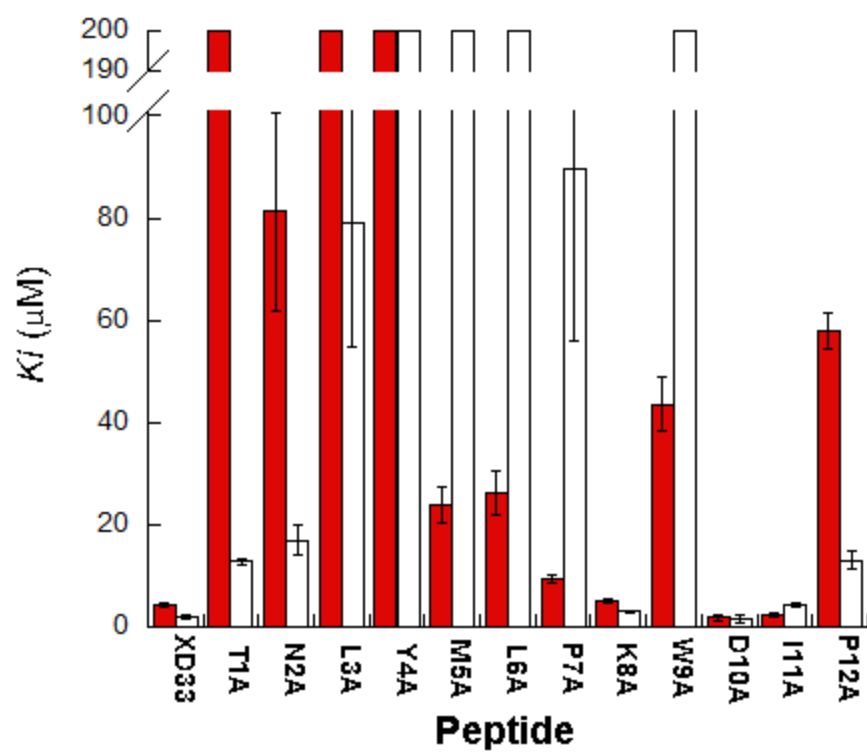
<b>Species</b>	<b>LpxA Acyl Length</b>	<b>LpxA <math>K_d</math></b>	<b>LpxD Acyl Length</b>	<b>LpxD <math>K_d</math></b>
<i>E. coli</i>	OH-C14	$6.21 \pm 0.44$	OH-C14	$0.66 \pm 0.03$
<i>A. baumannii</i>	OH-C12	$3.01 \pm 0.24$	OH-C14	$8.53 \pm 0.31$
<i>C. pneumoniae</i>	Unknown	$0.45 \pm 0.02$	Unknown	N/A
<i>H. pylori</i>	OH-C16	$55.4 \pm 3.4$	OH-C18	N/A
<i>N. meningitidis</i>	OH-C12	>100	OH-C14	$49.9 \pm 4.3$
<i>P. gingivalis</i>	OH-C15/16	>100	OH-C17	DNB
<i>P. aeruginosa</i>	OH-C10	$17.8 \pm 2.7$	OH-C14	>100

**Table 3.6:** Binding of FITC-RJPXD33 to various LpxA and LpxD. N/A indicates not tested as a result of being unable to get the protein soluble at high enough concentration for the binding assay. DNB indicates did not bind. The acyl chain lengths incorporated by *C. pneumoniae* LpxA and LpxD are currently unknown.

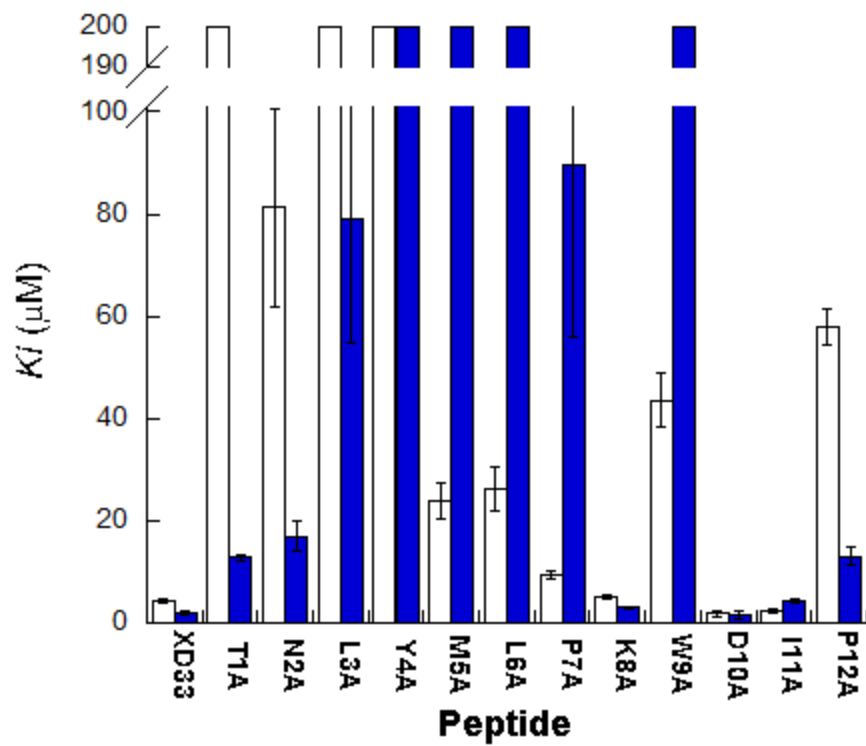


**Figure 3.1** Enzymatic activities of LpxA and LpxD in the Raetz pathway.

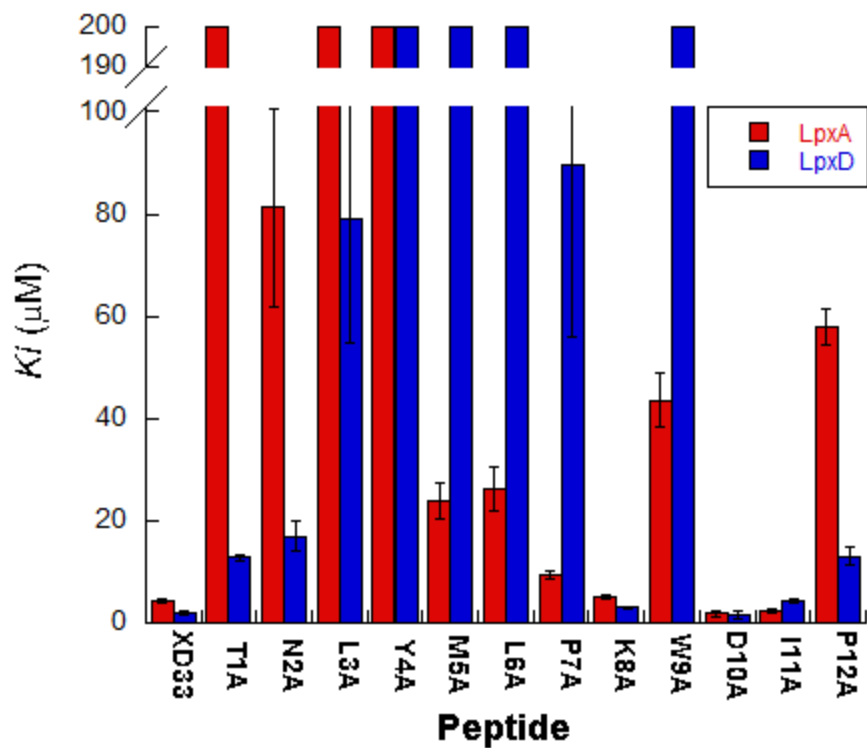




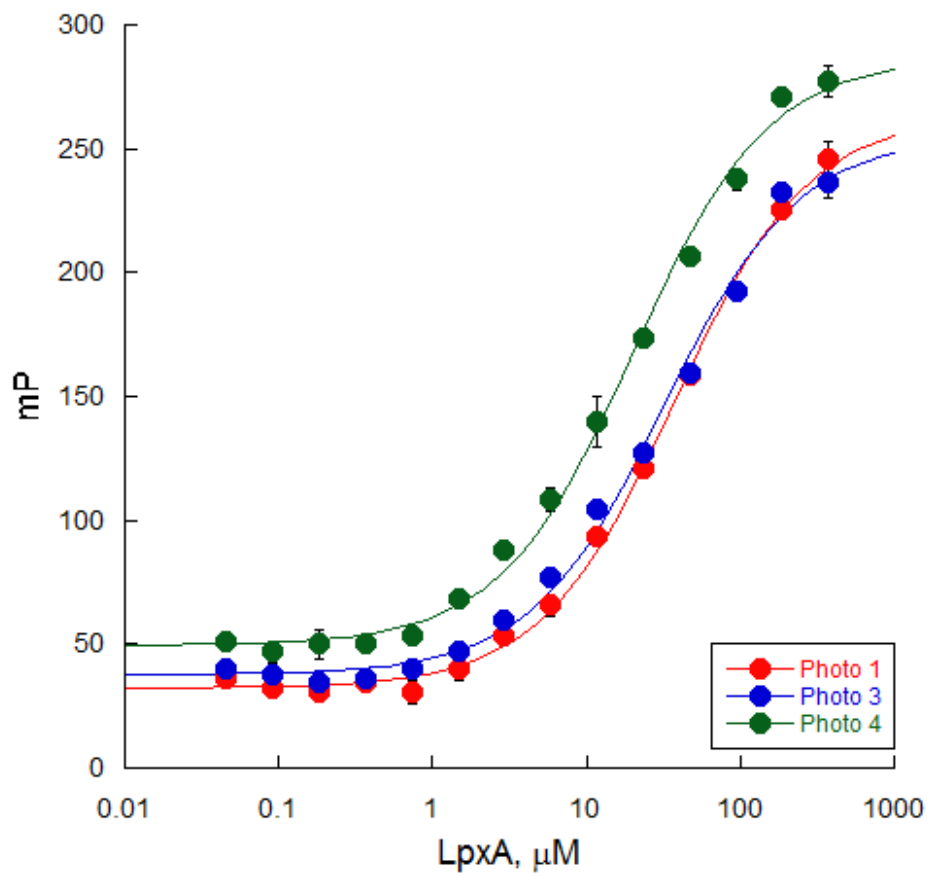
**Figure 3.2:** Alanine-substitution effects on RJPXD33 binding to LpxA.



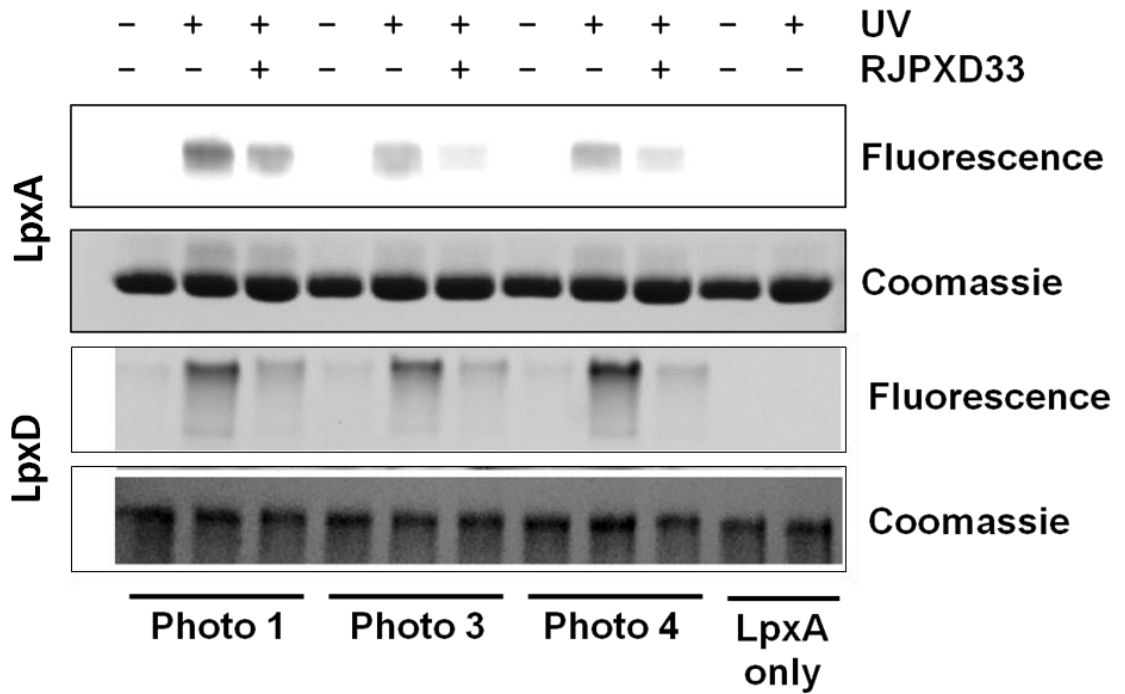
**Figure 3.3:** Alanine-substitution effects on RJPXD33 binding to LpxD.



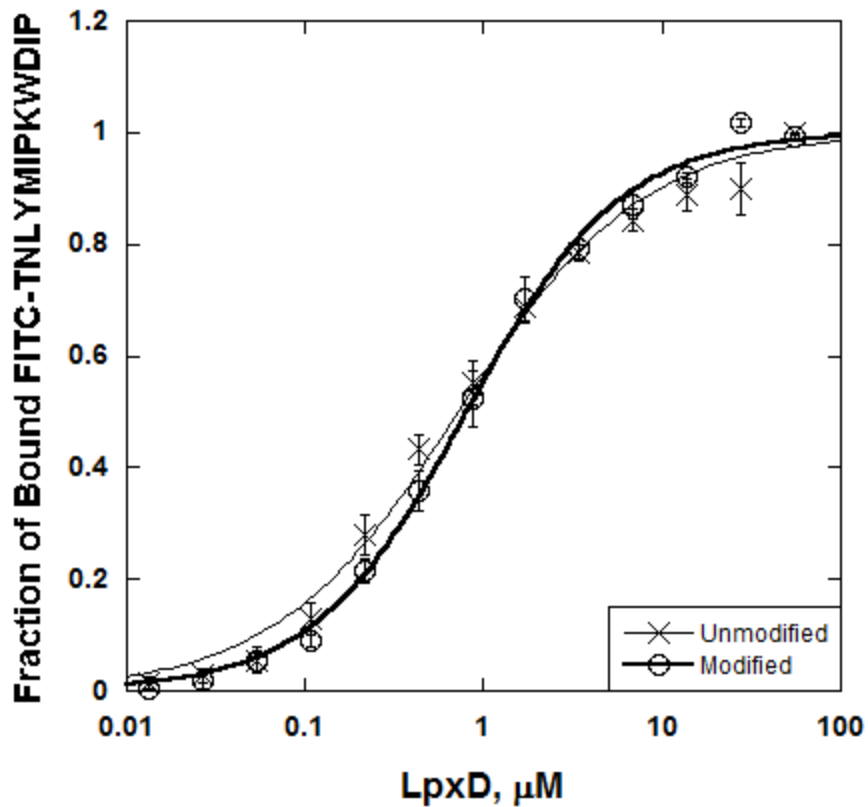
**Figure 3.4:** Alanine-substitution effects on RJPXD33 binding to LpxA and LpxD.



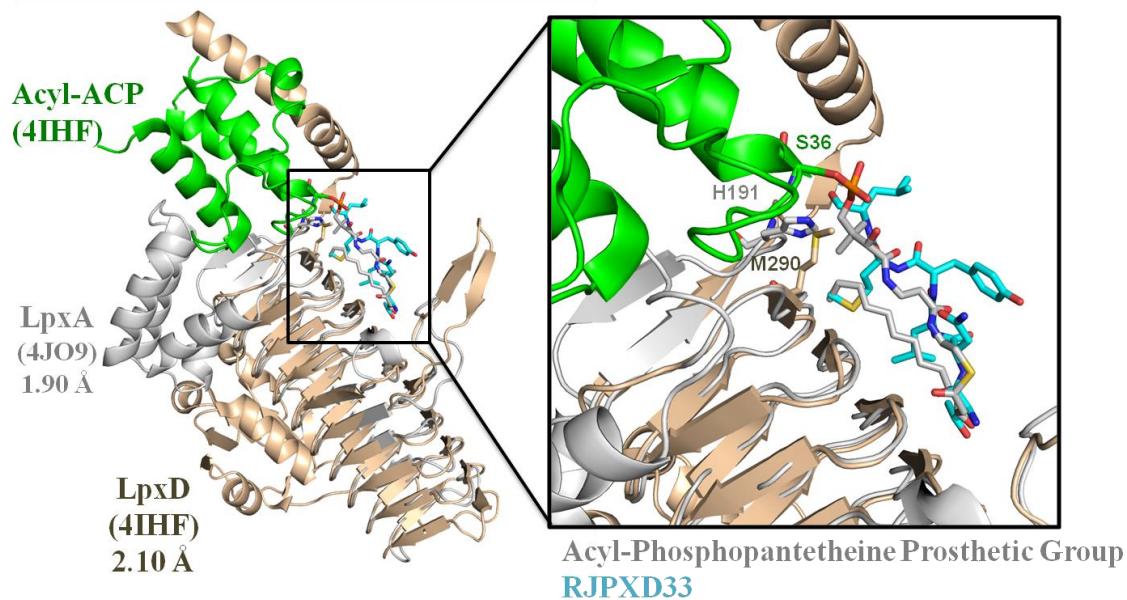
**Figure 3.5:** Direct binding curve of photopeptides to LpxA.



**Figure 3.6:** In-gel fluorescence of photocrosslinked LpxA and LpxD. Photopeptides 1, 3, and 4, were all able to crosslink both LpxA and LpxD and exhibit in-gel fluorescence. These photopeptides bound in the same location as RJPXD33, as addition of the unlabeled peptide to the mixture was able to compete with the photopeptide crosslinking.



**Figure 3.7** FITC-RJPXD33 titrations of native and iodoacetamide treated LpxD. Fluorescence polarization experiments were performed holding FITC-RJPXD33 constant (20 nM) while varying concentrations of LpxD. The peptide was able to bind both native and acylated LpxD with roughly the same affinity ( $K_d = 2.8 \mu\text{M}$  for native LpxD,  $K_d = 3.1 \mu\text{M}$  for iodoacetamide treated LpxD).



**Figure 3.8** Structural overlay of LpxA-RJPXD33 onto LpxD-acyl-ACP. The LpxA-RJPXD33 co-crystal structure monomer (4JO9) (28) is overlaid on the co-crystal structure of LpxD-acyl-ACP (4IHF) (29). The 6 C-terminal residues of RJPXD33 are in teal, with L6 in close proximity with S36 of acyl-ACP. This overlay suggests that the 6 N-terminal residues would further follow the proposed acyl-ACP association pocket to LpxA and LpxD, preventing the association of acyl-ACP to the acyltransferase.

## Chapter 4

### Conclusion & Future Directions

#### Conclusion

Phosphopantothenoylcysteine synthetase (PPCS; EC 6.3.2.5; *coaB*) is a critical enzyme in the CoA biosynthetic pathway, as it is responsible for the incorporation of the reactive thiol. PPCS performs a two step reaction. In the first step, a nucleotide triphosphate is utilized to activate phosphopantothenate by forming a cytidylate intermediate. In the second half reaction, cysteine attacks the cytidylate intermediate to produce phosphopantothenoylcysteine and CMP. PPCS is broadly divided into three types, with Types 1 and 3 existing in bacteria. Type 1 PPCS is found in most bacteria and is expressed as a bifunctional enzyme with PPCDC and solely utilizes CTP. Type 3 PPCS is a monofunctional enzyme that utilizes solely ATP and has recently been discovered in high priority pathogens, including *Streptococcus*, *Enterococcus*, and *Bacillus*.

Prior to the work of this thesis, the active site of *E. coli* Type 1 PPCS had been characterized and residues N210 and K289 were determined to be catalytic (1,2). K289 mediates the first half activation of phosphopantetheine and N210 mediates the second half cysteine condensation. A co-crystal structure of the cytidylate mimetic inhibitory compound **JDP03** bound to *E. coli* PPCS was previously solved by Patrone et. al. (3) but no structural data for the bacterial Type 3 PPCS existed.

This work represents the first molecular characterization of Type 3 PPCS. Through a novel multiple sequence alignment of strictly Type 1 and Type 3 PPCS, we



were able to identify residues conserved completely across bacterial PPCS. To explore Type 3 PPCS in a structural sense, a novel multiple sequence alignment between just bacterial PPCS was generated in order to determine completely conserved residues. These completely conserved residues were probed through mutagenic studies in order to determine their roles in the Type 3 enzyme.

In order to evaluate the activity of PPCS *in vivo*, we developed a double knockout model systems. This knockout strain capitalizes on the pantetheine shunt salvage pathway present in *E. coli*, which allows for genetic knockout of the *coaBC* (*dfp*) gene cluster to be rescued by environmental pantetheine. We showed that this system can be complemented with plasmid-based *coaB* (PPCS) and *coaC* (PPCDC), from different organisms and grow at a rate on par with that of wild-type *E. coli*. Additionally, this system can be used to validate that potential antimicrobials are in fact targeting PPCS, as the introduction of environmental pantetheine should recover the grow inhibition.

Through saturation mutagenesis of completely conserved PPCS residues, we were able to identify N22, D93, and K123 as those with stringent residue requirements. Follow-up *in vitro* characterization using activity assays to determine the binding affinity of the mutants to each substrate, we were able to identify that N22 and K123 share similar catalytic roles in Type 3 *S. pneumoniae* PPCS to those of N210 and K289 in Type 1 *E. coli* PPCS. Additionally, we determined D93 to be responsible for the required divalent cation of *S. pneumoniae* PPCS.

This thesis work also incorporated the characterization of the peptide probe RJPXD33. RJPXD33 is a 12-mer peptide able to bind and inhibit both LpxA and LpxD of the Raetz Lipid A biosynthetic pathway. The essential nature of lipid A in gram

negative bacteria, and the ability of RJPXD33 to target multiple enzymes in the pathway make it an ideal candidate as a starting point for the development of small molecule antimicrobials. To do so, we first needed to fundamentally understand the molecular binding mechanism of the peptide to both LpxA and LpxD.

RJPXD33 was characterized through direct and indirect fluorescence polarization binding assays, by synthesizing series of truncated and alanine-mutated peptides. From this work, we were able to identify the essential YML motif for the binding of the peptide to both LpxA and LpxD. Additionally, we identified Trp9 as integral to the inhibition of LpxA and LpxD, and that Lys8 and Asp10 were overall unimportant in the overall binding of the peptide. We also were able to test the utility of RJPXD33 as a broad spectrum chemical biological probe by testing the ability of the peptide to bind an array of bacterial acyltransferases. This research was essential in order to begin the rational design of small molecules to target both LpxA and LpxD.

TNLYMLPKW was identified as the optimal peptide for high affinity binding and inhibition of both acyltransferases, with a sub 6  $\mu\text{M}$  binding affinity to both LpxA (5.7  $\mu\text{M}$ ) and LpxD (0.5  $\mu\text{M}$ ), and inhibit LpxA with an  $\text{IC}_{50}$  of 26.7  $\mu\text{M}$  and LpxD with an  $\text{IC}_{50}$  of 2.4  $\mu\text{M}$ . Alanine substitution elucidated that K8 resulted in a slight improvement of inhibition of the full length peptide to LpxA (20.6  $\mu\text{M}$   $\text{IC}_{50}$ ). As a basic residue at this position appears to be of little inhibitory or binding consequence to either acyltransferase, TNLYMLPAW would be the best peptidic scaffold to begin rational design of small molecule dual targeting inhibitors.

## References

1. Kupke, T. (2002) *Journal of Biological Chemistry* **277**, 36137-36145
2. Kupke, T. (2004) *European Journal of Biochemistry* **271**, 163-172
3. Patrone, J. D. (2010) Investigating Phosphopantothencycysteine Synthetase as a Potential Antibacterial Target. in *Medicinal Chemistry*, University of Michigan, College of Pharmacy
4. Jenkins, R. J., Heslip, K. A., Meagher, J. L., Stuckey, J. A., and Dotson, G. D. (2014) *Journal of Biological Chemistry* **289**, 15527-15535
5. Masoudi, A., Raetz, C. R. H., Zhou, P., and Pemble Iv, C. W. (2014) *Nature* **505**, 422-426